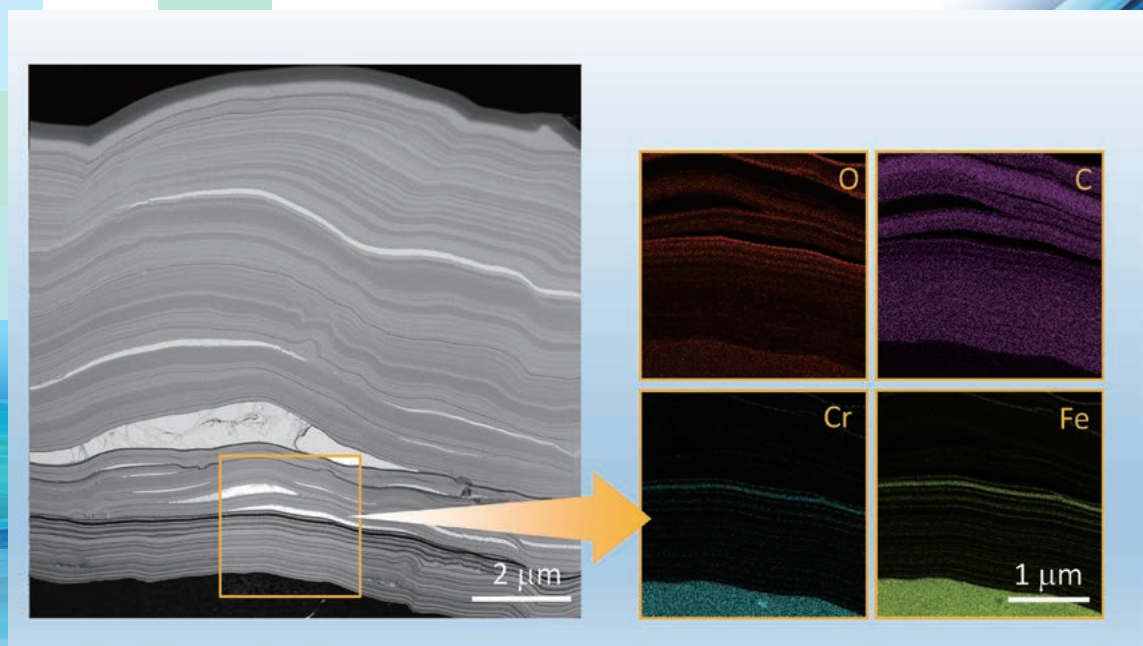


ANNUAL REPORT OF NATIONAL INSTITUTE FOR FUSION SCIENCE

April 2020 – March 2021



Front Cover Caption:

Cross-sectional TEM* image and corresponding EDS* element mappings of the mixed-material deposition layer formed on the LHD first wall in about 15 years of plasma campaign.

*TEM: Transmission electron microscope

*EDS: Energy dispersive X-ray spectroscopy

Provided by Fusion Engineering Research Project

Editorial Board

SEKI, Tetsuo

CHIKARAISHI, Hiroataka

GOTO, Motoshi

MIZUGUCHI, Naoki

MURAKAMI, Izumi

Inquiries about copyright should be addressed to the NIFS Library,
National Institute for Fusion Science, Oroshi-cho, Toki-shi, Gifu-ken 509-5292 Japan.
E-mail: tosho@nifs.ac.jp

<Notice about copyright>

NIFS authorized Japan Academic Association For Copyright Clearance (JAC) to license our reproduction rights and reuse rights of copyrighted works. If you wish to obtain permissions of these rights, please refer to the homepage of JAC (<http://jaacc.org/eng/>) and confirm appropriate organizations to request permission.

Printer: Arakawa Printing Co., Ltd.

2-16-38 Chiyoa, Naka-ku, Nagoya-shi 460-0012, JAPAN


Phone: +81-52-262-1006, Facsimile: +81-52-262-2296

Printed in Japan, ISSN 0917-1185



ANNUAL REPORT OF NATIONAL INSTITUTE FOR FUSION SCIENCE

April 2020 – March 2021



December 2021

Inter-University Research Institute Corporation
National Institutes of Natural Sciences

NATIONAL INSTITUTE FOR FUSION SCIENCE

Address : Oroshi-cho, Toki-shi, Gifu-ken 509-5292, JAPAN

Phone : +81-572-58-2222

Facsimile : +81-572-58-2601

Homepage on internet : URL = <http://www.nifs.ac.jp/>

Contents

National Institute for Fusion Science April 2020 – March 2021	iv
1. Large Helical Device (LHD) Project	1
2. Fusion Engineering Research Project	21
3. Numerical Simulation Reactor Research Project	31
4. Basic, Applied, and Innovative Research	43
5. Fusion Science Archives (FSA)	45
6. SNET Collaborate Research	47
7. Bilateral Collaboration Research	49
8. Activities of Rokkasho Research Center	61
9. Research Enhancement Strategy Office	63
10. The Division of Health and Safety Promotion	65
11. Division of Deuterium Experiments Management	67
12. Division of Information and Communication Systems	69
13. International Collaboraiton	71
14. Division of External Affairs	79
15. Department of Engineering and Technical Services	81

16. Department of Administration	95
APPENDIX 1 Organization of the Institute	97
APPENDIX 2 Members of Committees	98
APPENDIX 3 Advisors, Fellows, and Professors Emeritus	99
APPENDIX 4 List of Staff	100
APPENDIX 5 List of Publications I (NIFS Reports)	104
APPENDIX 6 List of Publications II (Journals, etc.)	000



National Institute for Fusion Science

April 2020 – March 2021





Towards a new era of fusion science

Fusion science is a comprehensive area encompassing various disciplines with extremely high potential. Not only the immense merit of fusion energy, but also the possibilities of new discoveries give us the motivation to climb a high mountain - the history of overcoming every challenge has brought academic depth and breadth to fusion science. While the physics of fusion reactions is already well known, we have yet to understand how a “system”, called high-temperature plasma, can maintain a stable condition. It is a macroscopic system

producing an internal energy by which autonomous dynamics sustains. The aim of fusion science is to elucidate the mechanism of such a spontaneous process; the fundamental principle must be common to the dynamics of the universe, society, or life. Recognizing the problem in a wide context, we pave the way in a zone of fundamental studies. On the way to fusion, the ultimate energy source, we will encounter many crossroads leading to future science and technology.

As we know, there are three different states of matter, i.e., solid, liquid, and gas. Even if the same molecules constitute matter, its “state” varies as the temperature is changed. At a high temperature, all matter becomes a gas, in which molecules are disconnected and distribute sparsely, moving freely. When the temperature is raised further, molecules are broken into ions (positively charged heavy particles) and electrons (negatively charged light particles) by disconnecting the electrical bonding of ions and electrons; we call such a high temperature state “plasma”. While plasma is not common on Earth, it is the most typical state of matter in the universe. Our sun is a huge mass of plasma, consisting mainly of hydrogen. Inside it fusion reactions produce enormous energy. A star is a naturally made sustainable system of high temperature plasma, energized by fusion reactions.

Although the fusion energy is often likened to a “sun on Earth”, we need to think of a system that is completely different from stars. The challenge of fusion science is, indeed, to build a sustainable fusion system, based on a thoroughly new mechanism that we cannot find an example of in nature. A star confines plasma by gravity, but it is a very weak force, only effective against huge masses such as celestial bodies. We have to invoke a much stronger force to create a compact confinement system; magnetic force is the recourse. However, magnetic force acts like “vortex” and its role in creating macroscopic structures is an interesting subject of contemporary physics and mathematics. We also need a much higher temperature than the center of the sun. In a typical star like our sun (the main sequence star), the reaction of synthesizing a helium atom from a hydrogen atom proceeds slowly. This reaction (a so-called p-p chain reaction) is too slow for producing sufficient fusion power in a compact system. We need to apply a faster reaction (a so-called resonant fusion reaction); the easiest is the deuterium-tritium fusion reaction, which produces helium and neutrons, but occurs at temperatures of around 100 million degrees Celsius. On the other hand, several meters away from the plasma, we have to place super-conducting magnets to generate the magnetic field, which are operated at ultra-low temperature. Therefore, fusion on Earth requires an extreme technology, dealing with ultra-high temperatures and ultra-low temperatures, separated only by several meters.

The road to fusion power is purgatory, which is much harder than the prediction made at the beginning (the mid-20th century). However, it is not necessarily unfortunate that we encounter unexpected challenges. As many great researchers say that discovery is born from failure, unknown truths exist outside the range that one can predict. Fusion energy is a steep peak for development researchers to climb, but it is also a treasure trove for academic researchers. The task of the academic researcher is to generate new knowledge from the input of difficult problems.

All members of the National Institute for Fusion Science (NIFS) are working on the construction of a lighthouse that illuminates the direction of fusion science in choppy academic waters ahead. NIFS is a broad avenue for many researchers, through which the scope of “fusion science” will extend in the world of science. We hope that many people will pay attention to our endeavor and participate in these activities.

YOSHIDA Zensho
Director General of National Institute for Fusion Science

1. Large Helical Device (LHD) Project

The experiment with deuterium plasma started in 2017 in the Large Helical Device (LHD). The achievements in FY2020 include: (1) Establishment of a high-temperature plasma generation method, (2) Discovery of the positive side of turbulence, and (3) Observation of plasma-wave interaction.

(1) Establishment of a high-temperature plasma generation method

In the LHD deuterium plasma experiment in FY2020, we succeeded in generating plasmas with electron and ion temperatures of 100 million degrees. One hundred million degrees is one of the conditions for nuclear fusion and is an important milestone. Until now, plasmas with high ion temperatures have had low electron temperatures, but with this success, a method for producing plasmas that reach 100 million degrees has been established. With this success, the LHD research has entered a new stage.

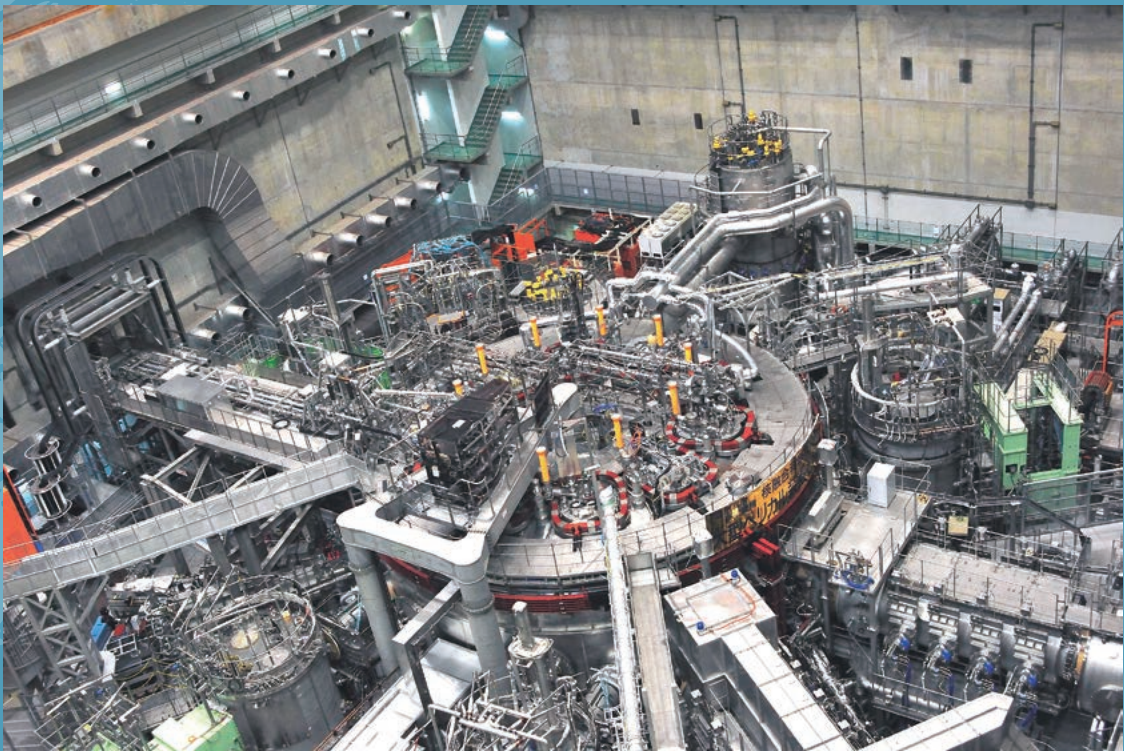
(2) Discovery of the positive aspects of turbulence

In nuclear fusion, isotope mixture plasmas consisting of hydrogen isotopes deuterium and tritium are used. The LHD isotope mixture plasmas experiment using hydrogen and deuterium was conducted to simulate isotope mixture plasma. The hydrogen isotope mixing was observed for the first time in the world. It was found that turbulence, which has a large size, effectively mixes the hydrogen isotopes. The other finding is turbulence spreading. Turbulence does not occur in the absence of temperature or density gradients, but turbulence generated elsewhere can propagate to a region with a zero-gradient area, which is called turbulence spreading. The non-uniform flow in the plasma blocks the spreading turbulence. Furthermore, when this turbulence block is mitigated by MHD instability to enhance turbulent spreading in the plasma periphery, the heat load at the device's wall is reduced. The experiment revealed that turbulence, which has been emphasized as a negative aspect of nuclear fusion, has a positive aspect, and this achievement will become a basis for future fusion research.

(3) Observation of the interaction between plasma and waves

Two types of plasma instabilities occur when the pressure gradient becomes steep: those that appear slowly and persist and those that appear suddenly. Suddenly appearing instabilities are like earthquakes in that they can occur at any time, but we do not know when they will occur. For this sudden type, important experimental results were obtained to clarify the "trigger" and the "effect" on the plasma. Sudden instability is accompanied by the generation of waves like the tremors of an earthquake. The plasma generates these waves, but it was found that the impurities in the plasma absorb the waves and distort the velocity profile function. This interaction between plasma and waves is called "Landau damping," which the former Soviet physicist Landau proposed in 1946. Landau damping is one of the most significant discoveries in plasma physics, and the fact that this phenomenon was observed in the LHD plasma experiment is of great academic significance.

(K. Ida)



High Performance

Highlight

Extension of high-performance plasma operational regime

In the Large Helical Device (LHD), a deuterium (D) experiment was initiated in March 2017. To seek higher performance plasmas and to study the mechanism of the increased performance by isotope effect are the important purposes of the D experiments. In the FY2020 experimental campaign, we focused on the extension of the high temperature operational regime, of the high neutron emission ratio (S_n), and of the plasma stored energy (W_p).

Figure 1 shows the summary of the extension of the plasma performance [1]. We were able to successfully expand the high ion temperature (T_i) and the high electron temperature (T_e) regime due to the optimized heating combination of a neutral beam injection (NBI) and an electron cyclotron resonance heating (ECRH). Representative achievements are (1) $T_{i0} = 10$ keV with $T_{e0} = 8.1$ keV, and (2) both T_{i0} and $T_{e0} = 8.7$ keV (100 million degree). We renewed the S_n record of D pellet discharge as 4.1×10^{15} n/s from 3.3×10^{15} n/s using NB, ECH, and ICH. The experiments were conducted in the inward-shifted configuration of the $R_{ax} = 3.55$ m, where the EP confinement is better. The NB#1 and HAS were half and the new gyrotron was on low power operation. Thus, higher S_n is expected in the next campaign with heating operation in perfect condition. We also achieved a new record of W_p as 2.1 MJ with all NBs, ECH, and ICH. Under the n-NBI dominant condition, the achievable W_p is maximum at $R_{ax} \sim 3.6$ m, where the plasma volume is the maximum and is consistent with previous experiments. On the other hand, the achievable W_p increased as R_{ax} shifted inward under the p-NBI dominant, implying a better confinement of perpendicular beam components. In the $R_{ax} = 3.75$ m and 3.9 m, the SDC discharges were observed both for the H and the D pellet operation.

(H. Takahashi, K. Ogawa, R. Sakamoto)

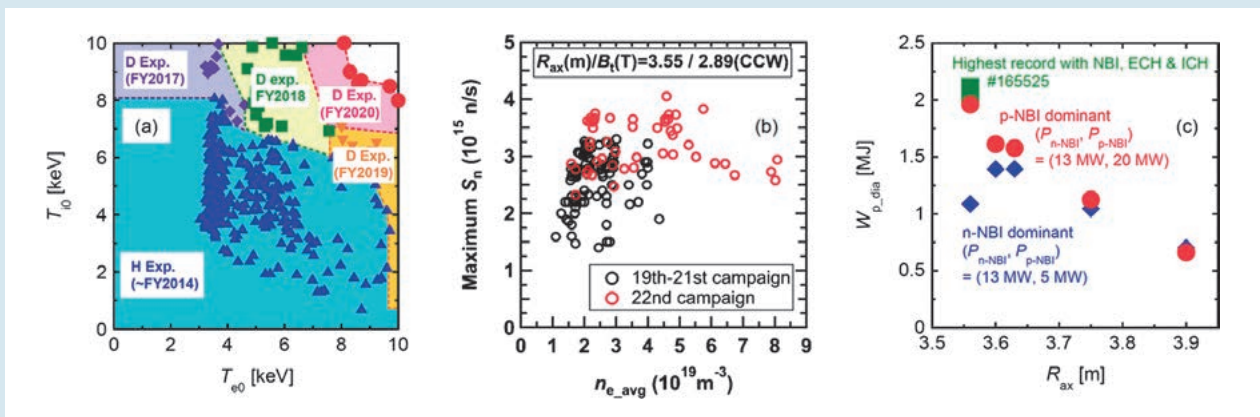


Fig. 1 (a) The operational map of high temperature plasmas, (b) the dependence of the S_n on the averaged n_e , and (c) the configuration dependence of the W_p [1].

Effect of an electron heating on high T_i operations

In the D experiments in the LHD, the simultaneous high T_i and high T_e regime has been successfully extended mainly due to the suppression of the EIC modes and control of the T_e/T_i value [2]. The EIC is triggered by helically trapped ions at a lower order magnetic resonant surface and the EIC causes loss of high energy ions, leading to the decrease in T_i [3]. The mode width of the EIC depends on $T_e^{-1/2}$ thus the increase in T_e at the resonant surface is expected to be effective to suppress the EIC. Figure 2 shows the comparison of the time evolution of (a) the heating power, (b) the line-averaged-electron density n_{e_fir} , (c) the poloidal magnetic fluctuation amplitude b_θ , (d) the neutron emission rate S_n , (e) the T_{i0} without and with 0.95-MW ECRH superposition. The bursty increase of b_θ and the synchronized drop in the S_n correspond to the EIC occurrence and the loss of the high energy ions, respectively. Due to the ECRH the EIC was clearly suppressed. Then the S_n , which is reflected the amount of the confined high energy ions, increased and this contributed to realizing the higher T_{i0} .

Although the ECRH is effective in mitigating the EIC, the increase in T_e/T_i causes a destabilization of the ITG mode [4], leading to a degradation of the ion thermal confinement. Figure 3 shows the ECRH power dependence of (a) number of the EIC bursts during the high T_i discharges and (b) the T_{i0} and the T_{e0} . The plasmas were produced using high power NBIs with the $n_{e_fir} \sim 1 \times 10^{19} \text{ m}^{-3}$ and the ECRH was superposed on the high T_i plasmas. The numbers of the EIC burst clearly decreased with increase in the superposed ECRH power. The T_i value increased in low power ECRH conditions due to the EIC suppression. On the other hand, the T_i decreased in higher ECRH power superposition. This is due to the degradation of the ion thermal confinement in the plasma core region, due to the increase in the T_e/T_i .

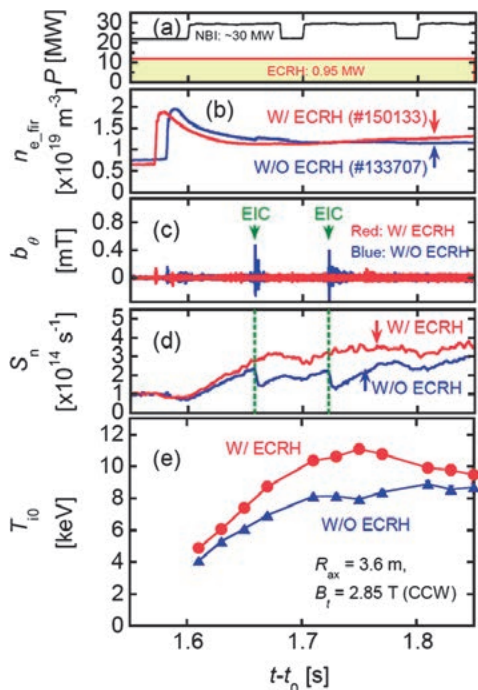


Fig. 2 The time evolution of (a) the heating power, (b) the n_{e_fir} , (c) the b_θ , (d) the S_n , and (e) the T_{i0} without and with ECRH superposition.

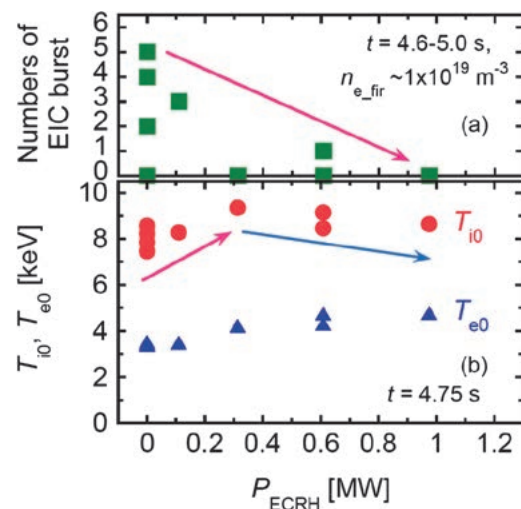


Fig. 3 The ECRH power dependence of (a) the numbers of the EIC burst during the high T_i discharges and (b) the T_{i0} and the T_{e0} .

Figure 4 shows the dependence of the normalized scale length of T_i on the T_e/T_i at the effective minor radius of $r_{\text{eff}} = 0.1$ m. These data were obtained in the high T_i operation with the superposed on-axis ECRH power from 0 to 5.4 MW. A significant degradation of the R/L_{T_i} was observed both in the H and D plasmas when the T_e/T_i exceeded ~ 0.7 . These results show that not only the mitigation of EIC by ECRH but the control of T_e/T_i in the moderate range is important for realizing high T_i and high T_e simultaneously.

(H. Takahashi)

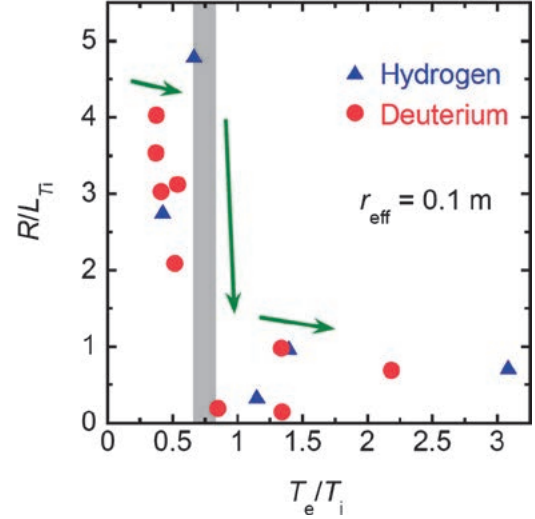


Fig. 4 The dependence of the R/L_{T_i} on the T_e/T_i at the effective minor radius of $r_{\text{eff}} = 0.1$ m.

Extension of the high total neutron emission rate of steady-state deuterium discharge guided by a data-driven approach.

One of the direct parameters for showing the path to a fusion reactor is fusion output which is connected to electrical power generation. In previous deuterium LHD campaigns, the total neutron emission rate (S_n) dependence on the electron density was surveyed in wide experimental conditions, i.e., the toroidal magnetic field strength (B_t) and the magnetic axis position (R_{ax}). It was reported that the relatively high $S_n \sim 3.1 \times 10^{15}$ n/s was achieved in a steady-state deuterium gas puff discharge at the so-called inward shifted and subcooled condition $B_t = 2.89$ T and $R_{\text{ax}} = 3.55$ m [5,6]. In the 22nd LHD campaign, we newly employed the data-driven approach, which is a complementary technique of physics-based methodology with no physics concerns, to guide a high S_n discharge scenario. The regression analysis, using externally controllable parameters, e.g., electron density and heating power, obtained in the previous campaign was executed to inspect the parameter importance toward high S_n achievement. In this analysis, data points fulfilling the following conditions were selected. (1) $B_t = 2.89$ T, and $R_{\text{ax}} = 3.55$ m. (2) A deuterium gas puff discharge without deuterium pellets. (3) All deuterium NBs were injected. (4) Deuterium dominant plasma with line-averaged electron density $n_{e,\text{avg}}$ of 1×10^{19} m^{-3} . (5) The plasma initiation phase is excluded. The regression analysis is performed using only controllable parameters from the outside, e.g., $n_{e,\text{avg}}$ [10^{19} m^{-3}], injection power of negative-ion based NB $P_{\text{N-NB}}$ [MW], injection power of positive-ion based NB $P_{\text{P-NB}}$ [MW], and injection power of electron cyclotron heating P_{ECH} [MW]. The regression expression $S_n = 10^{14.25} \times n_{e,\text{avg}}^{0.52} \times P_{\text{N-NB}}^{0.69} \times P_{\text{P-NB}}^{0.37}$ is obtained [7]. Note that P_{ECH} was excluded from this regression analysis because the importance of P_{ECH} was relatively low, compared with the other parameters. The experimental scenario for high S_n was decided based on the obtained regression expression.

Figure 5 represents the time evolution of steady-state discharge that we achieve the new S_n record [8]. In this discharge, $P_{\text{N-NB}}$, $P_{\text{P-NB}}$, P_{ECH} , and the injection power of ion cyclotron heating P_{ICH} were 6.9 MW, 19.3 MW, 4.3 MW, and 2.4 MW, respectively. Especially, $P_{\text{N-NB}}$ injection power increases by 0.9 MW more than the previ-

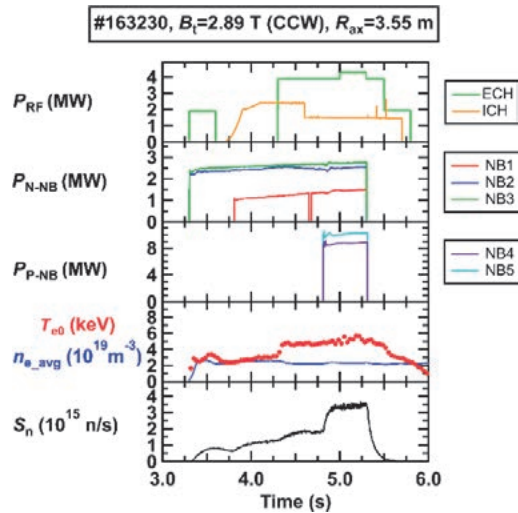


Fig. 5 Highest S_n steady-state discharges.

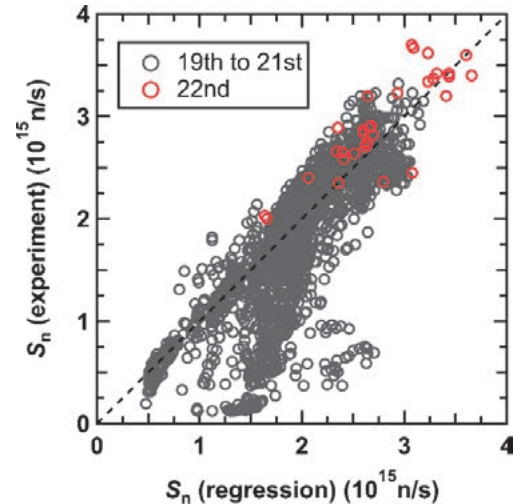


Fig. 6 Comparison of S_n measured in experiment and calculated by regression analysis in steady-state discharges.

ous high S_n discharge in steady-state conditions. The highest S_n of 3.7×10^{15} n/s in the steady-state discharge was successfully achieved in discharge number 163230 at $t = 5.236$ s. We have extended the S_n by approximately 20% from the previous campaigns. The relation between experimentally obtained S_n in a steady-state discharge and S_n , calculated by the regression expression, is indicated in Fig. 6. Here, the data taken through the 22nd campaign, indicated by the open red circles, are overplotted with the data taken through previous campaigns represented by the open gray circles. Although the regression expression is only applicable in a range of utilized databases, it is found that this regression approach can be used for showing a guideline to extend the parameter range slightly beyond the employed database.

(K. Ogawa)

- [1] H. Takahashi *et al.*, presented in the 4th LHD Workshop, Toki, #2 (2021).
- [2] H. Takahashi *et al.*, proc. 28th IAEA Fusion Energy Conference (virtual), CN-781 (2021).
- [3] K. Ogawa *et al.*, Nucl. Fusion **58**, 044001 (2018).
- [4] M. Nakata *et al.*, Plasma Phys. Control. Fusion **58**, 074008 (2016).
- [5] M. Isobe *et al.*, Nucl. Fusion Nuclear Fusion **58**, 082004 (2018).
- [6] K. Ogawa *et al.*, Nucl. Fusion **59**, 076017 (2019).
- [7] K. Ogawa *et al.*, Plasma Fusion Res. **15**, 1202087 (2020).
- [8] K. Ogawa *et al.*, Fusion Eng. Des. **167**, 112367 (2021).

Transport and Confinement

Highlight

Progress in the development of turbulence diagnostics

To improve our understanding of the effects of turbulent transport on toroidal plasma confinement, we are studying the interaction of turbulence on various scales at the LHD. Mixed micro-scale turbulence phenomena, which include both the ion and the electron scale turbulences, is of especial interest in the high temperature plasma confinement study at present, and there are many theoretical studies. The LHD already has several ion-scale turbulence diagnostics, such as CO2 laser used 2D phase constant imaging (PCI), microwave Doppler reflectometer/backscattering (DBS), and beam emission spectroscopy (BES). Recently, a 90 GHz W-band millimeter-wave back-scattering system [1] was designed and installed for measuring the electron scale turbulence such as the electron temperature gradient (ETG) driven mode which has a high wavenumber ($k_{\perp}\rho_s \sim 40$ and $k_{\perp} \sim 40 \text{ cm}^{-1}$). Figure 1 shows the cross-section of the observation line of sight of the back-scattering system. In order to achieve both high spatial resolution and spatial scanning, a metallic lens antenna was applied as an in-vessel focusing antenna.

Simultaneous measurements of each ion scale turbulence and electron scale turbulence have been obtained. As an example, a comparison of the turbulence intensities of different hydrogen isotopes, hydrogen (H) and deuterium (D), shows a seesaw behaviour as shown in Figure 2. The ion scale turbulence decreases more in the case of D than H, while the electronic scale turbulence increases slightly in the case of D. These results are qualitatively consistent with the predictions of the gyrokinetic simulation (GKV code) calculation [2], and provide a basis for discussion of the future importance of comparing the results of such multi-scale turbulence experiments and theoretical simulations.

[1] T. Tokuzawa *et al.*, Rev. Sci. Instrum. **92**, 043536 (2021).
 [2] K. Tanaka *et al.*, Plasma Phys. Control. Fusion **62**, 024006 (2020).

(T. Tokuzawa)

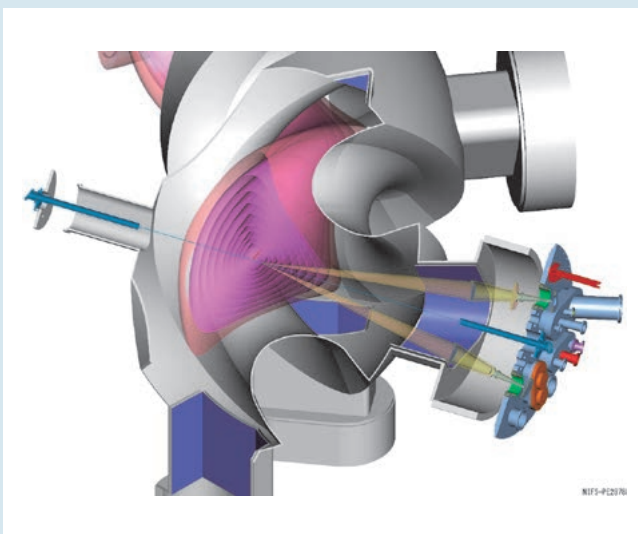


Fig. 1 In-vessel antenna pair for the back-scattering system. The millimeter wave beams of the launcher and receiver are represented by yellow triangles. [1]

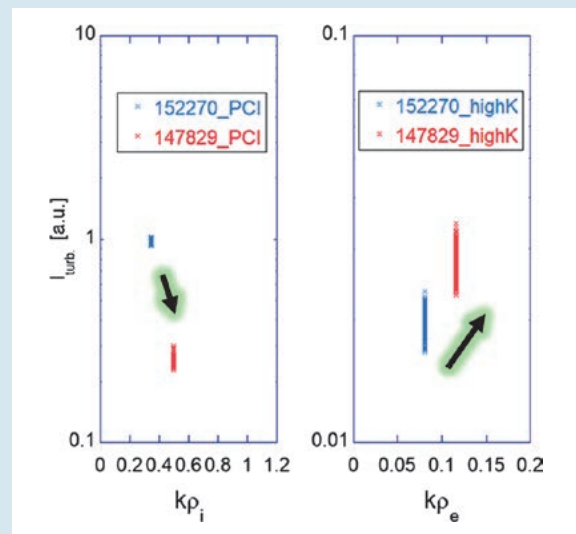


Fig. 2 Comparison of turbulence intensity in hydrogen (blue crosses) and deuterium (red crosses) plasmas. Ion scale turbulence (left) and electron scale turbulence (right).

Observation of heat flux driven by turbulence pulse during minor collapse of electron internal transport barrier [3]

Minor collapses of the electron internal transport barrier (e-ITB) are repeatedly observed by controlling the rotation transform profile with the electron cyclotron current drive (ECCD) and the neutral beam current drive (NBCD) to form a magnetic island in the central region of the plasma, which increases the pressure gradient in the e-ITB region. Figure 3 shows the time evolution of the electron temperature profile and the electron temperature gradient near the e-ITB foot, measured by a newly developed high time resolution (repetition rate: 20 kHz) Thomson scattering diagnostics. As shown in Fig. 3 (b), the pressure gradient near the e-ITB foot increases due to the formation of the magnetic island, and reaches a threshold value of about 12 keV/m. When the pressure gradient reaches this value, the e-ITB collapses. After the collapse, the temperature gradient increases again, leading to another subsequent collapse.

At the timing of the collapse of the e-ITB, the time evolution of the electron temperature, the electron scale turbulence, and the magnetic field fluctuation are investigated by an ECE measurement, a backscattering measurement, and a magnetic probe, respectively (Fig. 4). It is suggested that the formation of a magnetic island in the central region of the plasma causes a strong pressure gradient, which leads to MHD instability, and the resulting turbulent transport propagates the heat flux outward, causing minor collapses of the e-ITB. Since the electron-scale turbulence rises and falls in a very short time of about 300 μsec , it is considered to have a pulse shape with a spatial width of the line of sight. The electron-scale turbulence is scanned shot-by-shot at the spatial position to investigate the radial propagation speed. The turbulence pulse propagates outward at a speed of about 10 km/s from the core ($r_{\text{eff}}/a_{99} \sim 0.1$) to the edge region ($r_{\text{eff}}/a_{99} \sim 1.0$), while the thermal pulse propagates at a speed of 1.5 km/s.

In this research, strong pressure gradients are generated by forming magnetic islands inside the e-ITB plasma, which induce instabilities and generate observable turbulence that is larger than the background turbulence. Such a large turbulence enables us to observe the propagation of the turbulence pulse. This method can artificially induce turbulence spreading and avalanche, caused by the collapse of e-ITB, and is beneficial for understanding the physics of avalanche and turbulence spreading.

[3] N. Kenmochi *et al.*, submitted to Communications Physics.

(N. Kenmochi)

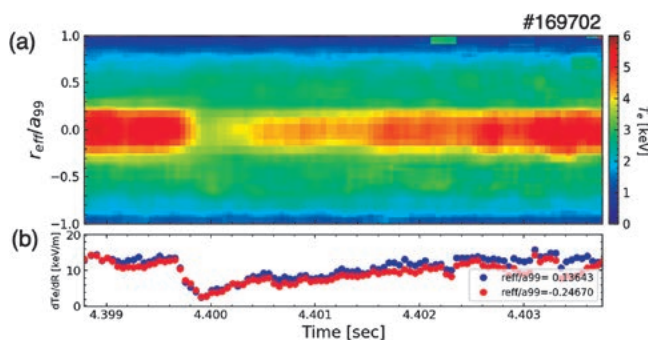


Fig. 3 The time evolution of (a) the electron temperature profile and (b) the electron temperature gradient near the e-ITB foot observed by the newly developed high time resolution (repetition rate: 20 kHz) Thomson scattering measurement.

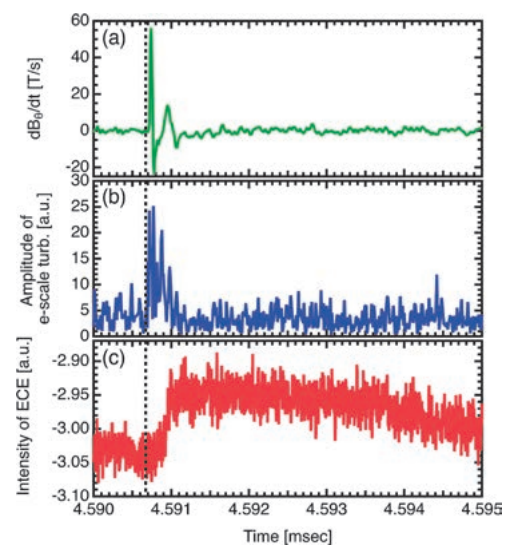


Fig. 4 The time evolution of (a) magnetic fluctuation, (b) electron scale turbulence, and (c) electron temperature measured by magnetic probe, W-band back scattering measurement, and ECE measurement, respectively.

Development of fast charge exchange spectroscopy system with fast camera

As the energetic ion driven mode and non-local transport and hysteresis phenomena have been observed in the plasma, the velocity distribution of ions and electrons have been a target of study to understand these behaviors. In the LHD, the energetic ion driven resistive interchange (EIC) mode, a rotating bursting $m/n = 1/1$ tearing parity mode, which resonates with the precession motion of helically trapped energetic ions, has been observed during the heating by neutral beam injection with positive ion source (p-NBI).

The charge exchange system with a high sampling frequency (10 kHz) has been developed to observe the time change of the velocity distributions of carbon ion on the various plasma behaviors. Figure 5 shows the components of the spectrometer system. The fast camera (FASTCAM Nova PHOTRON LIMITED.) and image intensifier (C10880 Hamamatsu Photonics K.K.) are used as the detector of the spectra image instead of the CCD camera for the high sampling frequency. A bundle consisting of 200 optical fibers (400 μm core), arranged in four slits of 50 fibers each, with smile curve correction, is used for the incident side. The 50 fibers are binned in a vertical direction to increase the signal light coming from the plasma and the system can be observed from four positions in space. The pixel size of the fast camera is 20 μm , but since the image intensifier shrinks the image, the effective pixel size is 29 μm . The inverse dispersion is 0.724 nm/mm, and the instrument width (FWHM) is 0.471 mm. The tangential lines of sight on the 90 port are used for this measurement because the lines of sight have a lot of channels (15 lines of 104 horizontal channels each) with a 1 cm pitch. The emission from the area of 14 cm vertically times 4 cm radially, is collected with the 50 channels of the slit in the incident bundle.

Figure 6 (a) shows the time traces of the W_p and RF probe signal in the discharge in which are observed MHD burst events. The stored energy W_p is dropped down associated with the spikes in the RF probe signal, which indicates the activities of the energetic ions. The magnetic axis position R_{ax} , toroidal magnetic field B_T , canceling ratio of the quadrupole component B_q , and pitch parameter are 3:6 m, -2.75 T, 100%, and 1.254, respectively. The electron density and temperature at the plasma center are $2.5 \times 10^{19} \text{ m}^{-3}$ and 1.3 keV, respectively. Figure 6 (b) shows the time change of the CVI (529.05 nm) spectra around $R = 4.25$ m, measured with the sampling frequency of 10 kHz. The CVI spectra were observed to spread only to the longer wavelengths when the event

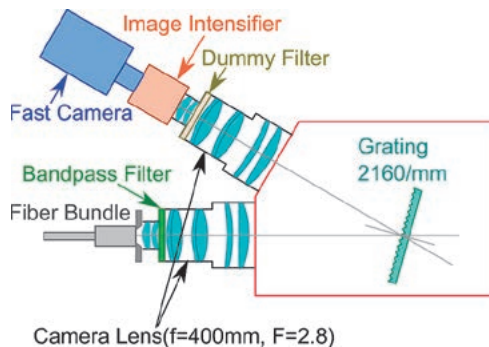


Fig. 5 Schematic view of the spectrometer for the fast charge exchange spectroscopy system.

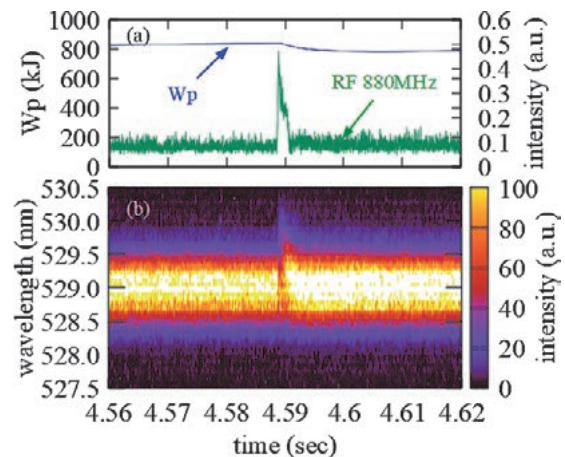


Fig. 6 (a) time trace of W_p and RF probe signal. (b) time change of CVI spectra around the MHD burst event (#164344).

happened and it recovered in a very short time. From the spectra obtained in this way with high time resolution, the distortion of the velocity distribution of ions from the Maxwell distribution when the event happened can be investigated using moment analysis.

(M. Yoshinuma, K. Ida, T. Kobayashi)

Study of ICRF minority hydrogen ion heating characteristics in deuterium plasma in the LHD

The characteristics of the ion cyclotron range of frequency (ICRF) minority ion heating with hydrogen minority and deuterium majority plasma were studied by an ICRF modulation injection experiment in the LHD. In recent experimental conditions with deuterium plasma, a significant increase of the neutron emission rate by ICRF second harmonic deuteron heating was not observed [4]. Therefore, in this study, the neutron emission rate is used to refer to the information regarding the thermal ion component. The experimental and simulation results of the heating efficiencies in the various minority hydrogen ion ratios are shown in Fig. 7 (a). The heating efficiencies of the HAS antenna and FAIT antenna were observed separately. The dashed lines are the results of the estimation of the total heating efficiency and that of the electron direct heating, using a simple-model simulation [5]. The experimental results showed good agreement with the simple-model simulation of the ICRF wave absorption. Fig. 7 (b) shows the simulation result of the spatial distribution of the absorbed power in the case of a minority hydrogen ratio of 2%. The strong absorption can be seen at around the region where the left-hand polarized electric field is locally. During these experiments, the accelerated minority hydrogen ions were observed by neutral particle analyzers (NPAs) [6]. As shown in Fig. 7 (c), the counting rates of the energetic particles were higher in the lines of sight of passing through the helical ripple than that of across the magnetic axis. The counting rate decreased as the minority hydrogen ion ratio increased. The dependence of the minority hydrogen ion ratio on the density of the energetic ions was consistent with the heating efficiencies experimentally observed and of simulation. The heating efficiency of the ICRF minority ion heating could be well explained by simple-model simulation in the LHD deuterium experiment.

[4] R. Seki *et al.*, 2020 *Plasma Fusion Res.* **15**, 1202088.

[5] K. Saito *et al.*, 2001 *Nucl. Fusion* **41**, 1021-1035.

[6] S. Kamio *et al.*, 2019 *JINST* **14**, C08002.

(S. Kamio)

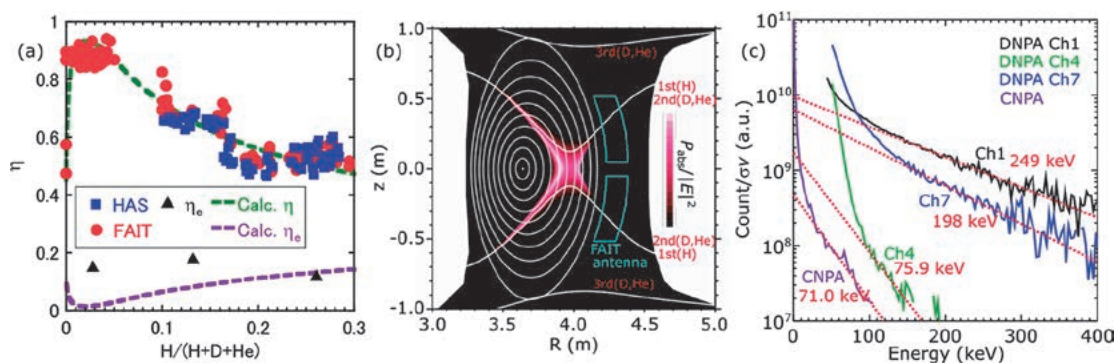


Fig. 7 (a) Experimental and simulation results of the heating efficiencies depending on the minority hydrogen ratio. (b) Spatial distribution of the absorbed power in the calculation in the case of the minority hydrogen ion ratio of 2%. (c) Energy distributions of the accelerated energetic particles observed by NPAs.

Edge/Divertor/Atomic and Molecular Processes

Highlight

Confinement mode transition during detached phase with RMP application in LHD

Compatibility of good core plasma performance with divertor heat load mitigation is mandatory for future reactors. In LHD, impact of the edge magnetic field structure on the core confinement and divertor detachment is being observed. The RMP (resonant magnetic perturbation) field ($m/n = 1/1$) application creates edge magnetic island. It has been found that the edge island has stabilizing effect on the detachment operation [1]. In the deuterium experiments with the RMP application, confinement mode improvement is observed [2]. Figure 1 shows time traces of plasma stored energy (W_p), divertor particle flux, magnetic probe signal, and pressure gradient profile. The detachment transition occurs at $t = 3.95$ sec as confirmed with the reduction of the divertor particle flux. At the same time, increase of W_p is observed together with formation of edge pressure gradient. In the latter phase of the detachment, further increase of W_p occurs spontaneously at $t = 4.5$ sec, where strong edge transport barrier (ETB) is formed as shown in the pressure gradient profile in Fig. 1 (d). The ELM like burst appears in the magnetic probe signal as well as in the divertor particle flux. The density fluctuation measured by the 2D phase contrast imaging decreases by an order of magnitude during the ETB formation. These are clear signature of the confinement mode transition as observed in the H-mode in tokamaks. It has been found that the ETB develops at the inner edge of the magnetic island created by the RMP. It is also found that the ETB is stronger in the deuterium plasmas than the hydrogen plasmas as shown in Fig. 2, where edge pressure profiles in detached phase are compared between deuterium and hydrogen plasmas. The results clearly show the importance of the edge magnetic field structure and isotope effect on the core confinement compatible with the divertor detachment for the heat load mitigation. The mechanism of the confinement mode transition is under investigation to extrapolate to a future reactor operation scenario.

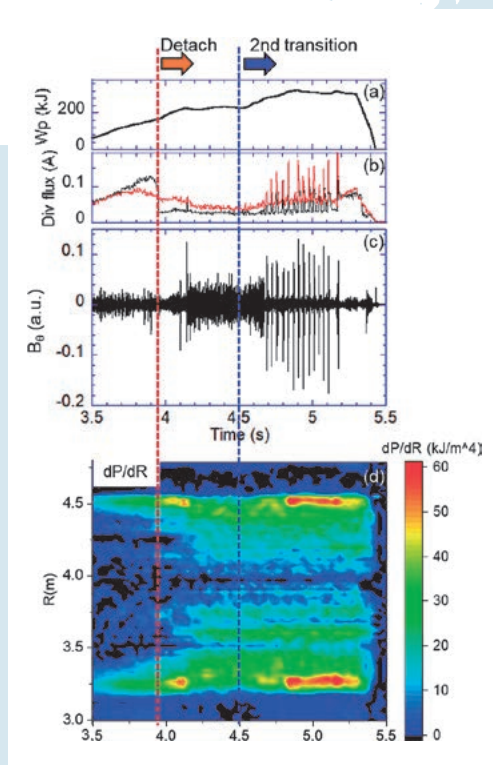


Fig. 1 Time traces of (a) plasma stored energy (W_p), divertor particle flux, (c) magnetic probe signal, (d) radial profile of pressure gradient, with RMP application in deuterium plasma.

It has been found that the ETB develops at the inner edge of the magnetic island created by the RMP. It is also found that the ETB is stronger in the deuterium plasmas than the hydrogen plasmas as shown in Fig. 2, where edge pressure profiles in detached phase are compared between deuterium and hydrogen plasmas. The results clearly show the importance of the edge magnetic field structure and isotope effect on the core confinement compatible with the divertor detachment for the heat load mitigation. The mechanism of the confinement mode transition is under investigation to extrapolate to a future reactor operation scenario.

[1] M. Kobayashi *et al.*, Nucl. Fusion **59**, 096009 (2019).
 [2] M. Kobayashi *et al.*, IAEA FEC 2020, EX/2.

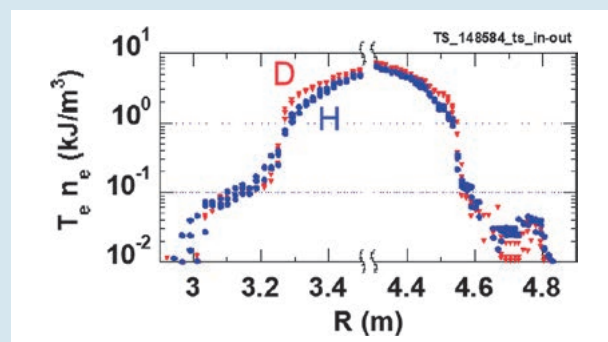


Fig. 2 Radial profile of pressure at the edge region during divertor detachment operation with RMP application. Red: deuterium, blue: hydrogen.

Impact of boron powder dropping on plasma operation

Impurity powder dropping (IPD) experiment has been conducted in the Large Helical Device (LHD) for a collaborative research between PPPL and NIFS to investigate the effects of the real-time wall conditioning on plasma and plasma-wall interactions [3–6]. Boron (B) powder was dropped from a top port (see the middle figure in Fig. 3) to high temperature plasmas with central electron temperature of several keV with a typical dropping rate of several tens of mg/s.

It has been observed that emission intensities of $H\alpha$ and low-Z impurities decreases with the B powder dropping as shown in the left figure in Fig. 3. The figure which shows time evolutions of the emission intensities with and without the B dropping in two hydrogen discharges with the same line averaged density. The figure clearly shows that the real-time wall conditioning with the B powder dropping works effectively as expected.

The figure also shows that the emission intensity of Fe XVI decreases with B powder dropping. On the other hand, it has been observed that emission intensities of low charged Fe ions do not decrease with the B powder dropping (not shown in Fig. 3). This suggests that generation of Fe impurity does not change but transport changes with the B powder dropping.

Neutral pressure measured at an outer horizontal port also decreases with the B dropping suggesting wall pumping works during the dropping. The suppression of fuel recycling has been observed not only for hydrogen isotopes but also helium. It is well known that hydrogen isotopes are absorbed by a B film on plasma facing wall. In the case of the B dropping, absorption on the formed B film and co-deposition of fueled particles and B simultaneously work. As a result, it is possible that helium recycling is also suppressed by the co-deposition.

Another interesting effect of the B powder dropping has been observed in ion and electron temperatures as shown in the right figure in Fig. 3. Line averaged densities in the two discharges shown in the figure were the

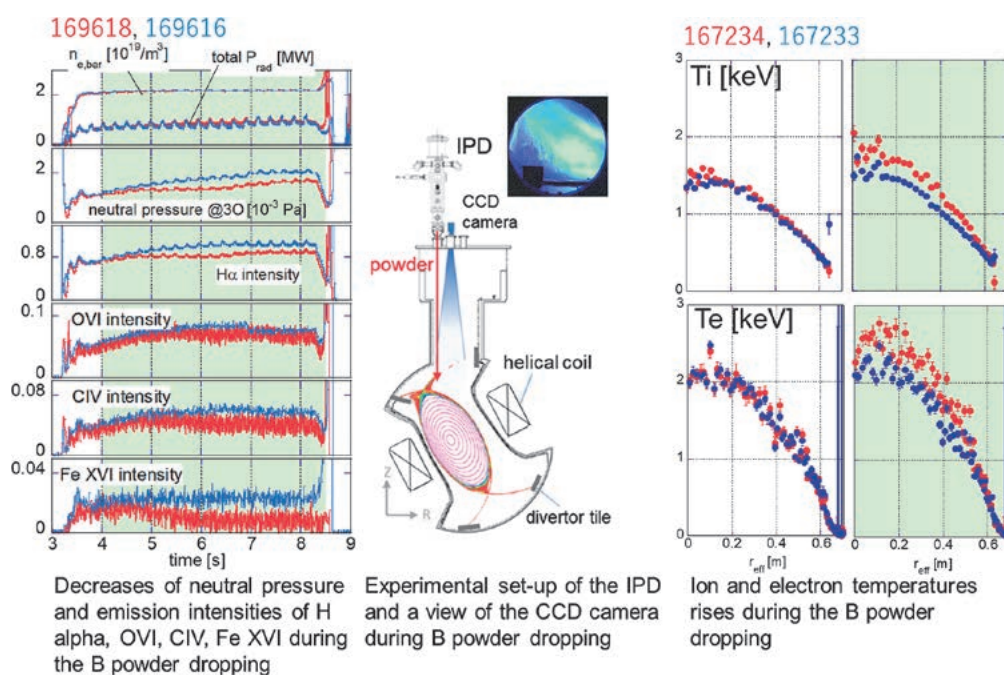


Fig. 3 Effects of the B powder dropping on plasma operation. In all graphs, red and blue show data with and without the B powder dropping, respectively, and the terms of the B powder dropping are shown by the green hatched parts.

same. By the B powder dropping, both ion and electron temperature rises. This temperature rises have been observed not only in NBI heated plasmas but also an ECH and ICH plasma. A suppression of density fluctuation has been observed during the B powder dropping by the Phase Contrast Imaging (PCI) measurement, and that suggests a reduction of turbulent transport. That can cause the temperature rises.

[3] F. Nespola *et al.*, Nucl. Mater. Energy **25**, 100842 (2020).

[4] F. Nespola *et al.*, 28th IAEA Fusion Energy Conference.

[5] M. Shoji *et al.*, Nucl. Mater. Energy **25**, 100853 (2020).

[6] T. Oishi *et al.*, Plasma Sci. Tech. **23**, 084002 (2021).

(S. Masuzaki)

Polarization spectroscopy for the study of anisotropy in the electron velocity distribution function

The polarization of the Lyman- α line has been measured with an accuracy of 1%. The analysis of the polarization angle showed that the electron motion perpendicular to the magnetic field is more dominant than that parallel to the magnetic field, which supports our intuitive understanding of the electron confinement characteristics in the plasma edge region where the Lyman- α line emission mainly takes place.

The motion of electrons in the plasma can be divided into two components: the translation velocity in the magnetic field direction and the rotation velocity in the plane perpendicular to the magnetic field direction. Electrons with a large velocity component moving in the magnetic field direction will continue to move along the magnetic field lines, while particles with a large rotational velocity component will tend to be trapped in regions with low magnetic field strength when the magnetic field strength along the magnetic field lines has a modulation.

Electrons in the plasma edge, when flung out of the confinement region due to collisions with other particles, are guided along the magnetic field lines to the vessel wall and are lost, while electrons with a large rotational velocity component tend to stay in the plasma for the reasons mentioned above. It has been therefore pointed out that the directional distribution of electron motion outside the confinement region may be anisotropic. This anisotropy in electron motion affects the ionization rate of the atoms which influences the plasma production characteristics and is also thought to be involved in the formation of the electric field that plays an important role in determining the confinement performance of the plasma.

A possible clue for understanding the anisotropy of electron motion is the light emitted by atoms or ions in the plasma [7]. When an atom collides with an electron, it receives a portion of the electron's kinetic energy and is excited to a higher energy state. Since the excited states are unstable, it returns to its original low energy state after a short period of time (typically about a nanosecond), and the energy difference between the two states is emitted as a photon or a light.

The light is a kind of electromagnetic wave. Electromagnetic waves oscillate in a direction perpendicular to their direction of motion. The azimuthal angle of oscillation is arbitrary, and most of the light we see in our daily lives is a mixture of waves oscillating at various azimuthal angles to the same degree. However, there are some

cases where the intensity of the waves differs depending on the azimuth angle. Such light is called “polarized”.

The azimuthal angle of the light oscillation coming out of an atom colliding with an electron is affected by the direction of the colliding electron’s motion as shown in Fig. 4. We are studying the magnitude of the polarization of the light emitted by hydrogen atoms to determine the anisotropy of the electron motion in the plasma [8].

In LHD and other plasmas aimed at nuclear fusion, the expected polarization degree is so small that it is necessary to detect a difference in light intensity of about 1%. Based on the hints obtained in the joint research with the Solar observation group of the National Astronomical Observatory of Japan (NAOJ) [9], and after several years of development of measurement instruments, we finally succeeded in realizing high-precision polarization measurement at the LHD and actually detected the polarization as shown in Fig. 5. It was confirmed that the polarization of the emission lines occurs between the direction of the magnetic field and the direction perpendicular to it, and initial analysis showed that electrons moving perpendicular to the magnetic field, i.e., rotating electrons, have dominant distribution characteristics [10].

[7] T. Fujimoto and A. Iwamae, Eds., *Plasma Polarization Spectroscopy*, Springer, Berlin (2008).

[8] M. Goto and N. Ramaiya, *Symmetry* **13**, 297 (2021).

[9] R. Kano *et al.*, *ApJL* **839**, L10 (2017).

[10] N. Ramaiya *et al.*, *J. Quant. Spectrosc. Radiat. Transf.* **260**, 107430 (2020).

(M. Goto)

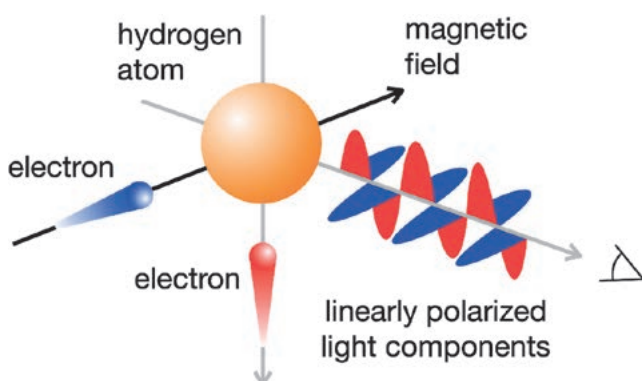


Fig. 4 Schematic diagram of the principle of polarization of light emitted by an atom in collision with an electron. Emission lines from collisions between blue and red electrons mainly correspond to the blue and red waves, respectively.

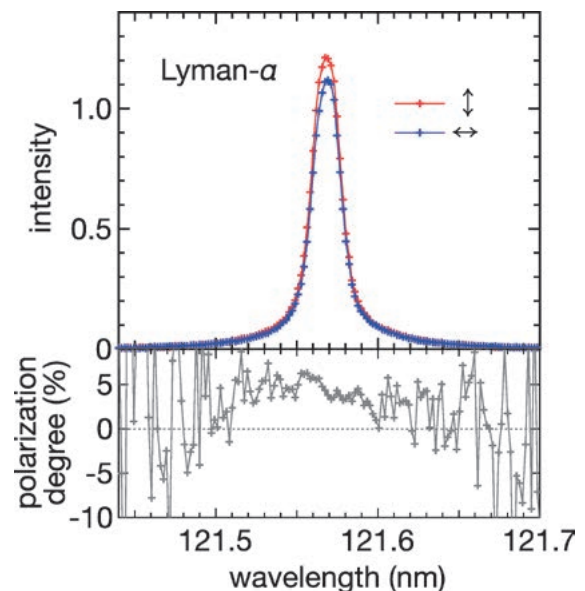


Fig. 5 An example of a polarized hydrogen atom emission spectrum observed at LHD. The upper figure shows the line profiles, with the red and blue lines showing the linearly polarized light components in the vertical and horizontal directions, respectively. The lower figure shows the difference between the red and blue lines in the upper figure divided by the sum of the two lines, which is called the polarization degree.

High-beta/MHD/Energetic Particles

Highlight

High-beta plasma production examined in Deuterium experiment

An aim of the LHD project is the realization of the reactor-relevant high-beta plasma, where the volume averaged beta, $\langle\beta\rangle$, is 5%, at $B = 1\sim 2$ T. In the hydrogen experiment before the 19th campaign, the beta value achieved 3.4% and 4.1%, which are the quasi-steady state by the gas puffing and the transient by the pellet injection, respectively. However, in the deuterium experiment, due to the power degradation of the tangential NBI, the plasma start-up in the low field was impossible. For solving that problem, in the 21st campaign, only one tangential NBI keeps the hydrogen operation for expecting the high heating power. Then the high-beta production examined comparing with the hydrogen plasma.

Figure 1 shows the dependency of the achieved beta value on the line averaged density. The circle symbol indicates the quasi-steady state discharge by the gas puffing, and the triangle symbol indicates the transient discharge by the pellet injection. The color indicates the pre-set vacuum magnetic axis. For both quasi-steady state and transient discharges, the highest beta values were achieved at $R_{ax} = 3.55$ m. For discharges of the gas puffing, it seems the degradation due to the increased density, but for the pellet injection, there is no degradation by the increased density. The fine-tuning of the density is the next step.

(Y. Suzuki)

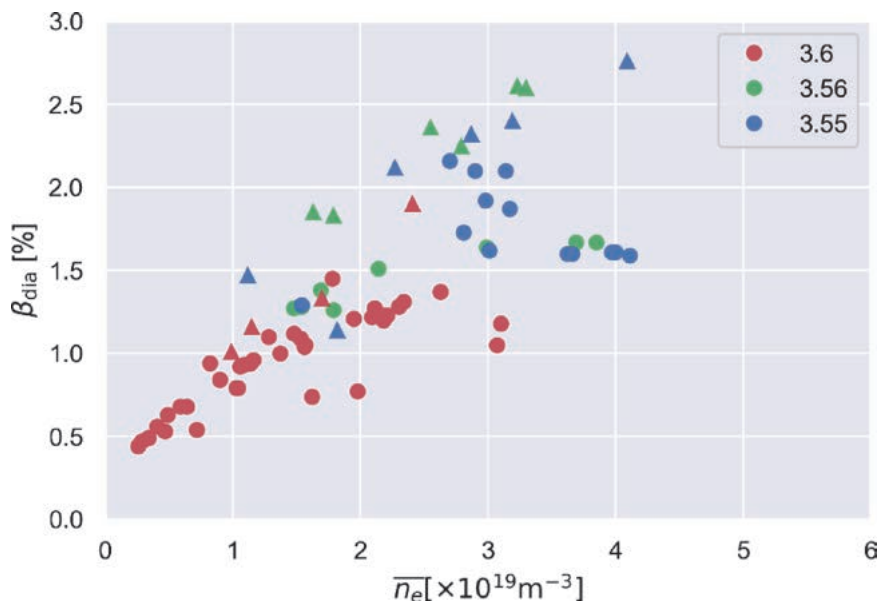


Fig. 1 the dependency of the achieved beta value on the line averaged density.

Energetic Particle Transport by Helically-trapped Energetic-ion-driven Resistive Interchange Mode in LHD

In high-ion temperature experiment performed in relatively low-density plasma with intense positive-ion-source based perpendicular neutral beam injections (P-NBI) in the Large Helical Device (LHD), the helically-trapped energetic-ion-driven resistive interchange mode (EIC) is often observed [1,2] and limits sustainment of the high-ion-temperature state [3]. To sustain the high-ion-temperature state for a longer period, a study of energetic ion transport due to EIC was performed using neutron diagnostics in LHD [4].

We used two vertical neutron cameras (VNCs) to measure the time evolution of the neutron profile. VNC1 [5] characterized by a high spatial resolution based on stilbene fast-neutron detector and VNC2 characterized by high detection efficiency based on EJ410 fast-neutron scintillator were installed under the floor concrete of the torus hall. VNC1 and VNC2 were installed in the vertical elongated poloidal cross section and the diagonal poloidal cross section, respectively. Figure 2 shows the typical density profile of helically-trapped beam ion created by P-NB injection in relatively low-density plasma calculated by MORH code [6] with sightlines of VNCs.

Figure 3 shows line-integrated neutron profiles measured by VNC1 and VNC2 before and after the EIC burst.

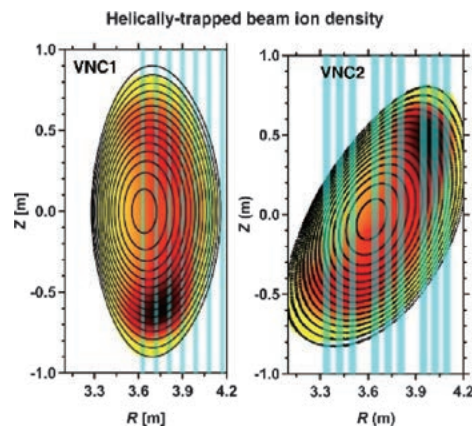


Fig. 2 Helically trapped beam ion density created by P-NB injection and sight lines of VNCs.

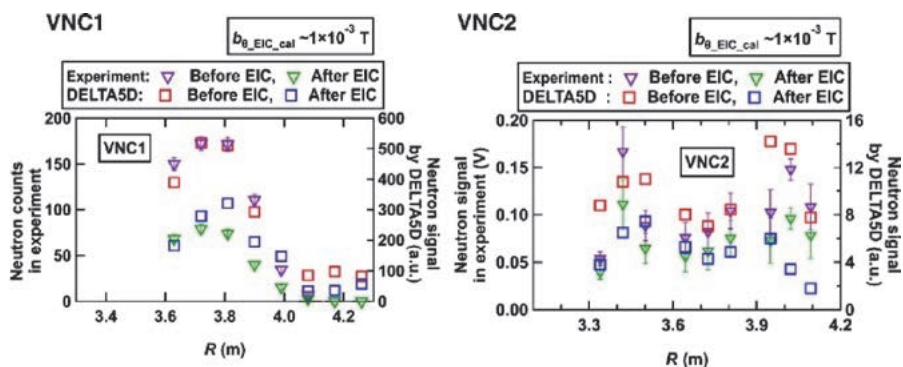


Fig. 3 Line-integrated neutron profile before and after the EIC burst.

Here, the neutron counts measured by VNC1 at a time interval of 20 ms and the averaged signals over 20 ms measured by VNC2 are plotted. These results showed that the neutron profiles were substantially changed due to the EIC burst. Guiding-center orbit-following simulations, including EIC fluctuations, were performed to understand the helically-trapped beam ion transport due to EIC. A comparison of the line-integrated neutron profile before and after the EIC burst measured in the experiment and obtained by the numerical simulation is shown in Fig. 3. The neutron profile for VNC1 shows a single peak appeared at R of approximately 3.75 m, which is nearly equal to the peak position measured in the experiment. The neutron counts for VNC1 at the central channel (R from 3.6 m to 3.9 m) becomes almost one-half after the EIC burst, as measured in the experiment. Although there are relatively wide peaks for line-integrated neutron profile for VNC2 compared with the experiment, the neutron signal shows two peaks in numerical calculation. A decrease in the neutron signal due to the EIC burst at two peaks corresponding to helical ripple valley is reproduced.

- [1] Du X. D. *et al.*, 2015 Phys. Rev. Lett. **114**, 155003.
- [2] Du X. D. *et al.*, 2015 Nucl. Fusion **56**, 016002.
- [3] Takahashi H. *et al.*, 2018 Nucl. Fusion **58**, 106028.
- [4] Isobe M. *et al.*, 2018 IEEE Trans. Plasma Sci. **46**, 2050.
- [5] Ogawa K. *et al.*, 2018 Rev. Sci. Instrum. **89**, 113509.
- [6] Seki R. *et al.*, 2015 Plasma Fusion Res. **10**, 1402077.

(K. Ogawa)

Observation of the Transported Particles Using an Upgraded Neutral Particle Analyzer during TAE Burst in the Large Helical Device

The bursting toroidal Alfvén eigenmodes (TAEs) [1] are often observed in relatively low magnetic field experiments in the Large Helical Device (LHD). In previous studies, by measuring the transported neutral particles by the TAE burst using the E-parallel-B type neutral particle analyzer (E||B-NPA) [2] and using the lost ion using scintillator-based fast-ion loss detector (FILDA), the existence of the hole-clump pairs was suggested in real space [3–5]. To measure the time evolution of the energetic particles transported by TAE bursts in more detail, the E||B-NPA was upgraded. The time duration of the observed single TAE burst is approximately 0.5 ms with the frequency chirping down. Therefore, the measurement time resolution is important for measuring the detailed structure of the transported energetic particles during the TAE burst. The measurement electronic circuits of the E||B-NPA were updated, and the time resolution was improved up to 100 kilo samples per second [6].

During the tangential neutral beam (t-NB) #1 injection in the magnetic field at the magnetic axis is 0.6 T, TAE bursts were observed by the Mirnov coils and the E||B-NPA. Figure 4 shows the (a) signal of the Mirnov coil, (b) the spectrogram of the magnetic fluctuations, and (c) the energy spectrum of the particle flux Γ observed by E||B-NPA. The TAE bursts were observed with the time intervals of approximately 10 ms. During and after the TAE bursts, the transported particles were observed by E||B-NPA. Figure 5 shows the result of the conditional averaging technique for the amplitude of the magnetic fluctuation and the changing of the observed particle flux $\Delta\Gamma$ measured by E||B-NPA with using 72 TAE bursts. The peak amplitude of the magnetic fluctuation of 70 kHz is set to 2.0 ms. By the conditional averaging technique, the structure of the transported particles is clearly con-

firmed during and after the TAE burst. The highest detected energy of the transported particles is 150 keV, which is less than the injection beam energy of 180 keV. The energy slowing down time was 1.0–1.5 ms during the TAE burst, and 6–8 ms after the TAE burst. The energy slowing down during the TAE burst is considered to be related to the TAE burst frequency chirping down, and the energy slowing down after the TAE burst can be considered as the classical energy slowing down time.

- [1] Cheng C. Z. and Chance M. S. 1986 Phys. Fluids **29**, 3695.
- [2] Medley S. S. and Roquemore A. L. 1998 Rev. Sci. Instrum. **69**, 2651.
- [3] Osakabe M. *et al.*, 2006 Nucl. Fusion **46**, S911-S917.
- [4] Ogawa K. *et al.*, 2009 J. Plasma Fusion Res. SERIES **8**, 655.
- [5] Ogawa K. *et al.*, 2010 Nucl. Fusion **50**, 084005.
- [6] Fujiwara Y. *et al.*, 2020 JINST **15**, C02021.

(S. Kamio)

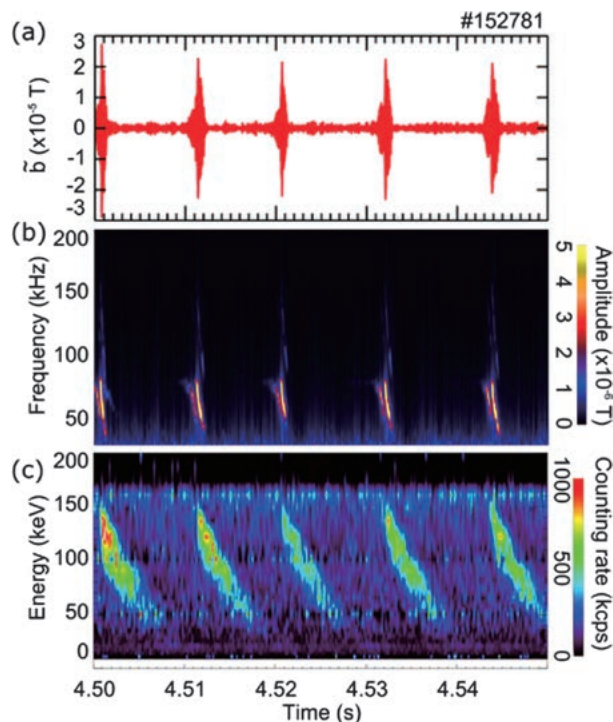


Fig. 4 Time evolutions of (a) the signal of the Mirov coil, (b) the spectrogram of the magnetic fluctuations, and (c) the energy spectrum of the particle flux Γ observed by E||B-NPA.

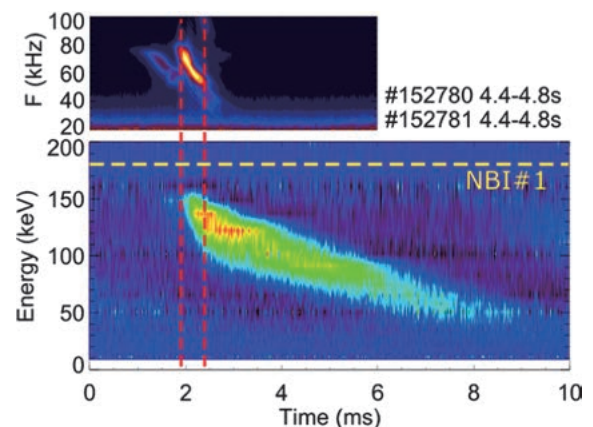


Fig. 5 The conditional averaged spectrogram of the magnetic fluctuation and the $\Delta\Gamma$ observed by E||B-NPA. Red dashed lines are the timing of the start and the end of the TAE bursts. Yellow dashed line is the injection energy of the NB #1.

Research and Development collaboration program for LHD-project

A special collaboration program, which is aimed to support the research and development activities in domestic universities for advanced diagnostics or heating scenarios, is established for future application on the LHD. One of the examples of such activity is shown in this section.

(M. Osakabe)



Figure. Inside the Large Helical Device

An RF induced transport model for the study of RF wave sustained plasmas

An RF transport model is constructed to understand the energy, momentum and particle confinement properties of lower hybrid wave sustained plasmas. Using the model, major properties of RF wave sustained TST-2 spherical tokamak plasmas are reproduced. The reproduction indicates that electrons are accelerated by the RF wave, and simultaneously transported toward a limiter and are lost.

Plasma current generation and sustainment by RF wave are important issues for spherical tokamak research. In most of the experiments so far, the obtained plasma density and the plasma current are relatively low. In such a case, RF induced transport of high energy electrons can be the dominant process determining the energy, momentum (i.e., current) and particle confinement of electrons. In the constructed model, the velocity evolution of an electron is obtained through the equation $\Delta V_{\parallel} = \widetilde{\Delta V}_{\parallel} - v_{\parallel} V_{\parallel} \Delta t - \frac{eE}{m} \Delta t$, where the terms in the RHS represent a random velocity change due to RF wave, collisional slowing down and acceleration by electric field, respectively. The orbit of an electron can be calculated from the velocity, and the electron is lost when the orbit touches one of the limiters. The electron velocity distribution function (EVDF) is obtained by following many electrons, and the plasma current, the deposited RF power, energy and particle confinement times are calculated from the EVDF. Some model parameters are adjusted to reproduce the measured plasma current, electron density and RF wave power. The model results suggest that major fraction of the deposited RF power, which generates fast electrons, is lost by the electrons hitting a limiter, while minor fraction is used to heat bulk electrons and ions. From the energy distribution of the lost electrons, we can calculate the hard X-ray generation and the energy spectrum of measured hard X-rays. Figure 1 shows the calculated and the experimental hard X-ray spectra, and qualitative agreements between the experimental and the model results are shown.

[1] A. Ejiri *et al.*, Nuclear Fusion, being submitted.

(A. Ejiri, The University of Tokyo)

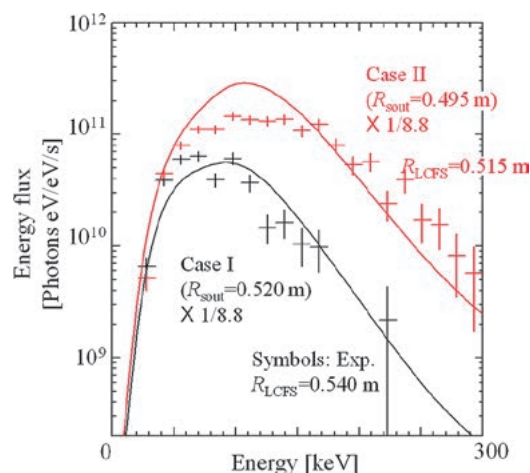


Fig. 1 Calculated (solid curve) and experimental (plus symbols) energy spectra. The calculated spectra are obtained by using the energy distribution of lost electrons in the model. They are multiplied by a factor of 1/8.8 in the plot to reproduce the experimental spectra. Two cases with different plasma sizes are shown by black and red.

2. Fusion Engineering Research Project

The Fusion Engineering Research Project (FERP) started in FY2010 at NIFS. Along with the conceptual design studies for the helical fusion reactor FFHR, the FERP has been developing technologies of key components, such as the superconducting magnet, blanket, and divertor. The research is also focused on materials used for blankets and divertors, the interaction between the plasma and the first wall including atomic processes, handling of tritium, plasma control, heating, and diagnostics. The FERP is composed of 13 tasks and 44 sub-tasks with domestic and international collaborations. Cooperation with the Large Helical Device Project, the Numerical Simulation Reactor Research Project, and the Task Force for Next Research Project have been promoted.

(T. Muroga)

Design Studies on Helical Fusion Reactor

Regarding the fusion reactor design study, the step-by-step strategy towards the helical fusion power plant FFHR-d1 has been proposed, as shown in Fig. 1. In the last fiscal year, three intermediate step devices have been considered before the construction of FFHR-d1: FFHR-c1 (experimental/prototype reactor for the demonstration of steady-state operation of the power plant system, FFHR-b2 (volumetric neutron source for the early utilization of fusion fast neutrons) and FFHR-a1 (non-nuclear system for the examination of improved magnetic configuration and advanced engineering concepts). In this fiscal year, a new design called FFHR-b3 which can operate more than 5 years with a net electric output of 100 MW at twice the size of LHD has been proposed based on the progress in physics and engineering research, such as the improvement of plasma performance by optimizing the helical coil shape and the development of compact and high-efficiency engineering components. This new design has led to the proposal of a new development strategy to demonstrate steady-state electric power generation at an early stage and to accelerate the realization of a commercial power plant.

Various innovative ideas are being proposed in the design of a helical fusion reactor. The divertor, which is directly exposed to the plasma in order to exhaust impurities in the plasma, has the problem of how to remove the ultra-intense heat from the plasma. To solve this problem, the pebble divertor concept, a method of dropping small ceramic pebbles near the plasma boundary, is being investigated (Fig. 2). Such a concept had been studied in the past, but at that time, damage of pebbles due to drop impact had become an issue. To presently address this issue, the cooperative system of a pebble divertor and a liquid metal blanket has been proposed. In this cooperative system, the liquid metal, which is circulated to cool the blanket module, is pooled at the bottom of the vacuum vessel. The pebbles drop into the liquid metal pool for alleviating the impact and for efficient use of the heat flowing into the divertor.

(T. Goto)

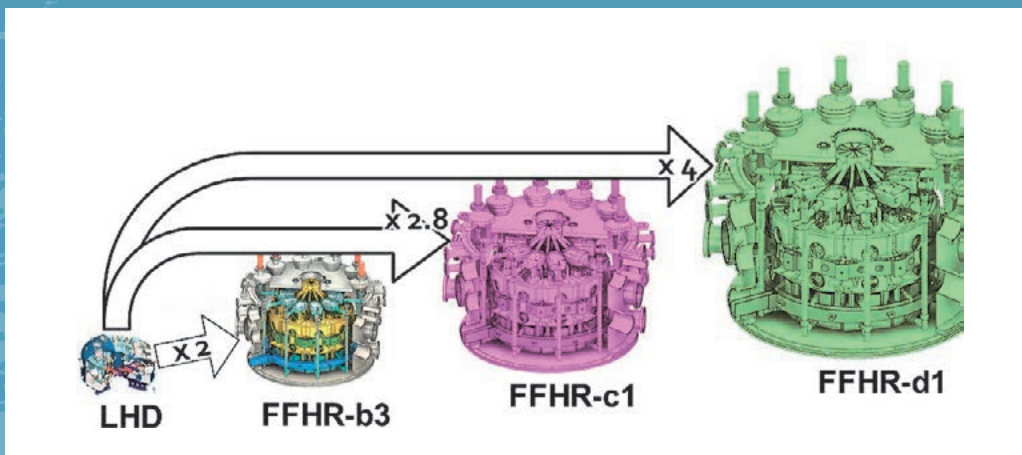


Fig. 1 Comparison of the size of helical fusion reactors. The latest design, FFHR-b3, is twice the size of the LHD and aims to generate net electricity of 100 MW.

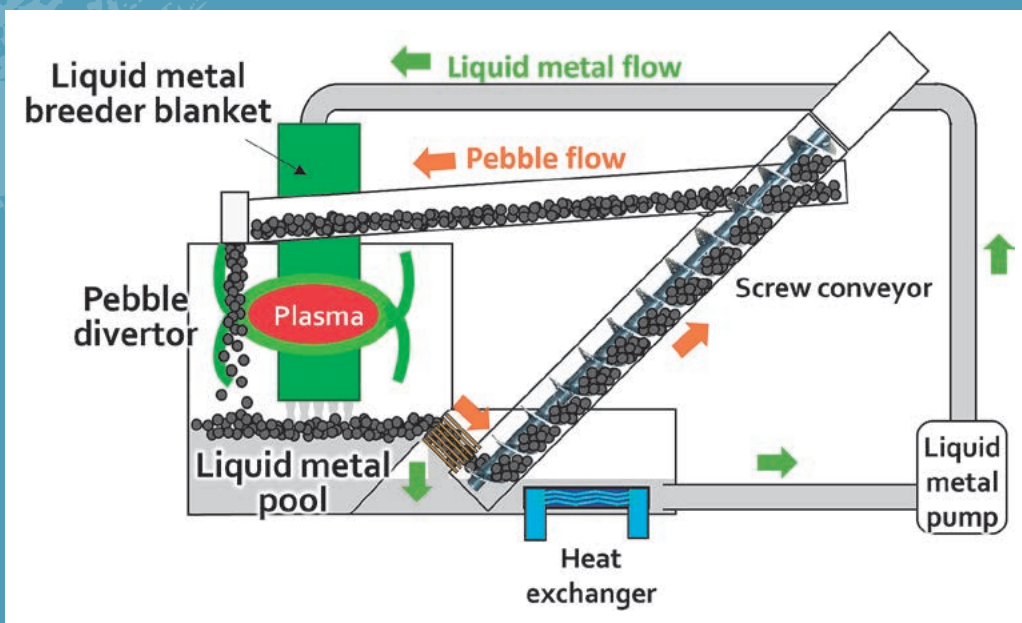


Fig. 2 Schematic view of the cooperative system of the pebble diverter and the liquid metal blanket.

Research and Development on Blanket

The FLiNaK/LiPb twin loop system Orosshi-2 (Operational Recovery Of Separated Hydrogen and Heat Inquiry-2) is operated at NIFS as a collaboration platform for integrated experiments on the liquid blanket technologies. In FY2019, two new testing sections have been installed in Orosshi-2: (i) a test chamber for demonstration of continuous and high efficiency hydrogen isotope recovery from LiPb by the vacuum sieve tray (VST) technique (Fig. 3 (a)) and (ii) a test section for evaluation of heat removal performance of a FLiNaK flow under an intense magnetic field (Fig. 3 (b)). In FY2020, experiments using these sections have been delayed significantly due to the severe influence of the COVID-19 pandemic, but preparation works have continued despite this situation. Regarding the test section of the VST technique, it was confirmed that dissolution of deuterium gas into a circulated LiPb flow and measurement of the deuterium concentration in the flow were performed steadily. The VST test section is ready for the demonstration of hydrogen isotope recovery. The temperature control of the FLiNaK heat removal test section was checked, and it is also ready for starting the experiments in FY2021.

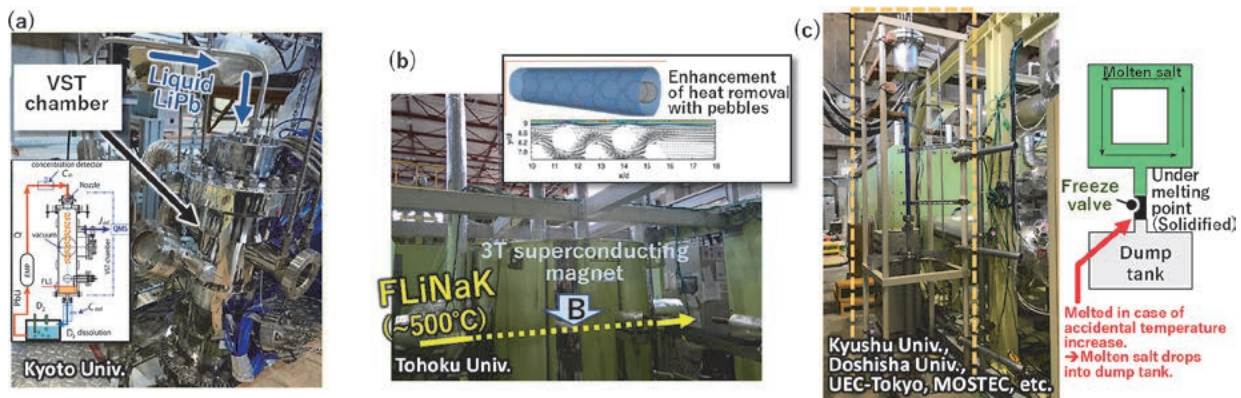


Fig. 3 Photos of test sections installed in Orosshi-2. (a) LiPb vacuum sieve tray (VST) chamber, (b) FLiNaK heat removal test section penetrating the 3-Tesla superconducting magnet, and (c) FLiNaK freeze valve test section.

(T. Tanaka and Y. Hamaji)

Development of advanced structural materials for fusion reactor blanket

Low-activation vanadium (V) alloys are promising candidate structural materials for the first wall/blanket applications in advanced fusion reactor systems. One of the recent studies on the V-Cr-Ti system alloys is to further reduce the radioactive characteristic after use in fusion reactors. Effects of titanium (Ti) and chromium (Cr) concentrations on microstructure and tensile properties of high purity vanadium alloys, which contains less than 300 mass ppm interstitial impurities (e.g., carbon, nitrogen, oxygen), have been investigated. It has been found that Ti can be reduced from 4wt% to 1wt% for scavenger and precipitation. On the other hand, Ti reduction results in the strength degradation of V-Cr-Ti system alloy for both room temperature and high temperatures. Furthermore, it reveals that tensile strength gradually increases with increasing Cr concentration, indicating that a higher level of Cr can compensate for strength degradation by lowering Ti concentration. Comparing with the yield stress of V-4Cr-4Ti alloy, low-Ti and high-Cr candidates are V-6Cr-3Ti, V-8Cr-3Ti, V-10Cr-1Ti, V-12Cr-0.5Ti, and V-12Cr-1Ti alloys. The Ti and Cr concentrations will be further optimized according to irradiation damage resistance and ductile-to-brittle transition temperature investigations in the future.

(J. Shen)

Highlight

Corrosion of fusion structural materials in a molten salt with a hydrogen fluoride solution

NIFS has collaborated with universities and institutions worldwide to study lithium-containing molten salt as a candidate coolant for the fusion reactor blanket. These salts are well-known to be chemically stable and less affected by magnetic field. Hence, molten salts can be used for self-cooled liquid breeders. However, one of the difficulties with these salts is corrosion. Although these salts themselves hardly corrode with structural materials, the corrosive oxidants, such as water, hydrogen fluoride, and isotopes of these, are easily mixed or produced, corrode with structural materials. Nevertheless, the unknown was the quantitative relationship between the concentration of these corrosive oxidants and the corrosion mechanisms of the structural materials. Therefore, in this study, the effect of hydrogen fluoride (HF) in the molten fluoride salt (LiF-NaF-KF; FLiNaK in short) on the corrosion mechanism of the reduced-activation ferritic steel (JLF-1 steel) is investigated.

Fig. 4 (a) shows the apparatus developed and used to measure the corrosion in the salt under the controlled HF concentration similar to the blanket condition. A long-time weight-change measurement and a short-time electrochemical measurement determine the corrosion rate, reaction, and form. Fig. 4 (b) shows the current-potential relationship of JLF-1 steel and pure iron in FLiNaK at 773 K. It is easily seen that the current density of pure iron, which is equivalent to the corrosion rate, increases with the increase in the HF concentration in FLiNaK. Furthermore, the HF concentration is proportional to the cathodic limited current density, which means that the rate-determining step of the corrosion is the HF diffusion occurring at the liquid-solid boundary. These tendencies are also matched for JLF-1 steel. In addition, surface and cross-sectional observations have gradually exhibited that HF prefers to attack the specific microstructure (lath boundary).

NIFS possesses the large circulation loop of a molten salt equipped with a 3-Tesla superconducting magnet (the “Oroshhi-2 loop”). Therefore, corrosion tests under flowing and magnetic field conditions are prospective.

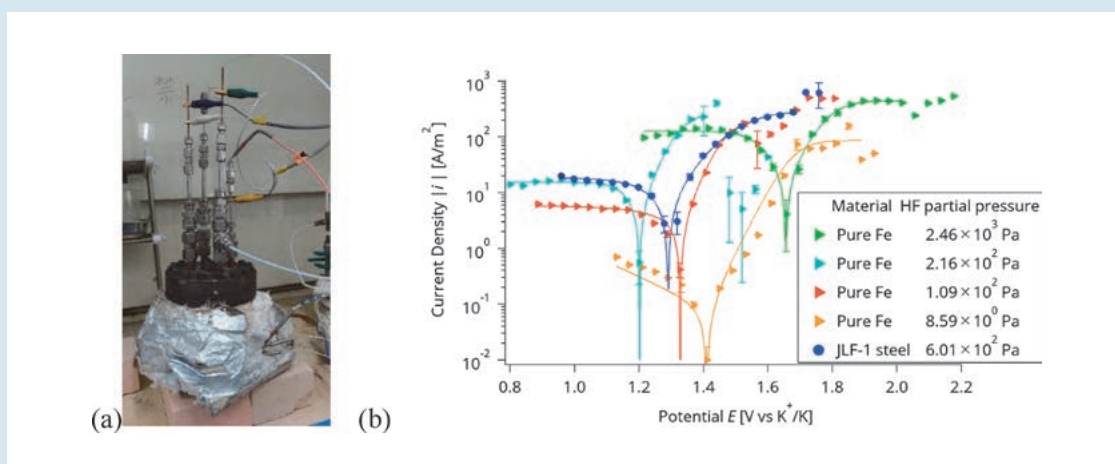


Fig. 4 (a) Apparatus for the corrosion tests. (b) Current-potential relationship of JLF-1 steel and pure iron in the molten salt (FLiNaK), depending on the HF concentration. Points are experimental results whereas lines are the fit results.

(G. Yamazaki and T. Nagasaka)

Research and Development on Divertor

Superior fabrication technique of the Advanced Multi-Step Brazing (AMSB) for fabricating the plasma facing component has been developed. The AMSB is based on the repetitive application of the Advanced Brazing Technique (ABT), in which the ABT was originally developed for joining tungsten (W) and oxide dispersion strengthened copper alloy (ODS-Cu; GlidCop®) in our previous work. The AMSB has large advantages for fabricating the high heat flux component with rectangular-shaped cooling flow path channel and V-shaped staggered rib structure because pre-processed cooling flow path channel can be tightly sealed via AMSB process with leak-tight condition. The new AMSB-type divertor heat removal component with rectangular-shaped cooling flow path channel and V-shaped staggered rib structure was developed, in which a pre-processed cooling flow path of the GlidCop® heat sink was sealed with stainless steel lid structure and then, W armor tiles were jointed on the GlidCop® heat sink. The component showed excellent heat removal capability under reactor-relevant conditions with a heat flux of $\sim 30 \text{ MW/m}^2$. The AMSB type divertor component was inserted into the divertor strike point of the Large Helical Device (LHD) in the FY2020 plasma campaign, and has demonstrated the excellent heat removal capability and structural reliability by being exposed 1,180 plasma shots.

The AMSB is expected to be developed not only for a divertor heat removal component but also for a first-wall component with a W armor. For developing the first-wall component, very thin W armor (W sheet) should be jointed on the base metal such as stainless steel (SS) or ferritic/martensitic steel. The prototype first-wall component with W sheet armor and SS substrate was developed using the AMSB process. In this fabrication procedure, intermediate material of GlidCop® was inserted between the W sheet and SS. Fig. 5 shows a schematic drawing of the AMSB joining scheme and photograph of the fabricated AMSB first-wall component. The interface between GlidCop® and SS (GlidCop®/SS) and W and GlidCop® (W/GlidCop®) were jointed by the ABT with BNi-6 filler material. The very high joint area ratio was confirmed even in the 40 mm \times 40 mm area by the ultra-sonic testing (UT). The AMSB technique is expected to be applied not only to the fusion engineering but also to other industrial fields.

Using a combined process of Mechanical Alloying (MA) and Hot Isostatic Pressing (HIP), new dispersion strengthened tungsten (DS-W) alloys containing TiO_2 particles on grain boundaries is being studied for the improvement of Plasma Facing Materials (PFM) on divertor components. The initial materials were mixed and mechanically alloyed in a planetary-type ball mill using tungsten carbide MA balls and pot. The mechanically alloyed powders were compressed by cold isostatic pressing (CIP) and then pre-sintered in hydrogen gas

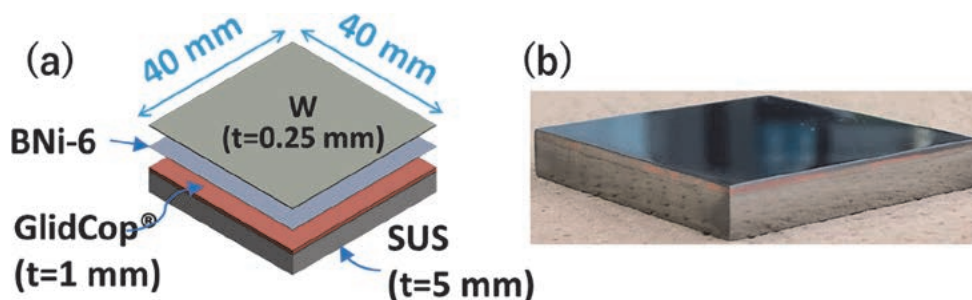


Fig. 5 (a) Fabrication scheme of the W/GlidCop®/SS first-wall component using the AMSB process. (b) Photograph of the prototype W/GlidCop®/SS first-wall component by AMSB.

atmosphere at high temperature (preliminary sintering). The pre-sintered W alloys were then sintered by HIP at 1750°C for 1.5 hours with a pressure of 186 MPa. For comparison, a pure tungsten supplied by the A.L.M.T. Corp. (hereafter named ITER-Pure W), was prepared. The HIPed DS-W and ITER-Pure W were annealed at 1600–1800°C for 1.5 hours in vacuum. The annealed tungsten materials were characterized by the four-point bending tests and the microstructure analysis. Fig. 6(a) shows EBSD (Electron Back-Scatter Diffraction) map images before and after annealing. The ITER-Pure W and the DS-W before annealing exhibited textures of fine grains by rolling and the equiaxed-fine grains of non-texture by HIP treatment, respectively. Grains of ITER-Pure W after annealing at 1600 and 1800°C coarsened drastically, indicating completion of the secondary recrystal-

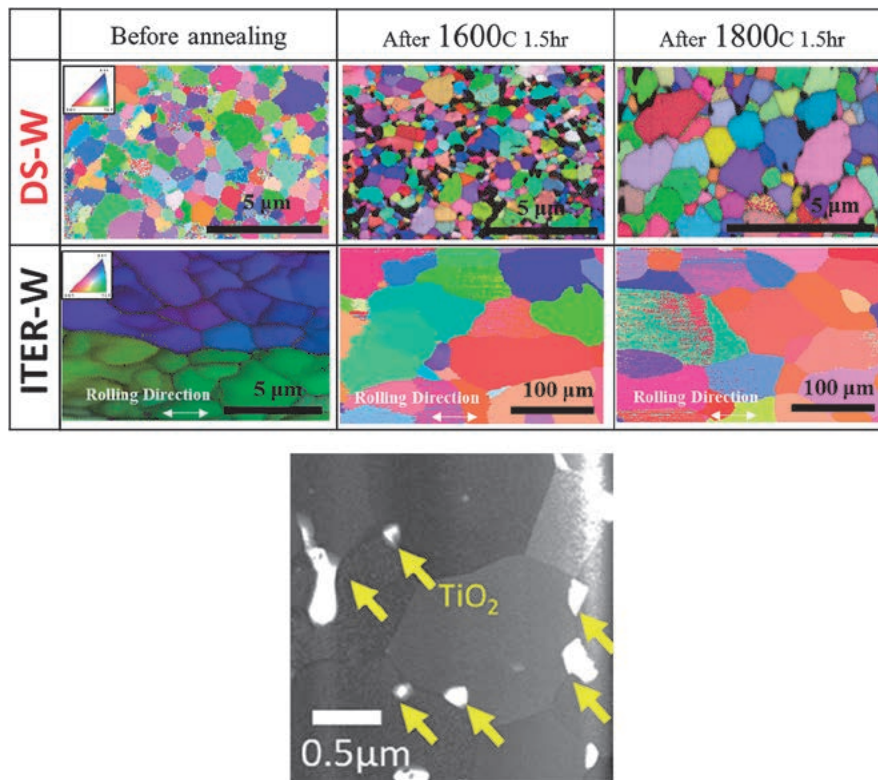


Fig. 6 (a) EBSD map images of the ITER-Pure W and DS-Ws before and after annealing. (b) Transmission Electron Microscope (TEM) image of nano-titanium oxide at grain boundaries after annealing at 1800°C.

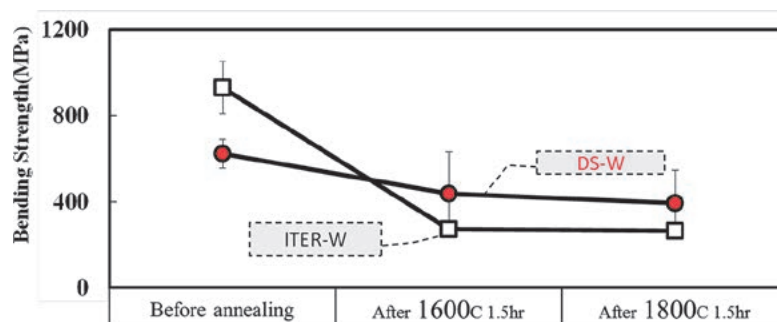


Fig. 7 Bending strength of the ITER-Pure W and DS-Ws before and after annealing.

lization. On the other hand, grains of DS-W after annealing at 1600 and 1800°C showed limited coarsening. As seen in Fig. 6(b), TiO₂ particles in DS-W were finely dispersed after annealing. The present result suggested that the dispersed particles of TiO₂ is stable up to 1800°C, maintaining the pinning effect on grain boundaries. Fig. 7 shows the fracture strength derived by four-point bending tests before and after annealing. Fracture strength of ITER-Pure W decreased drastically with grain coarsening after annealing. On the other hand, the fracture strength of DS-W after annealing decreased slightly, but was still higher than that of ITER-PURE W. This was attributed to the effect of fine dispersion of TiO₂ in DS-W.

We have been acquiring highly-charged tungsten (W) ion spectroscopy data for spectral identification of fusion plasmas using the electron beam ion trap, “CoBIT” (Fig. 8(a)). In FY2019, for the first time in the world, we successfully observed a very strong forbidden transition line called “electric octupole transition (E3)” of “W²⁷⁺4f-5s”. In FY2020, the atomic number dependence of this E3 transition was successfully measured in Re (rhenium), Os (osmium), and Ir (iridium) ions (Fig. 8(b)).

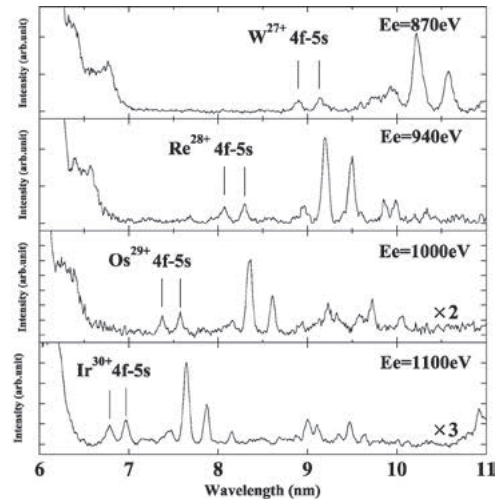
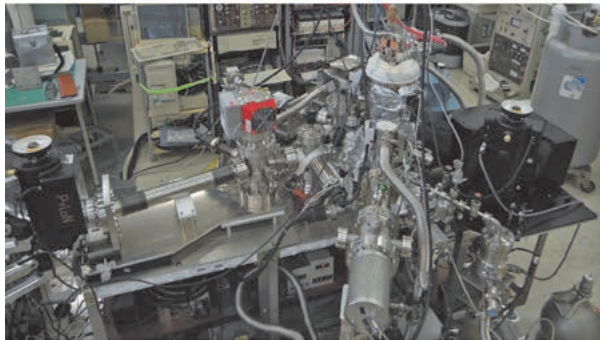


Fig. 8 (a) Photo of the electron beam ion trap “CoBIT” with installed spectrometers, (b) the E3 transition lines spectra of the highly-charged W, Re, Os, and Ir ions.

(M. Tokitani, H. Noto and H. Sakaue)

Research and Development on the Superconducting Magnet

In the recent designs of the helical fusion reactor series FFHR, the High-Temperature Superconducting (HTS) magnet is considered and a 100-kA-class HTS conductor has been developed. It is noted that large-current capacity HTS conductors are being developed also in the world to be applied to a variety of designs of fusion reactors. As a prior phase to fusion reactors, it is now being explored to apply HTS magnets to the next-generation helical experimental device. For this purpose, a relatively smaller conductor is required, and presently, the target is found at 6–18 kA current in the magnetic field of ~10 Tesla at temperature of 20 K. Three types of HTS conductors with different internal structures are being developed with all using REBCO tapes, as shown in Fig. 10. For these

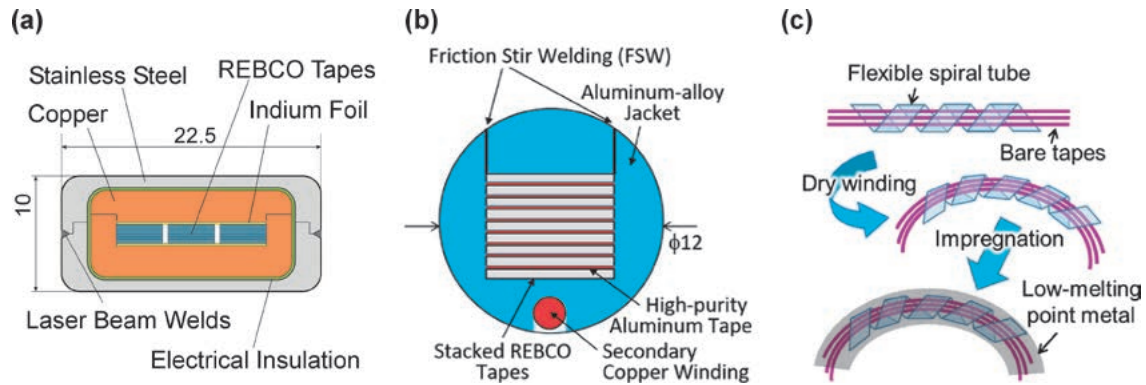


Fig. 10 Schematic drawings of the three types of large-current HTS conductors being developed to apply to the next-generation helical device: (a) STARS, (b) FAIR, and (c) WISE conductor.



Fig. 11 Experimental setup of the STARS conductor sample to be installed into the NIFS superconductor testing facility.

conductor types, 1–3 m-long samples have been fabricated and tested in liquid nitrogen (77 K) with no external magnetic field, and the fabrication method has been improved. Then, the conductors are being tested in high magnetic field (<8.5 Tesla) and low temperature (20–50 K) using the large-superconductor testing facility by installing 2-m-long conductor samples, such as shown in Fig. 11.

Development of mechanically reinforced Nb_3Sn multifilamentary wires has progressed for the Low-Temperature Superconducting (LTS) magnet option, as an extension of the ITER technology. We employed an internally reinforced matrix method using ternary bronze alloys (Cu-Sn-X), where X is a solute element such as Zn or In, as shown in Fig. 12(a). After the formation of the superconducting region of Nb_3Sn , the ternary alloy “hishimatrix” is transformed to a Cu-based solid solution such as (Cu, Zn) or (Cu, In), which contributes to the improvement of mechanical strength of the whole wire. When a Cu-Sn-In ternary alloy is used as the matrix material, the critical current (I_c) degradation under the compressive stress is restricted compared with the conventional bronze processed and CuNb-reinforced Nb_3Sn wire, as shown in Fig. 12(b).

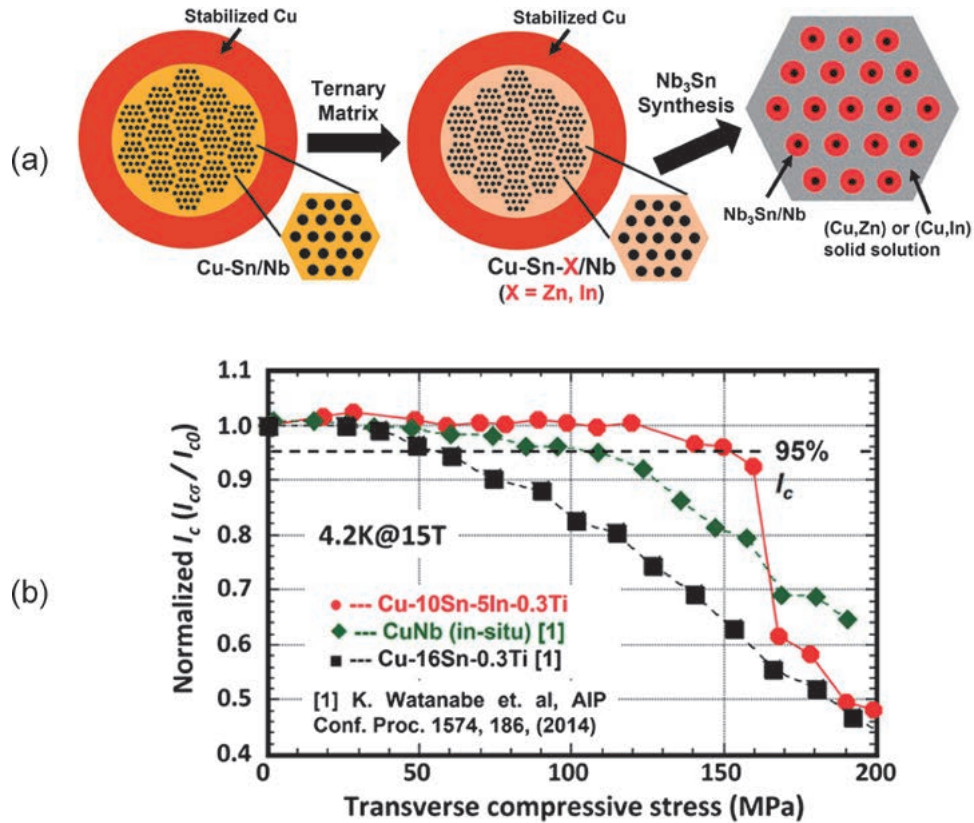


Fig. 12 Typical cross-sectional image of the internally reinforced Nb₃Sn multifilamentary wire using several ternary alloy matrices. (b) The comparison of I_c degradation under the compressive stress between several Nb₃Sn wires.

(N. Yanagi and Y. Hishinuma)

LHD-Project Research Collaboration

The LHD Project Research Collaboration program has been contributing to enhancing both the scientific and technological foundations for the research related to the LHD project as well as to the future helical fusion reactors. The feature of this collaboration program is that each research is performed at universities and/or institutions outside NIFS. For the fusion engineering, the following ten subjects were conducted in FY2020:

1. Engineering study on lithium isotope enrichment by ion exchange
2. Tritium behavior in a secondary cooling system in a fusion DEMO reactor
3. Field estimation for improvement of environmental tritium behavior model
4. Development of highly ductile tungsten composite systems
5. Fundamental engineering of tritium recovery process for liquid blanket of helical reactor
6. Development of new rapid-heating and quench processed Nb₃Al large-scaled cables for the helical winding due to the react and winding method
7. Evaluation of heat-transfer-enhanced channel under high magnetic field for liquid molten salt blanket development
8. Evaluation of multi hydrogen isotope transfer behavior on plasma driven permeation for plasma facing

materials

9. Studies on liquid hydrogen cooled HTC superconducting magnet
10. The analysis of biological effects elicited by organically bound tritium using life science techniques
11. Technological development of FeCrAl-ODS alloys coexisting with liquid metal cooling system of helical fusion reactor

From the above ten collaborative research items, the research 4 is briefly described below:

4. Development of highly ductile tungsten composite systems

A highly-deformed tungsten (W) foil shows excellent low-temperature ductility, even at room temperature. A pure W foil laminated composite (PWF-L) has been proposed for applying to the plasma-facing material of divertors. This is a composite material consisting of stacked pure W foils, and degradation of low-temperature ductility due to recrystallization is a concern for PWF-L. Potassium (K) doping is known as a method to suppress recrystallization, in addition to improving the low-temperature ductility. Therefore, a K-doped W foil laminated composite (KWF-L) was developed in the present study, which has a possibility to show improved mechanical properties. In FY2020, development of a fracture map to predict fracture behavior of KWF-L with various structures has been done by performing heat load tests of divertor target mockup in the ACT-2 (a 300 kW electron beam facility) at NIFS to clarify the performance of KWF-L in the actual fusion reactor environments. As shown in Fig. 13, heat conduction ability of the mockup was kept up to 20 MW/m^2 of steady-state heat load.

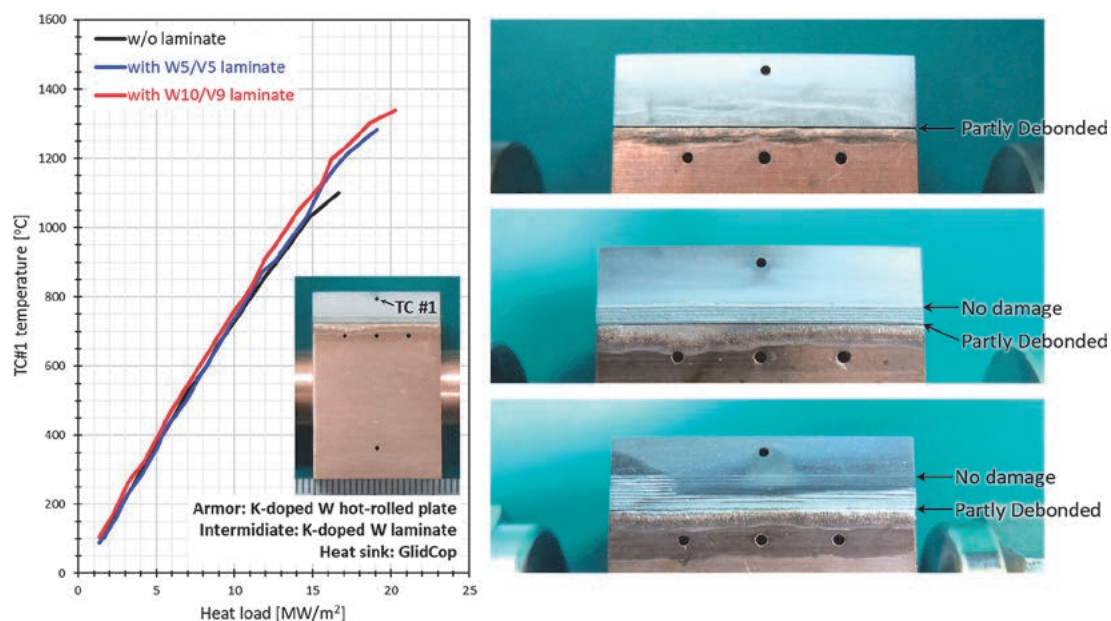


Fig. 13 Near-surface temperature during heat load tests of divertor target mockups using KWF-L (left) and their appearances after heat load tests (right).

(T. Nagasaka and S. Nogami (Tohoku University))

3. Numerical Simulation Reactor Research Project

Fusion plasmas are complex systems which involve a variety of physical processes interacting with each other across wide ranges of spatiotemporal scales. In the National Institute for Fusion Science (NIFS), we are utilizing the full capability of the supercomputer system, Plasma Simulator, and propelling domestic and international collaborations in order to conduct the Numerical Simulation Reactor Research Project (NSRP). Missions of the NSRP are i) to systematize understandings of physical mechanisms in fusion plasmas for making fusion science a well-established discipline and ii) to construct the Numerical Helical Test Reactor, which is an integrated system of simulation codes to predict behaviors of fusion plasmas over the whole machine range.

The Plasma Simulator was replaced to a new model (Fig. 1) in July 2020. It consists of 540 computers, each of which is equipped with 8 “Vector Engine” processors. The 540 computers are connected with each other by a high-speed interconnect network. The computational performance is 10.5 petaflops. The capacities of the main memory and the external storage system are 202 terabytes and 32.1 petabytes, respectively. The nickname of the Plasma Simulator is “Raijin (雷神)” which means a god of thunder.

Presented below in Figs. 2 and 3 are examples of successful results from collaborative simulation researches in 2020–2021 on the collisional merging process of field-reversed configuration (FRC) plasmas and on plasma shaping effects on ion temperature gradient (ITG) instability, respectively. Also, highlighted in the following pages are achievements of the NSRP on plasma fluid equilibrium and stability, energetic-particle physics, neoclassical and turbulent transport, plasma-wall interaction, and integrated transport simulation.

(H. Sugama)



Fig. 1 The Plasma Simulator, “Raijin (雷神)”

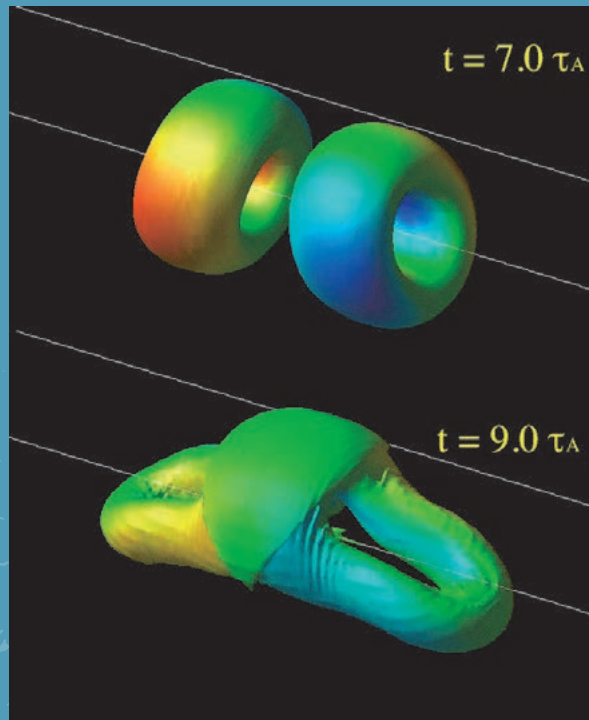


Fig. 2 Simulation results of the collisional merging process of field-reversed configuration (FRC) plasmas [presented by Dr. N. Mizuguchi (NIFS) collaborating with Nihon University]. The toroidal field strength on the isobaric surface is represented by color.

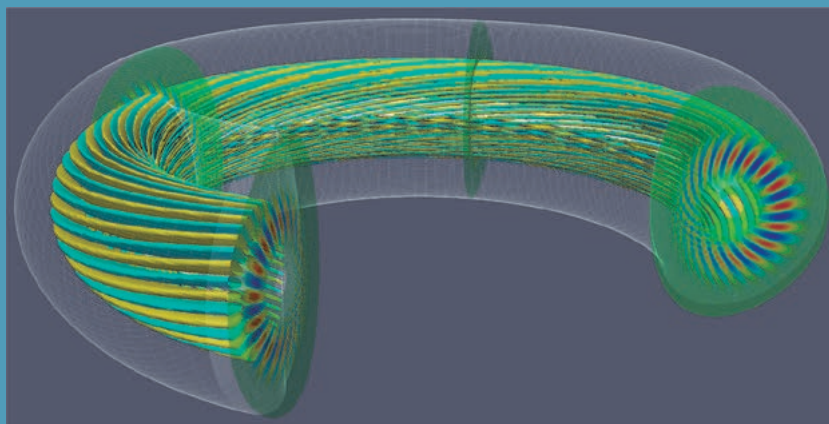


Fig. 3 Structure of the three-dimensional eigenfunction of the toroidal ITG mode obtained by the global gyrokinetic code (GKNET) for the non-circular tokamak configuration with the elongation $\kappa_0 = 1.5$ and the triangularity is $\delta_0 = 0.3$ [presented by Dr. K. Imadera (Kyoto University)]. Reference: K. Imadera *et al.*, Plasma Fusion Res. **15**, 1403086 (2020).

Progress of optimization scheme for magnetic field configuration

Highlight

A novel numerical optimization code of external-current system opens new window of stellarator/heliotron reactor concept

Stellarator/heliotron devices can confine hot plasma without driving net toroidal plasma current, owing to the twisted magnetic field generated by the external coil currents. Optimization of the magnetic configuration is one of the important issues in fusion plasma research based on the stellarator/heliotron concept because the magnetic configuration largely affects confinement of particle orbit, magnetohydrodynamic stability, micro-instability, edge plasma, etc. Conventional optimization of heliotron device is done by adjusting a small number of parameters describing a helical coil and comparing predicted plasma performances and engineering feasibility. For stellarator devices using modular coils, magnetic equilibrium is numerically optimized and external coils are designed to reproduce the optimized magnetic configuration.

A novel numerical optimization suite consisting of multiple numerical codes, OPTHECS, that can directly optimize the vacuum magnetic field/free-boundary equilibrium through modifying the shape and current of the external coils, has been developed. The developed code can not only treat the conventional parametric expression of helical coils but also cubic B-spline curve expression both of helical and modular coils, opening a new window of designing of stellarator/heliotron device. Using OPTHECS, it has been investigated if the magnetic configurations of advanced stellarators with robust divertor legs can be produced with helical coils. Fig. 1 shows a quasi-helically symmetric configuration obtained using OPTHECS. This configuration is realized using three helical coils and a pair of poloidal field coils. It has been found from the analysis of the field-line connection-length outside of the last-closed flux surface that the divertor legs exist in this configuration. The generation of divertor legs in other types of magnetic configurations with helical coils, including quasi-axisymmetric configuration and quasi-omnigeneous configuration, has also been found. Application of OPTHECS to the improvement of the engineering design of heliotron-based fusion reactors has also started, taking advantage of the coil-based optimization scheme of the suite. Fig. 1 (c) shows the initial results of improved divertor clearance of a heliotron configuration obtained with helical coil expressed with a B-spline curve.

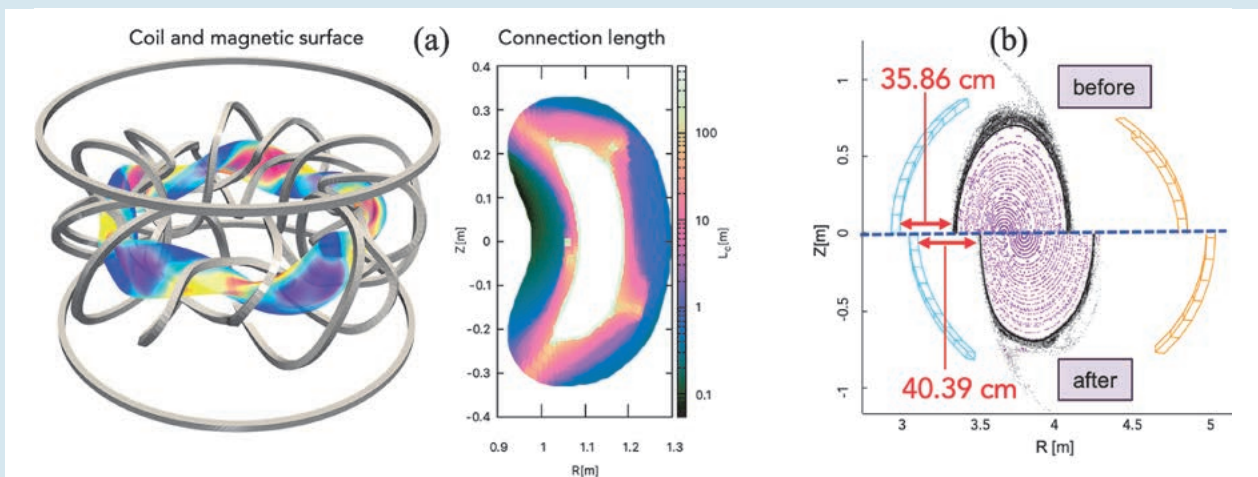


Fig. 1 (a) A quasi-helically symmetric configuration with helical coils obtained by OPTHECS. (b) Optimization of a heliotron configuration aiming at improved divertor clearance.

(H. Yamaguchi)

Transition from interchange mode to non-resonant mode in LHD collapse phenomena

In the MHD simulation of the LHD plasma collapse, a transition from $(m, n) = (3, 3)$ interchange mode to $(1, 1)$ non-resonant mode is obtained, where m and n are the poloidal and toroidal mode numbers, respectively [1]. In the LHD experiment with the net toroidal current that flows so as to increase the rotational transform, collapses are caused by the $(1, 1)$ mode [2]. Thus, we examined the dynamics of the LHD plasma for the case with the net toroidal current. In the case that the rotational transform has the low shear profile in the core region and the value close to unity in the region, a transition occurs in the nonlinear evolution of the dynamics. In the end of the linear phase, the $(3, 3)$ mode is destabilized first as shown in Fig. 1(a). This mode is localized around the resonant surface and shows a typical interchange mode. Then, the dominant mode changes to the $(2, 2)$ component in the nonlinear evolution as shown in Fig. 1(b). Furthermore, the $(1, 1)$ component becomes dominant in the further nonlinear phase as shown in Fig. 1(c). Thus, the mode number of the dominant component decreases as in the case of the inverse cascade. Since the collapses are caused by the $(1, 1)$ mode in the experimental observation, this transition is considered as one of the candidates to explain the observed mode number.

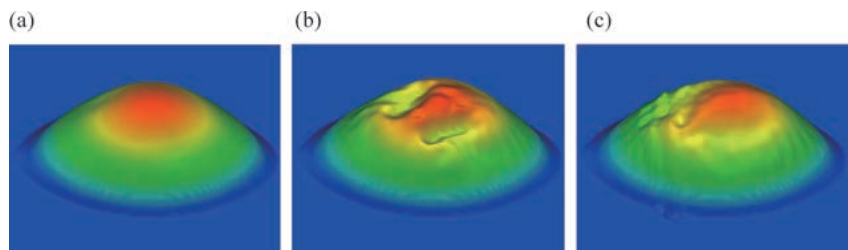


Fig. 1 Bird's eye view of the total pressure profile, (a) in the end of the linear phase, (b) in the early nonlinear phase and (c) in the further nonlinear phase.

[1] K. Ichiguchi *et al.*, submitted to Nucl. Fusion (2021).

[2] S. Sakakibara *et al.*, Nucl. Fusion, **55** 083020 (2015).

(K. Ichiguchi)

3D equilibrium study for a low shear stellarator with localized toroidal current density

Three-dimensional nonlinear MHD simulations study the core collapse events observed in a stellarator experiment. In the low magnetic shear configuration like the Wendelstein 7-X, the rotational transform profile is very sensitive to the toroidal current density. The 3D equilibrium with localized toroidal current density such as the ECCD (Electron Cyclotron Current Drive) is studied. If the toroidal current density follows locally in the middle of the minor radius, the rotational transform is also changed locally. For cases of 15 kA and 20 kA, the iota achieved to the unity, and then the topological change, where the magnetic island opens, is appeared.

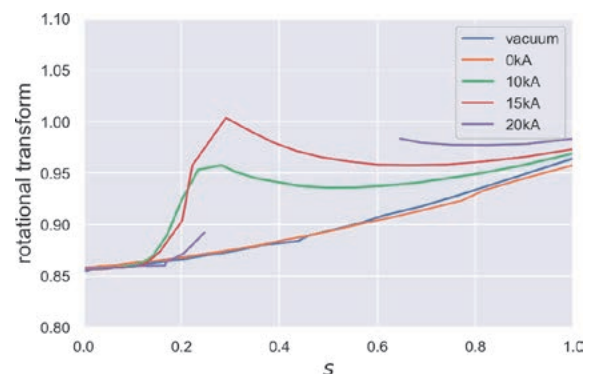


Fig. 2 Rotational transform profiles of the 3D equilibrium analyses for the sequence of the net toroidal current scan.

(Y. Suzuki)

Energetic-particle driven instabilities and energetic-particle transport in helical plasmas

Highlight

Precession drift reversal and rapid transport of trapped energetic particles due to an energetic-particle driven instability in the Large Helical Device

The effect of energetic deuterium ions with a distribution function consistent with a perpendicular neutral beam injection (NBI) was numerically investigated in a Large Helical Device (LHD) plasma reconstructed from a high-performance shot [1].

A fast growing $m/n = 2/1$ mode where m and n are poloidal and toroidal mode numbers, respectively is observed with its profile centered at the $r = 0.5$ radius. At the end of the linearly-growing phase, the mode saturates and its frequency chirps very rapidly and changes the sign. Fig. 1(a) shows the evolution of the mode amplitude and frequency, and the rapid frequency chirping can be seen in orange. This mode is important because it causes a rapid energetic particle perpendicular pressure redistribution, as can be seen in Fig. 1(b), where the pressure profile is shown for different times. It should be noted that the radial gradient of the energetic particle pressure profile even becomes positive for a short time after the saturation. An analysis of the energetic particle behavior shows that, at the start of the frequency chirping, a large portion of helically trapped energetic particles have their precession direction reverse. As shown in Fig. 1(c), the typical particle affected by this phenomenon reverses its precession drift direction, and at the same time is expelled from the plasma center, before going back to an equilibrium trajectory with the classical precession direction at a higher radius. The precession drift reversal is attributed to the poloidal ExB drift strong enough to counter the grad-B drift responsible for the precession drift motion, and at the same time a smaller radial ExB drift that pushes the particles from the center. This phenomenon is responsible for the energetic particle redistribution.

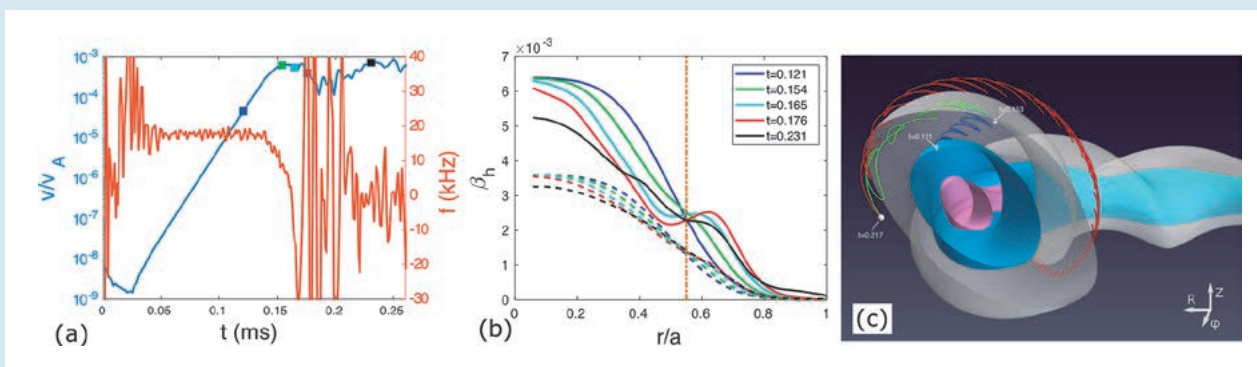


Fig. 1 (a) Time evolution of the radial plasma velocity amplitude of the mode shown in blue and the frequency in orange. The colored squares correspond to the different pressure profile times shown in Fig. 1(b). (b) Energetic particle pressure profiles for different times in the evolution. Solid (dashed) lines represent the perpendicular (parallel) energetic particle pressure profiles. (c) Trajectory of a typical energetic particle experiencing precession drift reversal. The blue line represents the trajectory at the end of the linear phase, the green curve during the drift reversal, and the red curve the return to an equilibrium trajectory at a higher radius.

[1] M. Idouakass *et al.*, "Numerical Observation of an $m/n = 2/1$ Mode with Strong Energetic Particle Redistribution in LHD", in the 29th International Toki Conference on Plasma and Fusion Research (2020).

Magnetohydrodynamic hybrid simulation of Alfvén eigenmodes in Heliotron J

Energetic-particle (EP)-driven MHD instabilities in Heliotron J, a low shear helical axis heliotron, were numerically investigated with MEGA, a hybrid MHD-EP simulation code [2]. The global Alfvén eigenmode (GAE) with poloidal/toroidal mode numbers $m/n = 4/2$ observed around $r/a = 0.5$ in the experiment was successfully reproduced; however, the energetic particle mode (EPM) with $m/n = 2/1$ at $r/a > 0.7$ was not reproduced. Instead, an $m/n = 2/1$ GAE at $r/a = 0.5$ was weakly destabilized. For the initial EP distribution function (f_{h0}), the bump-on-tail and the slowing-down velocity distributions were considered. The bump-on-tail distribution reflects the experimental observation (high charge exchange loss), while the slowing-down distribution represents the ideal case. For the bump-on-tail case, the majority of the EP drive arises from the toroidicity-induced resonance for high-velocity particles. The contribution of the helicity-induced resonances is weaker because they are localized in the low-velocity region. These helicity-induced resonances are more significant for the slowing-down distribution. The different initial EP distributions also cause differences in the redistribution of EP pressure profile. The hollow (flat) EP pressure profile is formed after the saturation of the EP-driven MHD modes in the bump-on-tail (slowing-down) distribution.



Fig. 2 Radial MHD velocity profile of the $m/n=4/2$ GAE in Heliotron J.

[2] P. Adulsiriswad *et al.*, Nucl. Fusion **60**, 096005 (2020).

(P. Adulsiriswad)

Hybrid Simulations of fast ion transport and losses due to the fast ion driven instabilities in the Large Helical Device

Hybrid simulations for energetic particles interacting with a magnetohydrodynamic (MHD) fluid were conducted using the MEGA code to investigate the spatial and the velocity distributions of lost fast ions due to the Alfvén eigenmode (AE) bursts in the Large Helical Device (LHD) [3]. The numerical fast-ion loss detector “numerical FILD” which solves the Newton-Lorentz equation was constructed in the MEGA code. Fast ions which are transported by the AE burst near the Last Closed Flux Surface (LCFS) were detected by the numerical FILD. Most of the fast ions detected by the numerical FILD are re-entering fast ions which re-enter in the plasma after passing through the outside of the plasma as shown in Fig. 3. The velocity distribution of lost fast ions detected by the numerical FILD is in good agreement with the experimental FILD measurements.

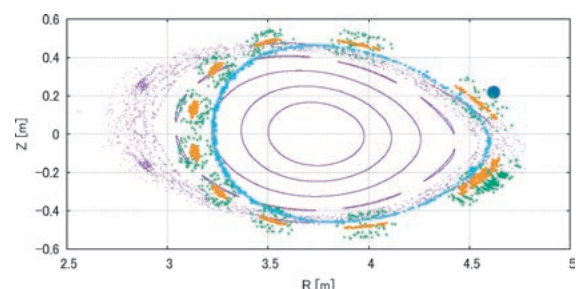


Fig. 3 Poincaré plots of fast ion orbits detected by the numerical FILD on the poloidal plane where the numerical FILD is installed. Gyro centers of a fast ion detected by the numerical FILD and the fast ion orbit before the AE burst are represented by yellow and blue dots, respectively. The Lorentz orbit of the detected fast ion is shown in green and the magnetic field lines are shown in purple. The blue circle represents the numerical FILD. The fast ion orbit represented by blue dots indicates that it is a re-entering particle.

[3] R. Seki *et al.*, “Hybrid Simulations of fast ion transport and losses due to the fast ion driven instabilities in the Large Helical Device”, in the 28th IAEA Fusion Energy Conference (2021).

(R. Seki)

Theory, simulation, and modeling of turbulent transport

Highlight

Reduced models of turbulent transport in helical plasmas including effects of zonal flows and trapped electrons

Using transport models [1], the impacts of trapped electrons and zonal flows on turbulence in helical field configurations are studied. The effect of the trapped electrons on the characteristic quantities of the linear response for zonal flows is investigated for two different field configurations in the Large Helical Device. The turbulent potential fluctuation, zonal flow potential fluctuation and ion energy transport are quickly predicted by the reduced models for which the linear and nonlinear simulation results are used to determine dimensionless parameters related to turbulent saturation levels and typical zonal flow wavenumbers. The effects of zonal flows on the turbulent transport for the case of the kinetic electron response are much smaller than or comparable to those in an adiabatic electron condition for the two different field configurations. It is clarified that the effect of zonal flows on the turbulent transport due to the trapped electrons changes, depending on the field configurations. The nonlinear simulation results (NL) can be predicted by the reduced models for the ion heat transport for the case of the kinetic electron response in the inward shifted magnetic field configuration for the plasma parameters in Fig.1 [2]. These plasma parameters for the case of the kinetic electron response in the inward shifted magnetic field configuration are out of the range for constructing the reduced models.

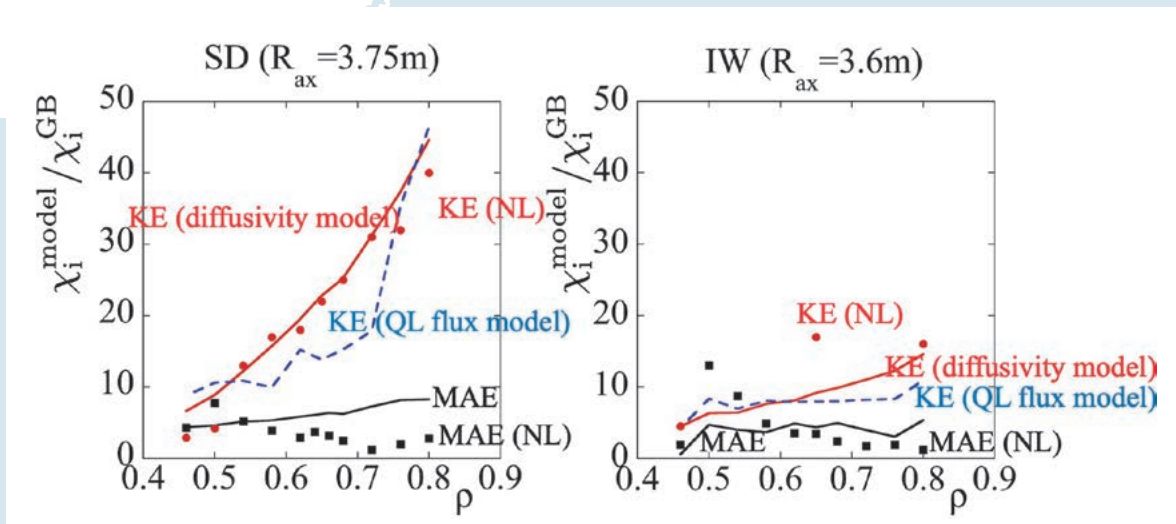


Fig. 1 The radial dependence of the normalized ion heat diffusivity is shown by the ion heat diffusivity model and the quasilinear (QL) flux model for the ion heat transport in the adiabatic (MAE) and kinetic electron (KE) conditions.

[1] S. Toda *et al.*, Phys. Plasmas **26**, 012510 (2019); doi: 10.1063/1.5058720.

[2] S. Toda *et al.*, M. Nunami, and H. Sugama, Journal of Plasma Physics **86**, 815860304 (2020); doi:10.1017/S0022377820000495.

Transport Prediction Scheme by Data Science and First-Principle Simulations

Transport of plasma heat and particle driven by the turbulence due to the micro-instabilities greatly affect the plasma confinement performances. The first-principle simulations based on the gyrokinetics are powerful to investigate the turbulent transport, not only qualitatively but also quantitatively. However, for the accurate estimate of the turbulences, a huge computational resources are demanded where we have to perform numerous numbers of the first-principle simulations for wide ranges of many physical parameters. Here, we have developed a new transport prediction scheme with as little as possible numbers of the first-principle simulations by using the technique of data science and the reduced transport model which approximately reproduces the turbulent transport levels. In the developed scheme, at first, we perform a mathematical optimization method of the techniques used in the data science for the reduced transport model to obtain the guesses of the input physical parameters needed for the first-principle simulation. Next, we perform the first-principle simulation under the guessed parameters. At last, based on the simulation result, we improve and optimize the transport model by employing the optimization technique again, we can obtain high accuracy transport model for each target plasma. See Fig. 2. The developed scheme enables us to perform the turbulent transport predictions with the minimum numbers of the first-principle simulations.

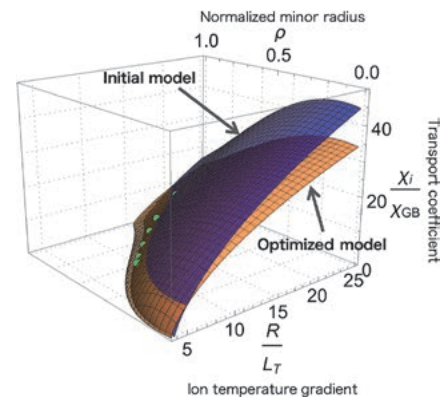


Fig. 2 Optimization of transport model by employing data science technique and the first-principle simulations. For the initial model (blue surface), a first-principle simulation at each radial position (green points) is performed and the optimized model (orange surface) is obtained.

(M. Nunami)

The variational formulation of the gyrokinetic system in general spatial coordinates

Gyrokinetics is a basic theoretical framework to study microinstabilities and turbulent processes in magnetized plasmas. Because background flow profiles are considered as one of the key factors for improving plasma confinement, momentum transport processes which determine the flow profiles are now being investigated extensively by large-scale gyrokinetic simulations. Thus, the momentum balance equation satisfied by the gyrokinetic model attracts our attention as a basis for theoretically and/or numerically investigating the physical mechanisms in the formation of the flow profiles. In the present work [3], our previous work [4] is extended to present the Eulerian variational formulation of the gyrokinetic system with electrostatic turbulence in general spatial coordinates and the invariance of the Lagrangian under an arbitrary spatial coordinate transformation is used to derive the gyrokinetic local momentum balance equation in an analogous manner to the theory of general relativity in which energy-momentum conservation laws are derived from the invariance of the action integral under arbitrary transformations of spatiotemporal coordinates. In the symmetric background magnetic field, the derived local momentum balance equation gives rise to the local momentum conservation law in the direction of symmetry. This derivation is in contrast to the conventional method using the spatial translation in which the asymmetric canonical pressure tensor generally enters the momentum balance equation. In the present study, the variation of the Lagrangian density with respect to the metric tensor is taken to directly obtain the symmetric pressure tensor, which includes the effect of turbulence on the momentum transport. In addition, it is shown in this work how the momentum balance is modified when the collision and/or external source terms are added to the gyrokinetic equation. The results obtained here are considered useful for global gyrokinetic simulations investigating both neoclassical and turbulent transport processes even in general non-axisymmetric toroidal systems.

[3] H. Sugama *et al.*, Phys. Plasmas **28**, 022312 (2021).

[4] H. Sugama *et al.*, Phys. Plasmas **25**, 102506 (2018).

(H. Sugama)

Numerical Simulations on Plasma-wall Interaction

Highlight

Simulations related to optical vortex — Molecular Dynamics simulation on Chiral Nano-Needle Fabrication by OV and Quasioptical simulation of OV beams in plasmas —

Omatsu group fabricated [1] chiral nanoneedles structure by vortex laser ablation. They used a ~2-mm-thick polished tantalum (Ta) as the target. Ta has a relatively low ablation threshold compared to other materials [2]. According their result [1], when the target Ta was irradiated with a circularly polarized Gaussian beam with the angular momentum quantum number $L = 0$ and the spin momentum quantum number $S = \pm 1$, no nanostructures, such as needles, were observed on the surface. In contrast, a linearly polarized optical vortex with $L = 0$ and $S = 0$ produced a chiral nanoneedle with a spiral conical surface at the center of the ablation zone. It is no exaggeration to mention that Omatsu's experiment is the start of research on optical vortex research in the field of optical physics. Against this backdrop, we used computer simulations instead of experiments to understand the interaction between light vortices and matter and addressed two issues: (1) molecular dynamics (MD) simulation on Chiral Nano-Needle Fabrication by optical vortex (OV) and (2) Quasioptical simulation of OV beams in plasma.

In the MD simulation on Chiral Nano-Needle Fabrication, the bcc Ta crystal at 300 K is prepared as the initial structure. We adopt EAM potential force field and NVT ensemble with Langevin thermostat [3,4]. We run the MD simulation with the external force field which is characterized by the Laguerre Gaussian beam [5]. As the result, we succeeded in fabrication of the chiral needle by the MD simulation (Fig. 1). Next, the background of the quasioptical simulation of OV beams in plasmas is as follows: Kato et al. demonstrated [6] that a single free electron in circular motion emits twisted photons carrying orbital angular momentum. However, OV property of radiation was not discussed well up, even though the physics of electron cyclotron motion and its radiation is essentially used for plasma confinements, heating, and diagnostics. Therefore, we started numerical studies to understand the behavior of OV in dispersive plasmas. Using the quasioptical ray tracing code named PARADE [8], we showed [7] the first PARADE simulations of optical vortex beams in various plasma situations, and especially discuss the differences between optical vortex beams and conventional Gaussian beams in plasmas as shown in Fig. 2.

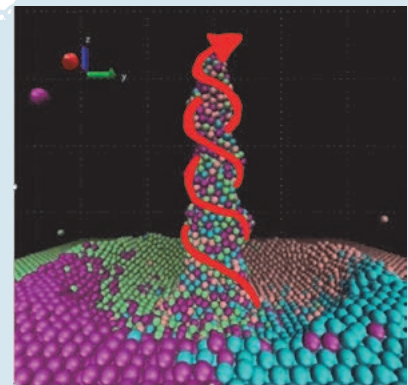


Fig. 1 Molecular Dynamics Simulation on Chiral Nano-Needle Fabrication. The red curve denotes the edge of the nanoneedle. It was found that a “ditch” is dug around the needle.

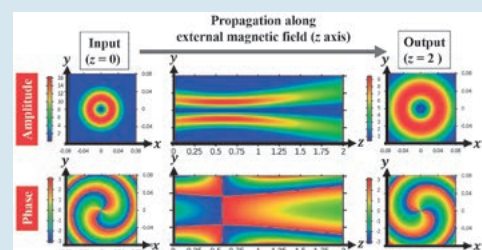


Fig. 2 Quasioptical simulation “PARADE” of OV beams in plasma. When an OV with Laguerre-Gaussian mode is input from $z = 0$, it propagates through the plasma along z axis which is parallel to the external magnetic field, and at $z = 2$ m, it becomes an output wave shown in the figures on the right. The upper figures show the amplitude distribution of the OV, and the lower ones show the phase distribution.

- [1] K. Toyoda *et al.*, Phys. Rev. Lett., **110**, 143603 (2013).
- [2] L. Torrissi *et al.*, J. Appl. Phys. **100**, 093306 (2006).
- [3] H. Nakamura *et al.*, “Molecular dynamics simulation on structural formation of chiral nanoneedle by optical vortex”, 38th JSST (2019).
- [4] S. Habu and H. Nakamura, “MD Simulation on Chiral Needle Fabrication in Radiation Force Field of Laguerre Gaussian Beams”, The 29th International Toki Conference (ITC29), 2020.
- [5] L. Allen *et al.*, Phys. Rev. A, **45**, 8185 (1992).
- [6] M. Katoh *et al.*, Phys. Rev. Lett. **118**, 094801 (2017).
- [7] K. Yanagihara *et al.*, “Quasioptical simulation of optical vortex beams in plasmas”, The 29th International Toki Conference (ITC29), 2020.
- [8] K. Yanagihara *et al.*, Phys. Plasmas **26**, 072112 (2019).

Development of Simulation Codes to Treat Hydrogen Molecules Process in Divertor Plasma Region including Divertor Plate

By combining the following three simulation codes, *i.e.*, (i) the Neutral-Transport code with the rovibrationally resolved Collisional-Radiative model (NT-CR) [9], (ii) EMC3-EIRENE code [10], and (iii) the Molecular Dynamics (MD) simulation [11], we successfully calculated each hydrogen molecule (H_2) population with vibrational state (v) and rotational state (J) at any position for carbon or tungsten divertor plate [12]. Neutral transport codes are widely used to analyze divertor plasmas. However, the H_2 rovibrational population is not considered. Using our codes, we calculated the H_2 rovibrational populations for a certain LHD plasma with carbon divertor plates.

As shown in Fig. 3, we found that the J -dependence of each H_2 population for $v = 0,1,2$ near the divertor plate becomes the Boltzmann distribution, which is consistent with the estimation by emission spectroscopy of the Fulcher- α band of H_2 in LHD [13].

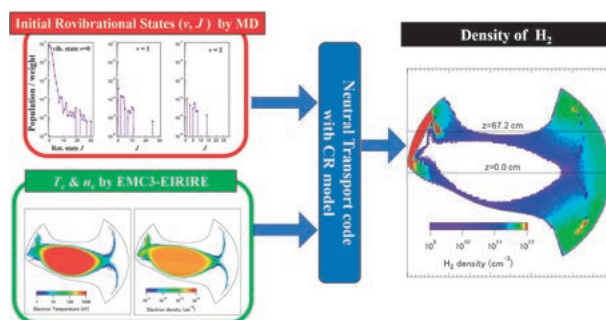


Fig. 3 Concept of the hybrid simulation among molecular dynamics, EMC3-EIRENE and Neutral-Transport code with the rovibrationally resolved Collisional-Radiative model.

- [9] K. Sawada and M. Goto, *Atoms* **4** (2016) 29.
- [10] G. Kawamura *et al.*, *Plasma Phys. Control. Fusion* **60** (2018) 084005.
- [11] S. Saito *et al.*, *Contrib. Plasma Phys.* (2020) e201900152.
- [12] K. Sawada *et al.*, *Contrib. Plasma Phys.* (2020) e201900153.
- [13] H. Ishihara *et al.*, *J. Quant. Spectrosc. Radiat. Transf.*, **267** (2021) 107592.

Structural Change of Tritium-substituted Macromolecules by β decays

A human telomeric DNA structure is found at the end of eukaryotic chromosomes and consists of a specific repeating base sequence (TTAGGG) and various proteins. It has been reported that telomere shortening can cause atherosclerosis and cancer. Adopting the nucleotide sequence of telomeric DNA, *i.e.*, TCTAGGGTTAGGGTTAG, we investigate the effect of tritium β decay on telomeric DNA by molecular dynamics (MD) simulation. In particular, we focus on both the hydrogen bond [15] and the covalent bond breaking in the telomere structure. For the latter purpose, we used the dynamic reactive force field (ReaxFF) [14], which is known to be able to handle covalent bond breaking.

In order to investigate the effect of the β decay on covalent bonds, we assume that the two hydrogens covalently bonded to the carbon at the 5' position of the sugar were decayed to helium (described as a scratch). When a lot of scratches are input to telomeric DNA, Fig. 4 shows snapshots at 1.85 ns from the initial structure. Furthermore, it also shows that covalent bond breaking has occurred and the structure is split into about three pieces. Thus, it was confirmed that when the number of scratches increases, the covalent bonds are broken and the telomere structure collapses.

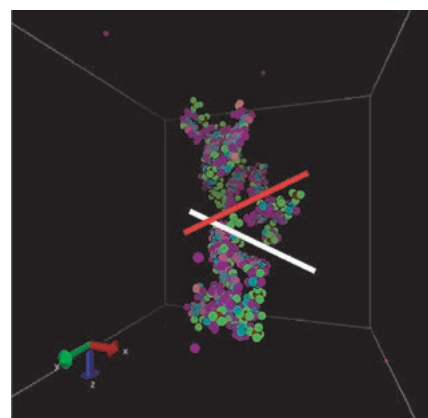


Fig. 4 A snapshot of the telomeric DNA structure at 1.85 ns after the initial structure. Figure shows that the double helix structure of the initial structure is broken into three pieces. For clarity, the broken parts are described with red and white lines.

- [14] van Duin *et al.*, *J. Phys. Chem. A*, **105**, 9396 (2001).
- [15] H. Nakamura *et al.*, *Jpn. J. Appl. Phys.* **59**, SAAE01 (2020).

Integrated Transport Analysis based on Data Assimilation Technique

Highlight

Data assimilation technique has made progress on a “whole-discharge” transport modelling of LHD plasmas

A data assimilation technique has been implemented into the integrated transport analysis suite, TASK3D [1], to make a transport model to be suitable for the actual plasmas, and then to predict and control the fusion plasmas [2]. The system is named as ASTI (Assimilation System for Toroidal plasma Integrated simulation). The temporal variations along with the change of profiles of the ion and electron temperatures have been successfully demonstrated by ASTI for an actual discharge of the Large Helical Device (LHD) (as shown in Fig. 1). Now, the ASTI development has been progressing towards controlling plasmas by implementing the new scheme, in addition to assimilate the measurement data. This will open up the new phase of general data assimilation methodology.

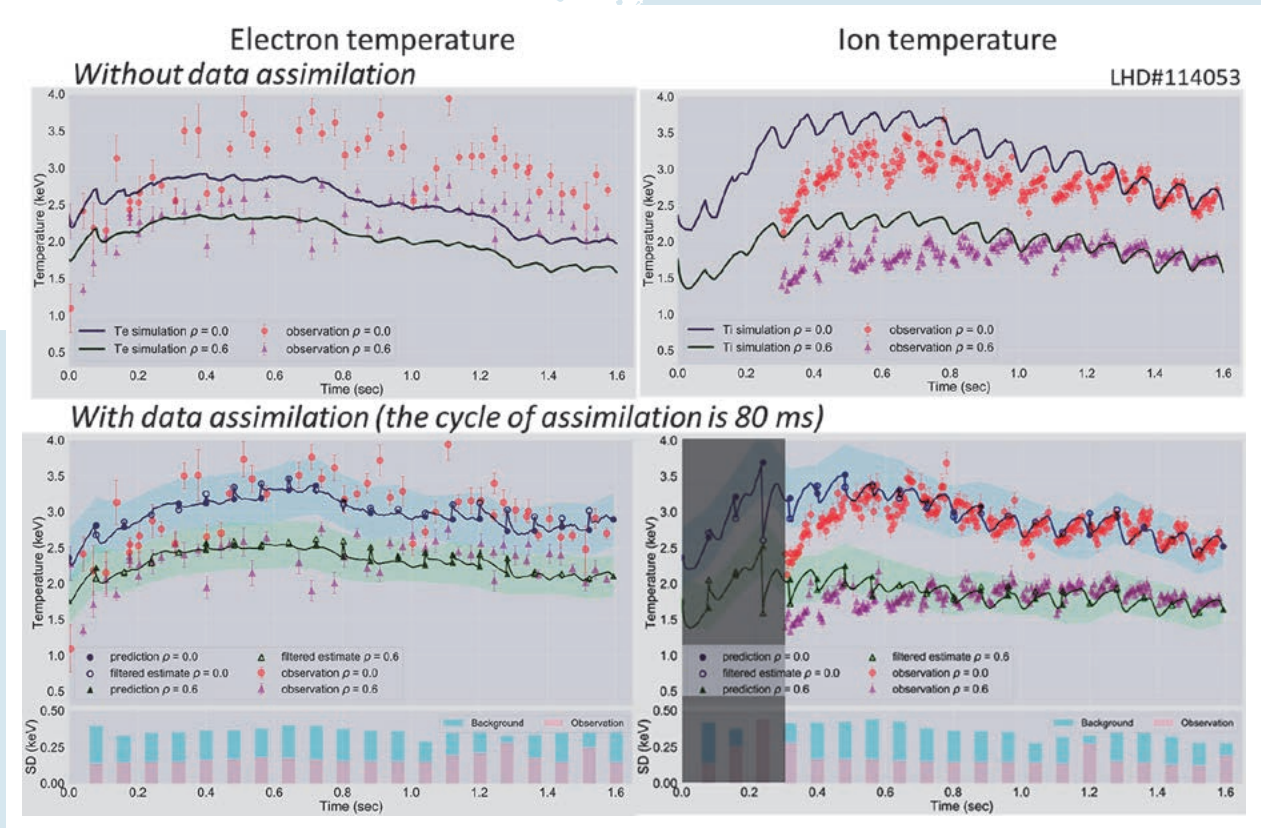


Fig. 1 Temporal change of electron (left) and ion (electron) temperatures at the plasma center (red dots with error bars for measurement and blue curve for simulation), and at 60% of the average minor radius (purple dots with error bars for measurement and green curve for simulation) for LHD discharge 114053. The upper column is for TASK3D only (without data assimilation), and the lower column is for ASTI (with data assimilation). Hatched region at the right-bottom is a part where the electron temperature is assimilated because the ion temperature measurement was not performed. The bars in the lower panels indicate the estimated standard deviations (SD) of the background error and observation noise before filtering.

The data assimilation technique is one of the statistical estimation methodologies. It has been widely developed and practically employed in meteorology and oceanology (weather forecast, prediction of El Niño and La Niña).

The time-series measurement data (profiles of the ion and electron temperatures) for a whole discharge of LHD experiment are assimilated into TASK3D in which one-dimensional diffusive heat transport equation is solved for ions and electrons. Here, previously obtained turbulent transport model, gyro-Bohm (for electrons) and gyro-Bohm-gradTi (for ions) models are employed in TASK3D. Utilizing the data assimilation technique, the state vector composed of physics variables (as shown in Fig. 2; notations are given in the figure caption) is estimated with employing the ensemble Kalman filter (EnKF) [3]. This prediction (TASK3D) and filtering processes make the given transport model to be adapted for the actual plasma behaviors. ASTI can also be used to estimate the variables not observed and the model parameters that can explain observed time series data. The ensemble Kalman smoother (EnKS), a data assimilation method for analysis, has also been implemented in ASTI [4].

Figure 2 shows the data assimilation results of the ion and electron temperatures in comparison to the results without the data assimilation (“usual” TASK3D simulation) for a particular LHD discharge (discharge number: 114053) as a whole. The implemented transport model is found not to be satisfactory to predict temporal variations of temperatures, but the data-assimilation can provide reasonably well alignment to the measured data. This is realized by “optimizing” the transport model to be suitable for the actual situations.

Now, it has been progressing towards data assimilation for a group of discharges so that widely applicable transport model is obtained, and in the meantime, towards “the ASTI for the control” for actual plasma control to be demonstrated.

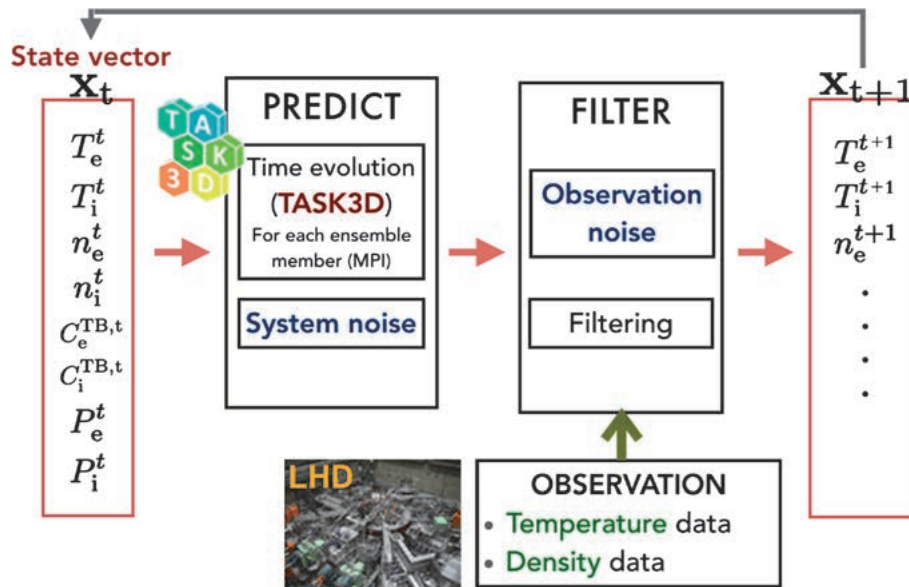


Fig. 2 A data assimilation scheme based on TASK3D and EnKF. Here, the state vector is composed of T (temperature), n (density), C^{TB} (coefficient of turbulent transport model) and P (NBI (neutral beam injection) heat deposition), with suffixes, e and i, for electrons and ions, respectively.

- [1] S. Murakami *et al.*, Plasma Phys. Control. Fusion **57**, 119601 (2015).
- [2] Y. Morishita *et al.*, Nucl. Fusion **60**, 056001 (2020).
- [3] G. Evensen, Ocean Dyn. **53**, 343–67 (2003).
- [4] Y. Morishita *et al.*, Plasma and Fusion Research **16**, 2403016 (2021).

(Y. Morishita, Kyoto University)

4. Basic, Applied, and Innovative Research

As an inter-university research institute, NIFS activates collaborations with researchers in universities as well as conducting world-wide top level researches. The collaboration programs in basic, applied, and innovative research support research projects motivated by collaboration researchers in universities. It is also important to establish the academic research base for various scientific fields related to fusion science and to maintain a powerful scientific community to support the research. Programmatic and financial support to researchers in universities who work for small projects are important.

For basic plasma science, NIFS operates several experimental devices and offers opportunities to utilize them in the collaboration program for university researchers. A middle-size plasma experimental device the HYPER-I is prepared for basic plasma research. The compact electron beam ion trap (CoBIT) for spectroscopic study of highly charged ions, atmospheric-pressure plasma jet devices for basic study on plasma applications, and other equipment are operated for collaborations.

(I. Murakami)

Simulations of negative ion extraction and transport for developing novel remote reactive ion processing system

A novel remote dry processing of specific reactive negative ions with a deflection and focusing system is being developed to precisely control their energy, flux and reaching position on the nanoscale. The trajectory simulations of the negative ion extraction and transport for the design of this processing apparatus have been carried out using SIMION software. It is found from the simulation results that the ion beams with good focusing characteristics, high directivity and appropriate current amount can be successfully extracted from the plasma source and transported to the reactor chamber through the deflection and focusing system. A typical result for the case of negative oxygen ions is shown in Fig. 1. As recognized from trajectories of O^- ion beams, the extraction and transport characteristics of the flat intermediate electrode are superior to those of the oblique one [1].

(T. Kanki, Japan Coast Guard Academy and H. Himura, Kyoto Institute of Technology)

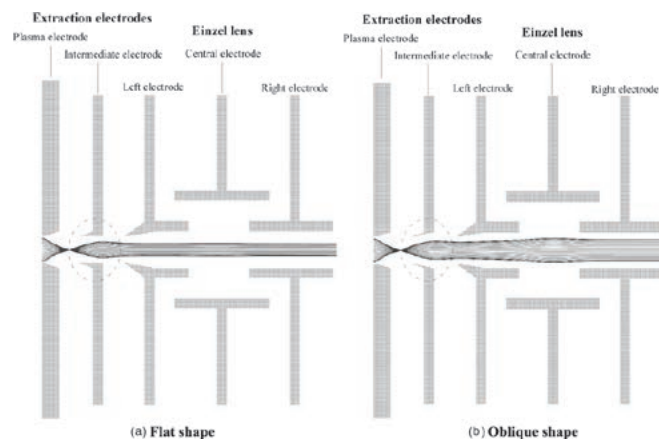


Fig. 1 Oblique and flat intermediate electrodes, and the trajectories of O^- ions near the electrodes for the case where the acceleration voltage is -7 kV. [1]

Toward the understanding of transport and self-organization mechanisms of flowing plasmas

Precise measurements of flow and potential structures are essential for the understanding of transport and self-organization phenomena commonly observed in various plasmas. For this purpose, development studies on a compact heavy ion beam probe (HIBP) system and coherence imaging system (CIS) are conducted for the RT-1 magnetospheric experiment. Based on the detailed analysis of laser irradiation conditions, a laser ion source was developed to provide a high brightness multi-charged beam for the HIBP system [2]. For the two-dimensional measurements of ion temperature and flow, a CIS system with a new CIS cell and electron multiplier CCD (EM-CCD) was developed, installed, and operated at the RT-1 (Fig. 2). For the calibration of wavelength, a new technique, using spectral line sources, was proposed as a reliable absolute calibration method [3]. Initial measurements in the RT-1 showed that the flow profiles are not simply explained by the grad-B and curvature drift in a dipole magnetic field especially in a strong field region, suggesting the existence of radial electric field in high-beta plasmas.

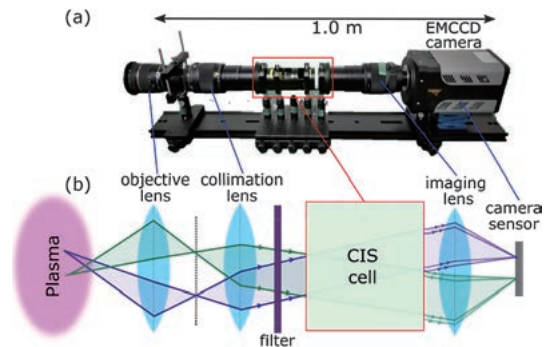


Fig. 2 CIS system for the 2-d measurements of ion temperature and velocity in RT-1 [3].

(H. Saitoh, Univ. Tokyo)

A broadband mid-infrared source for remote sensing

Fiber-optic sensors based on MIR absorption spectroscopy have great potential to be the next-generation gas detecting device. However, there is the remaining issue of the absence of a suitable MIR source exhibiting broadband spectrum and high-beam quality. In this work, the research team has demonstrated an ultra-broadband light source at the MIR region, which meets the requirements for developing the fiber-optic sensor. Er³⁺/Dy³⁺ co-doped ZBLAN optical fiber has been used to obtain broadband mid-infrared (IR) light sources pumped by commercially available laser diodes [4]. The demonstration shows that mid-infrared broadband emission, extending from 2515 to 3735 nm, was obtained by energy transfer between Er³⁺ and Dy³⁺, as shown in Fig. xx. To assess its potential for gas sensing applications, the fabricated light source was used to detect methane gas with concentrations at 1% and 5%. We can then say that the simple and stable construction of our light source is suitable for practical purposes.

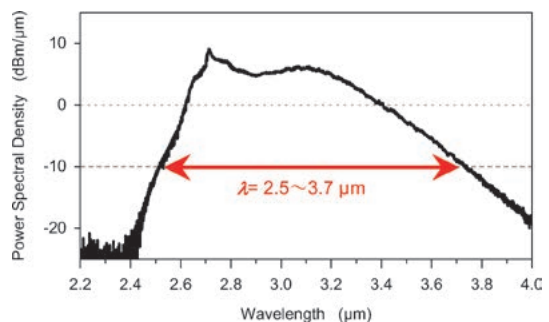


Fig. 3 Power spectral density of the developed MIR source.

(K. Goya, Akita Prefectural Univ.)

- [1] T. Kanki *et al.*, Japanese J. Appl. Phys. **59**, SJJE01 (2020).
- [2] K. Nakamura *et al.*, Rev. Sci. Instrum. **91**, 033503 (2020).
- [3] K. Ueda *et al.*, Rev. Sci. Instrum. **92**, 073501 (2021).
- [4] K. Goya *et al.*, Scientific Reports **11**, 5432 (2021).

5. Fusion Science Archives (FSA)

The Fusion Science Archives were established in 2005 to learn lessons from the past fusion science archives preserved and to maintain collections of historical documents and materials that are related to fusion research in Japan. These activities are important from the viewpoint of the historical evaluation of fusion research, its social accountability and making references for seeking future directions.

Since then, historical materials on fusion research and/or organizations related to fusion research have been collected and preserved at the FSA. They are stored in acid-free folders and boxes. The total number of registered items is now approximately 25,500. Most of those catalogues are available to the public through the internet in a hierarchical structure and can be accessed by the use of an electronic retrieval system.

The following collaborative works are performed this fiscal year along these lines:

- **Archival Studies on Collaborations in Heliotron Studies at Kyoto University (NIFS17KVXV015)**

T. Mizuuchi (Kyoto Univ.) *et al.*

The activities of this archival study are focused on the materials related to the development of plasma experimental devices, especially on the development of the series of Heliotron devices originating from Kyoto University. The range of objects in the archives covers not only the hardware but also related researchers, research groups, and their activities which have contributed to the development of the Heliotron concept. In these years, digitizing works of the minutes of research group meetings (PEC, etc.) from the Heliotron-E project has progressed. As of the end of this fiscal year, up to 28 of the 44 volumes of PEC files have been digitized, and electronic files are recorded and stored on DVDs and HDDs. Some other unfilled materials have been recorded on older recording media such as MO. We have started to transfer them to a new recording medium that can be easily accessed in the current PC environment.

- **History of the early days of Nuclear Fusion Research Group in Japan (NIFS17KVXV017)**

C. Namba (NIFS FSA) *et al.*

The organization “Nuclear Fusion Research Group of Japan” (KAKUYUGO KONDANKAI, hereafter referred as KK) was established in 1958. Dr. H. Yukawa was the first president of this organization. This KK continued to perform an important role in research and development of fusion science in Japan as a voluntary organization for researchers, until it became “The Japan Society of Plasma Science and Nuclear Fusion Research” in 1983. The theme of this work is to clarify the establishment process of the KK and how researchers organized and planned to promote fusion development research. We have examined the 1st to 6th volumes of the journal of KK called “KAKUYUGOU KENKYU” and the bulletins of the standing committee of the KK. We have confirmed that the KK organized research meetings and symposiums actively, that they provided places for discussion on the promotion policy of fusion research and issued timely detailed minutes, and that the KK played roles for selection of members for committees related to plasma-fusion research.

- **Collaborative Activities at NIFS Fusion Science Archives (NIFS FSA) (NIFS17KVXV018)**

S. Kubo (NIFS, FSA) *et al.*

The purpose of this collaboration is to arrange and promote the general archival activities under a NIFS collaboration framework.

One of the topics of this fiscal year in the archives activity is that the important relics of Professor Kodi Husimi

are added to the collection of the FSA. The collection of Koji Husimi which was originally collected and registered to the FSA is transferred from the so called “Husimi Salon” of Institute of Plasma Physics, Nagoya University and later from his house. An added new collection is from his second house in Nagano and includes several medals and certificates of awards he had received, pictures taken from 1950s, drawings during his childhood etc. The newly added collection was immediately digitized utilizing the equipment consolidated in FY2019.

- **Construction of Digital Library of Husimi Koji Archives (NIFS18KVXV019)** H. Iguchi (NIFS, FSA) *et al.*
Historical documents donated by Koji Husimi, who was the first director of Institute of Plasma Physics, Nagoya University, are key contents of the NIFS Fusion Science Archives. They are useful in tracing the history of research activities in plasma physics and fusion science in Japan, especially in universities. About 4,800 items are stored and registered in 120 storage boxes. Most of the documents are rather old. The quality of papers is poor and they are fragile. Printed letters in some documents are getting difficult to read. In order to preserve those documents for future reference, it is necessary to convert them into digital documents. The plan started three years ago. About 900 documents are digitalized as PDF files. However, it is still one fifth of the total Husimi documents. The final purpose of the program is to make a digital library of all the Husimi collections. It is still at the beginning stage of the program.
- **Trend of plasma spectroscopic research in Japan’s university laboratories surveyed from the chronicle of collaborative research meetings (NIFS19KVXV0020)** N. Yamaguchi (Comprehensive Research Organization for Science and Society (CROSS)) *et al.*
A workshop called the “Plasma Elementary Process workshop” or “Spectroscopy workshop” has been held as collaboration research between the Institute of Plasma Physics, Nagoya University (IPPJ) and NIFS from 1969 to the present. The chronological table of the history of the workshop has been compiled. The cumulative number of universities that contribute the workshop is 56, while the first workshop was attended by the nine major universities. University laboratories where researchers investigate plasma spectroscopy theoretically or experimentally are distributed around Japan.
- **Research study on the initiation phase of the Japanese fusion reactor technology (NIFS19KVXV021)**
S. Matsuda (Tokyo Inst. Technology) *et al.*
Based on archive documents kept in the JAERI, NIFS and Tokyo University, a study on the initiation phase of Japanese fusion reactor technology has been planned and started. The beginning of systematic development had to wait until fusion reactor studies started in 1970, when essential technologies were identified. Roughly, it started about ten years later than the plasma confinement researches. Although a power reactor for fusion is similar to one for fission, many fusion technologies are almost new and large scale and have to be developed for the first time. These include technologies for superconducting magnets, vacuum vessels, plasma heating systems, pumping systems, tritium fuel systems, plasma facing materials such as the first wall and divertor, and remote handling systems.

6. SNET Collaborate Research

NIFS is promoting the “Fusion Virtual Laboratory Initiative” to integrate fusion experiments and research environments in Japan using SNET, and is remotely collecting and storing data from plasma experiment devices such as QUEST at Kyushu University, GAMMA-10 at Tsukuba University, and TST-2 at the University of Tokyo.

In addition, NIFS is working with the ITER Remote Experimentation Center (REC) for the ITER project, which is an international collaboration, on the demonstration of the remote participation, the storage of large amounts of data, and with National Institute of Informatics (NII) on research related to the transfer of large amounts of data over long distances across national boundaries.

Research Highlights

The amount of data collection of TST-2 decreased to 40 GB in FY2020 compared to 96 GB in FY2019. This is due to a decrease in experimental opportunities due to COVID-19 countermeasures. In order to prevent noise around the device, a prototype of a trigger isolation circuit was developed and the circuit was examined under the following conditions: battery operation, short delay time, and positive logic TTL input/output.

In GAMMA-10, all the data are transferred to the LABCOM system through SNET after the experiment. In FY2020, data other than those collected by CAMAC system, such as oscilloscope measurement data, ADC measurement data for individual measurements, and high-speed camera data, were transferred to LABCOM system. 16 channels of Doppler reflectometer data have been added this year. The data from this system is directly transferred to LABCOM, and can be easily read out by the LabVIEW program.

The data acquired by the high-speed PXI digitizer in the QUEST experiment is remotely stored in the NIFS storage system, which provides a mechanism for sharing and redistribution to research institutes across the country. In addition, these collection systems can now be remotely monitored and controlled via the web to reflect the digitizer.

In the REC, LHD experimental data is used for the demonstration experiment for the remote participation for ITER project. The connection method between the computing resource and the experimental database, data format, storage method, backup, security, etc. were studied.

In collaboration with NII, we conducted a long-distance and multi-point data transfer experiment in anticipa-

tion of sharing measurement data of experimental fusion reactors in international joint research. This time, we connected the route around the world between NIFS and QST by L2VPN, and conducted a file transfer experiment using MMCFTP (Massively Multi-Connection File Transfer Protocol) developed by NII.

(M. Emoto)

7. Bilateral Collaboration Research

The purpose of the Bilateral Collaboration Research Program (BCRP) is to enforce the activities of nuclear fusion research in the universities by using their middle-size experimental facilities of the specific university research centers as the joint-use facilities for all university researchers in Japan. The current program involves five university research centers as follows:

- Plasma Research Center, University of Tsukuba
- Laboratory of Complex Energy Process, Institute of Advanced Energy, Kyoto University
- Institute of Laser Engineering, Osaka University
- Advanced Fusion Research Center, Research Institute for Applied Mechanics, Kyushu University
- Hydrogen Isotope Research Center, University of Toyama

In the BCRP, each research center can have its own collaboration programs, using its main facility. Researchers at other universities can visit the research center and carry out their own collaboration research there, as if the facility belongs to NIFS. That is, all these activities are supported financially by NIFS for the research subjects in the BCRP. The BCRP subjects are subscribed to from all over Japan every year as one of the four frameworks of the NIFS collaboration program. The collaboration research committee, which is organized under the administrative board of NIFS, examines and selects the subjects.

(S. Sakakibara)

FAST IGNITION OF SUPER HIGH-DENSE PLASMAS

Laser-driven inertial confinement fusion by the Fast Ignition (FI) scheme has been intensively studied as the FIREX-1 project at the Institute of Laser Engineering, Osaka University. The researches consist of target fabrication, laser development, fundamental and integrated implosion experiments, simulation technology and reactor target design, and reactor technology development. In FY2020, the following progress was made through Bilateral Collaboration Research Program with NIFS and other collaborators from universities and institutes (NIFS12KUGK057 as the base project).

Fundamental and Integrated Plasma Experiments

For the fast ignition of the inertial confinement fusion, we have developed several novel schemes, namely, stable generation of high-density core plasma using a solid ball fusion fuel, realization of an ultra-high contrast heating laser using a plasma mirror, low mean-kinetic energy beam of fast electrons, and focusing of the laser-accelerated electron beam using laser-driven strong magnetic field and self-generated magnetic field. The average energy of the electron beam accelerated by the heating laser must be kept as low as possible to achieve efficient heating. We have developed a high-contrast heating laser by introducing a plasma mirror into a kilojoule-class laser system. The average energy was reduced by about 80% as shown in Fig. 1, and the heating efficiency was improved by a factor of two compared with the previous experiments. We have shown that the pulse contrast is essentially important for plasma heating.

In the current fast ignition experiment, an external magnetic field using a laser driven coil is used. However, this method may not be suitable for realization of the laser fusion energy, which requires repetition rates of 10 Hz or higher. We have started experiments on guiding of the electron beams using a self-generated magnetic field formed spontaneously by the laser-accelerated electron beam itself.

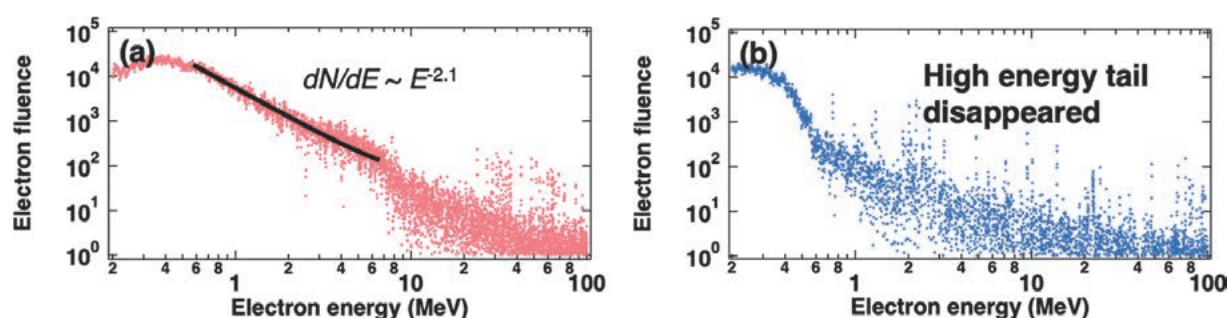


Fig. 1 Difference of electron energy distribution with (right) and without (left) a plasma mirror.

Target Fabrication

The low dense materials have been developed for laser fusion targets. In this year, the bromine (Br) doped trimethylolpropane trimethacrylate (TMPT) was developed, since Br doping to target materials is considered to be useful for suppression of the Rayleigh-Taylor instability. The Br-doped TMPT were fabricated by copolymerization of *p*-Bromostyrene and TMPT. After gelation, the co-polymer was dried by the supercritical carbon dioxide method. Figure 2 shows SEM images of the TMPT and the Br doped TMPT. The concentration of Br can be controlled up to 20 wt%. The spherical shaping was also successfully performed.

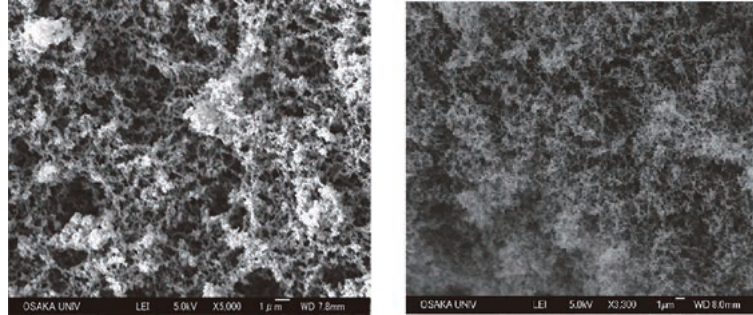


Fig. 2 SEM images of TMPT (left) and Br-doped TMPT (right).

Theory and Simulation of heating and ignition design

Heating of the dense plasmas by relativistic-intensity lasers has been considered to be effective in heating the core plasma by drag heating, resistive heating, and diffusive heating. The LFEX laser can maintain the heating surface at electron temperatures of 10 keV or higher and drive thermal diffusion with keV temperature as confirmed with simulations (Fig. 3). It can be seen that the core center is heated to a pressure above PPa. Energy conversion ratio from the laser energy to the core plasma is more than 15%. These results were published in Physical Review Letters [1].

Based on these results, we designed an ignition-scale experiment. The density of the imploded core was assumed to be 300 g/cc, and the heating laser was assumed to be 2ω light of 200 kJ/20 ps. All the heating processes and the radiation losses were taken into account in the calculation. The results are shown in Figs. 3 (d) and 3 (e). The maximum density of 300 g/cc set at 100 μm was heated to over 5 keV with the arrival of the thermal diffusion front at about 20 ps. From the calculation results, it is expected that the ignition temperature can be achieved by heating with 200 kJ 2ω light at about 20 ps.

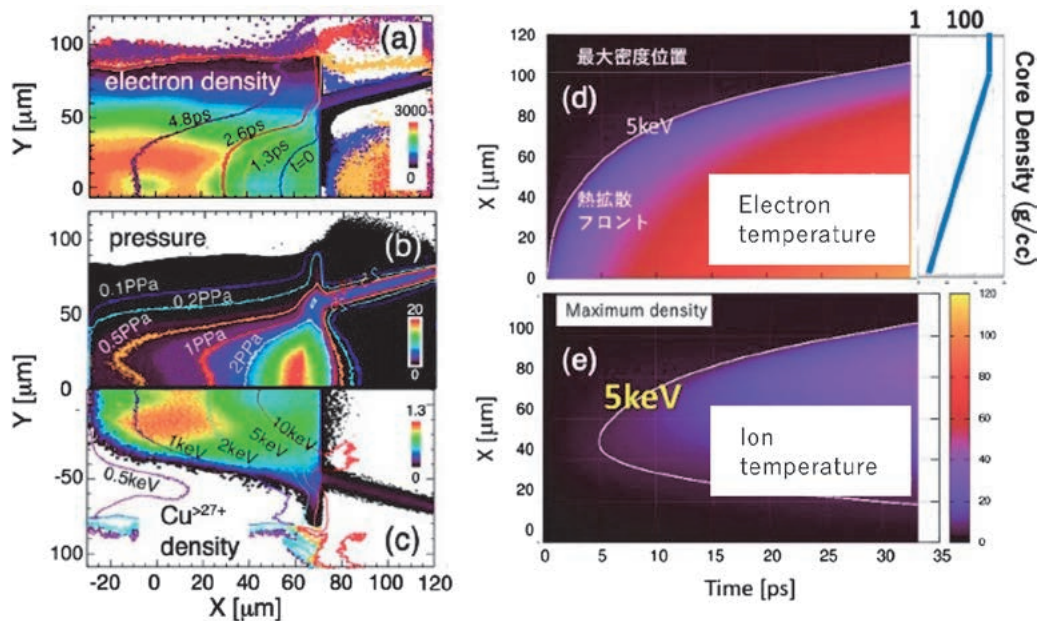


Fig. 3 Simulation of the FIREX experiment by the PICLS code. (a), (b) and (c) Results of the heating calculations for the ignition scale experiment. (d) Time evolution of the electron temperature. (e) Time evolution of the ion temperature.

Improvement of GXII and LFEX laser system

Replacement of various old devices by controllable devices on network has started for remote control of Gekko-XII (GXII) laser system. Based on a reconstructed timing chart of the whole system, a timing controller and a digital-controllable fiber oscillator have been renewed this year. The remote control of the oscillator has been implemented on September 2020 and already operated for many experiments.

In LFEX laser, a pulse energy and a spectral shape of a laser pulse from the front end have been improved by installing a fiber system instead of the conventional solid system for pulse stretching, amplification and spectral shaping. The concerned deterioration of a pulse intensity contrast due to introduction of the fiber system did not appear resulting in high contrast of 10^{10} as shown in Fig. 4.

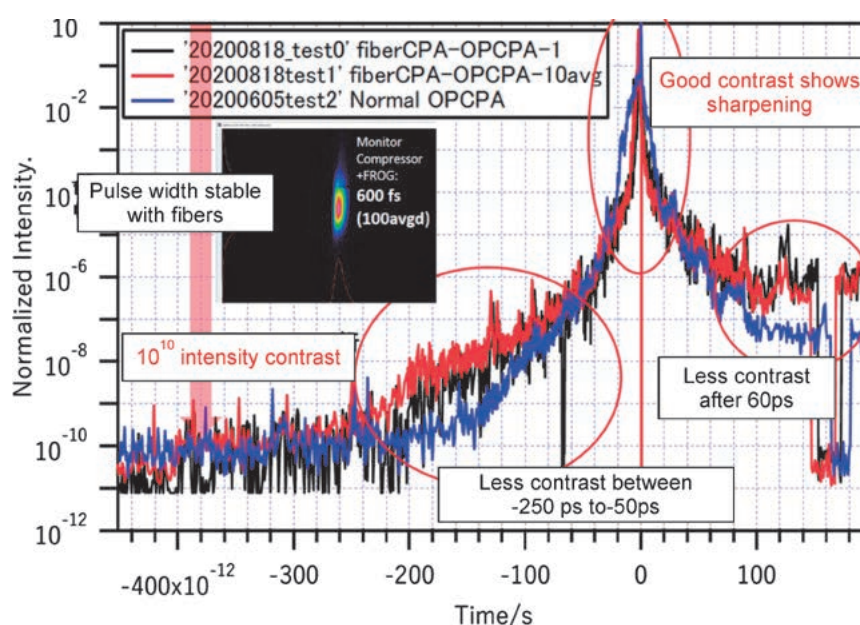


Fig. 4 Pulse intensity contrast measured with a third-order autocorrelator.

Individual Collaborations

In parallel to the main base project, 16 other collaborations by individual researchers including three from abroad as described below have been performed. Those were on electron-driven fast ignition (5 collaborations), ion-driven fast ignition (2), alternative scheme of laser-driven inertial fusion (3), implosion hydrodynamics (2), diagnostics of high-temperature and high-density plasmas (3), and reactor technology (1). 7 were projects continued from the previous year(s) and 9 were newly accepted in FY2020.

[1] K. Matsuo *et al.*, Phys. Rev. Lett. **124**, 035001 (2020).

(R. Kodama, H. Shiraga, S. Fujioka, K. Yamanoi, K. Shigemori, Y. Sentoku, and J. Kawanaka)

University of Tsukuba



Fig. 1 Bird's eye view of GAMMA 10/PDX.

Highlight

Study of boundary plasmas by making use of open magnetic field configuration and development in high power gyrotrons towards the DEMO project

In the Plasma Research Center, University of Tsukuba, studies of boundary plasma and development of high-power gyrotrons have been performed under the bilateral collaboration research program. The GAMMA 10/PDX (Fig. 1) is the world's largest tandem mirror device and has many plasma production/heating devices. By using a divertor simulation experimental module (D-module), shown in lower left of Fig. 1, which is installed at the west end region of the GAMMA 10/PDX, hydrogen recycling and plasma detachment have been extensively studied. The effective plasma detachment is clearly shown by the additional $N_2 + H_2$ gas injection into the D-module. As a ratio of the amount of N_2 gas to H_2 gas injection increases, the electron density and ion flux decrease more, indicating that nitrogen-induced molecular activated recombination efficiently contributes to the plasma detachment. Besides, enhancement of hydrogen recycling due to increase in the target temperature has been studied. A test of a new 28/35 GHz dual-frequency gyrotron has been carried out. The new linear plasma device with superconducting coils is designed and under construction to contribute to the DEMO divertor design.

In the Plasma Research Center, University of Tsukuba, studies of boundary plasma and development of high-power gyrotrons have been performed under the bilateral collaboration research program. In FY2020, 26 subjects including the base subject were accepted and produced a number of excellent results.

Effects of a combination of N_2 and H_2 gas-puff on the plasma detachment have been investigated. Figure 2 shows time evolution of pressure inside the D-module, electron temperature, density and ion flux in the cases of hydrogen gas-puff only and a combination of hydrogen and nitrogen gas-puff. It is found that as a ratio of the amount of N_2 gas to H_2 gas injection increases, the electron density and ion flux decrease more. The ratio of H_α line intensity to H_β line intensity, which is a good monitor of hydrogen activated molecular recombination (especially in the dissociative attachment process), is lower in the case of a combined gas-puff of hydrogen and nitrogen gases than hydrogen gas-puff only, suggesting processes of nitrogen-induced molecular activated recombination suppress the dissociative attachment process.

An effect of increasing the temperature of a tungsten target on hydrogen recycling has been studied. So far, enhancement of hydrogen recycling has been shown in the case of a high temperature target. Here, an effect of gas-puff on the recycling enhancement is studied. When the gas-puff is done, the electron temperature decreases more and the electron density increases more in the case of a high temperature target, compared to room temperature. However, there is no difference in the electron densities in the cases of high and room temperature targets. It is found that hydrogen recycling is enhanced due to the high temperature target when the amount of gas-puff is smaller than a certain value. When gas-puff exceeds a certain value, plasma seems to be detached.

An experimental test of a 28/35 GHz dual-frequency gyrotron has been carried out to achieve 0.4 MW CW at 28 GHz. In FY 2020, a cooling system was improved to suppress the temperature increase of cooling water at the collector up to 30°C in a 0.4 MW CW operation.

(M. Sakamoto)

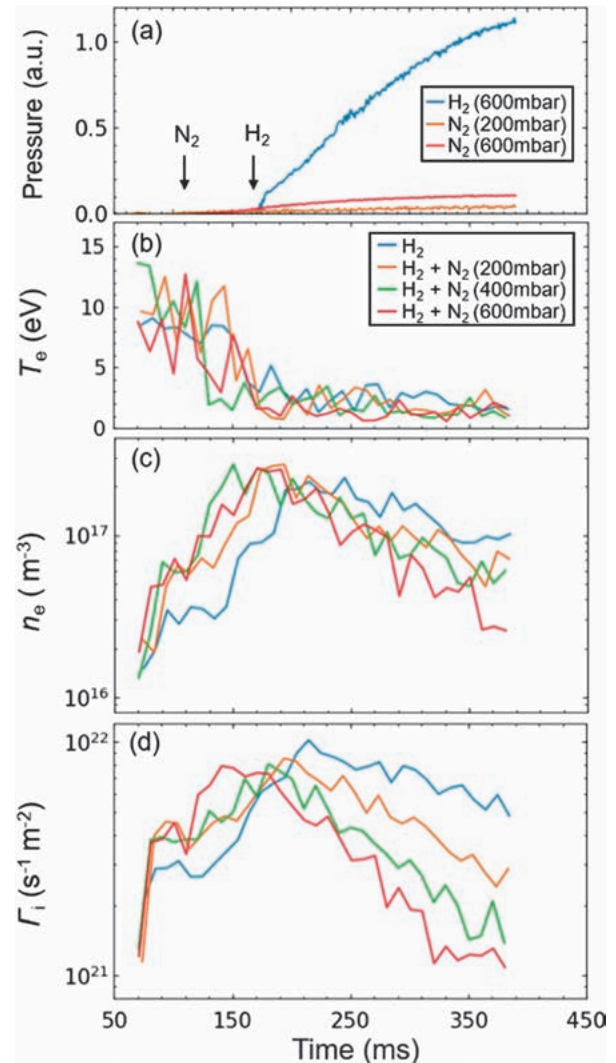


Fig. 2 Time evolution of (a) pressure inside the D-module, (b) electron temperature, (c) electron density, and (d) ion flux. The plenum pressure of hydrogen is fixed at 600 mbar.

Kyoto University

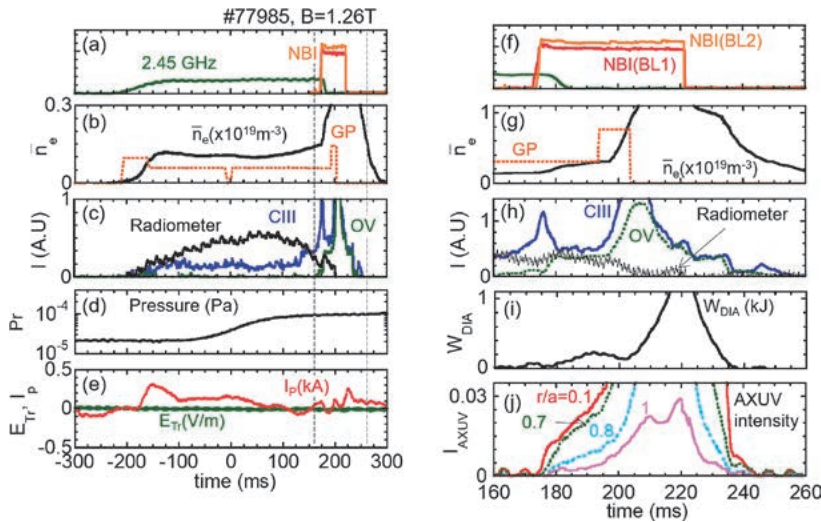


Fig. 1 Time evolution of plasma parameters in an NBI start-up plasma of Heliotron J assisted by non-resonant microwave heating. (a)–(e) in the pre-ionization by non-resonant microwave launch and (f)–(j) for the main plasma formation by NBI. The time response of the neutral gas pressure is in the order of 0.1 s.

Highlight

Study of NBI plasma start-up assisted by seed-plasma generation using non-resonant microwave heating:

Robust and reliable plasma start-up is an important topic not only in Tokamak but also in Stellarator/Heliotron (S/H) devices. In S/H configurations, since plasma pressure modifies the poloidal symmetry, development of operation scenario for high- β plasmas is required to study the β -effect on the confinement and transport. The plasma is often produced by electron cyclotron heating (ECH), and this heating scheme limits the operational magnetic field due to the resonance condition. To resolve this problem, a start-up technique using a high energy neutral beam injection (NBI) has been developed in some devices. However, experimental devices with large major radius and higher magnetic field strength are preferable for the plasma start-up by NBI alone. In order to mitigate this condition, we have developed a production method by use of non-resonant 2.45 GHz microwave, which enables us to realize the NBI plasma start-up even in the conditions of low NBI power (> 0.3 MW), low acceleration voltage (< 30 kV) and small device size (~ 1 m). Generation of relativistic electrons, which should be essential to produce the plasmas, has been confirmed experimentally with synchrotron radiation and hard X-ray emission measurements. A 0-D model analysis shows that the seed plasma has an important role in the rapid start-up. The physical processes of the rapid NBI start-up are as follows: (1) the beam ions are produced sufficiently to heat electrons by the collisions with the seed plasmas, (2) the electron heating promotes the dissociation and ionization of the deuterium molecules, molecular ions and atoms, and (3) the increase in electron density produces fast ions and heat electrons. In the successful start-up cases, the processes have a positive feedback loop, resulting that the electron temperature exceeds radiation barrier for low Z impurities. Since the beam fueling is not so effective to increase the electron density, an additional gas fueling with proper timing is required to ramp up the density under the condition that the seed plasma density is low. The key point for successful plasma start-up in the low NBI power condition is to produce the beam ions by the collisions with the seed plasmas to heat the background electrons sufficiently in the early phase of the beam injection. The pre-ionization technique developed in this study will be useful to realize the NBI plasma start-up in the low absorption power case such as the perpendicular or deuterium NBI.

Research Topics from Bilateral Collaboration Program in Heliotron J

The main objectives of the research in the Heliotron J device under this Bilateral Collaboration Program are to experimentally and theoretically investigate the transport and stability of fusion plasma in advanced helical-field, and to improve the plasma performance through advanced helical-field control. Picked up in FY2020 are the following seven key topics; (1) studies of plasma confinement improvement and related plasma self-organization through advanced helical magnetic field control, (2) study of plasma profile, plasma flow, and plasma current control for the confinement improvement, (3) study of fluctuation-structure formation and its control in plasma core region and peripheral region, (4) investigation of MHD instabilities of energetic particle modes and their control, (5) extension of high-density operation region, (6) optimization of particle supply and heating scenario, and (7) empirical research of new experimental methods and analysis methods.

Effect of magnetic configurations on energy confinement and formation of plasma structure:

The Heliotron J device has a feature of high freedom in confinement magnetic configuration. In the configuration control experiments, we have extended the bumpiness (toroidal mirror ratio) parameter in the magnetic field spectrum from the conventional low-, medium (standard)- and high-bumpiness configurations to an ultra-high-bumpiness configuration. We have measured the electron density and temperature profiles with a Nd:YAG Thomson scattering diagnostic. The injection angle and magnetic field strength are adjusted to have on-axis ECH heating, and the electron density is kept $1\text{--}1.2\times 10^{19}\text{ m}^{-3}$. The experiments have confirmed that the stored energy measured with a diamagnetic loop is the highest at the standard configuration, while the plasma profile depends on the magnetic configuration. The hollowness of the electron density profile is stronger as the bumpiness decreases. The reason may be the effect of trapped particles on radial particle transport. According to the TRAVIS ray tracing code, the ratio of the trapped electrons to the passing ones, produced by ECH is higher at a higher bumpiness configuration. Although the higher bumpiness causes a higher trapped particle population, the radial particle transport may be reduced through the bumpiness effect, resulting that the density profile is flatter.

Bumpiness dependence of electron confinement, and temperature and density distributions:

Electron internal transport barrier (e-ITB) is observed at on-axis ECH in helical plasmas. The ECH generates a radial electric field, which is determined by neoclassical transport, forming a large electron temperature gradient with the reduction in thermal transport coefficient. This phenomenon has been observed in many helical devices. On the other hand, in NBI plasmas, an ion internal transport is observed under some conditions, while no e-ITB is observed without ECH. In the Heliotron J device, we, for the first time, have observed an e-ITB in an NBI plasma without ECH. The NBI is injected tangentially in the co- and counter-directions. When a high intense gas puffing (HIGP) is applied to the NBI plasma, the electron density and stored energy increases, and the increase rate changes 20 msec after HIGP. In the core region, $r/a < 0.3$, the T_e gradient changes, and the central T_e increases up to 0.6 keV, which is typically 0.2 keV in conventional NBI plasmas. The n_e profile is not flat but peaked after the HIGP. A multi-channel AXUV diagnostic shows that the core intensity increases after the HIGP, and it is kept low at the edge region, indicating that the profile shape changes into a peaked one during the improvement phase.

Many research topics have been made progress on with collaborative researchers under Bilateral Collaboration Program in the Heliotron J project. The magnetic field configuration research including formation of a rational surface at the edge region is advanced, and the local fluctuation measurement is prepared by introducing a new beam emission spectroscopy, a Doppler reflectometer, and an upgraded Langmuir probe. A 0.7-mm ϕ pellet injector has been under operation for high-density plasmas. A laser blow-off system for the impurity transport measurement, and a multi-path Thomson scattering system for the high reliability measurement will be available soon. We will make effort to extend the plasma operation region to comprehend plasma self-organization and control instabilities according to the confinement field optimization.

(K. Nagasaki)

Research activities on QUEST in FY2020

We will summarize the activities of the Advanced Fusion Research Center, Research Institute for Applied Mechanics at Kyushu University during April 2020 – March 2021. The QUEST experiments were executed during 6th June – 28th Aug. (2020 Spring/Summer; shot no 42539–43470) and 9th Sep. – 5th Mar. (2020 Autumn/Winter; shot no 43471–45925). The main topics of the QUEST experiments in FY2020 are listed below.

- 1) Two 6 h discharges were achieved after modification of the center stack cover from the stainless steel type 316L, coated by atmospheric plasma spray tungsten (APS-W), bent in line with the circumference of the center stack, to more than 200 panels made of stainless steel type 316L. The center stack cover panels were cooled down by water-cooling channels. Wall stored hydrogen into the center stack panels was increased and wall pumping capability was significantly enhanced. Consequently, one 6h discharge could be obtained. The other was assisted by water-cooling of the hot wall located on the top side. The cooling down was executed during the discharge and clear recovery of wall pumping capability was observed.
- 2) The dependence of plasma current and electron temperature on a refractive index along the toroidal direction of the injected electron cyclotron wave (N//) was experimentally confirmed. The wave could be absorbed at higher harmonic electron cyclotron resonance. The presence of energetic electrons gave rise to enhancement of the wave absorption and efficiently drove plasma current in the case of high N//. While the wave was efficiently coupled with bulk electrons in the case of low N// and consequently high electron temperature could be achieved.
- 3) Radial distribution of atomic hydrogen flux to the walls, F, in steady-state discharges with inboard limiter configuration is measured using a reciprocate PdCu permeation probe for the first time. The F drops from 7.7×10^{16} H/m²/s in front of the radiation shield to a non-zero level of 4.3×10^{16} H/m²/s, inside the vacuum port.
- 4) The drift of the integrated signal of the magnetic sensor is the one of the most serious problems for a steady state tokamak operation.
The procedure compensating the integrated magnetic sensor signal with hall sensors has been developing based on the Cauchy condition surface method for equilibrium reconstruction of the QUEST long operation.
- 5) A CW 28 GHz is finally assembled. The output power of 400 kW is expected in the CW operation. It will be used in long-pulse discharges on plasma-wall interaction studies, as well as RF ramp-up of the tokamak plasma.
- 6) The use of liquid metals as the divertor surface materials has been receiving attention in the magnetic fusion community over the past two decades. The present work is intended to investigate the effect of forced convection on the behavior of heat transport in liquid metals such as GaInSn, safe to handle in a laboratory experiment. Data indicate that the convection induced by a JxB electromagnetic force can significantly increase the heat transport coefficient. However, it is also true that the effect of Joule heating can warm up the liquid metal. In the next fiscal year, the magnetic field will be increased so that the Joule heating effect can be controlled.
- 7) A large electrode system which can withstand high heat flux by water cooling during steady state tokamak operations at QUEST has been developed for edge voltage biasing experiments and scrape-off layer plasma measurement. Preliminary SOL measurements using the system succeeded in detecting locally the bulk electron temperature, intermittent dynamics of the high energy electron flux, and coherent and broadband fluctuation spectra of the floating potential during SSTOs.
- 8) A high-field side biased electrode configuration successfully initiated discharges in the injector region after the deployment of a new gas injection manifold that directed gas directly towards a cylindrical electrode attached to the electrode plate. There were some indications of the toroidal current persisting after the CHI

discharge was over. These results are encouraging for a planned upgrade, which involves lowering the cylindrical electrode structure closer to the CHI injector coil and further improvements to the gas injection system.

- 9) The design of the HIBP has been initiated to investigate heat and particle transport in core plasmas under controlling particle recycling. The ion species of the probe beam is cesium and the required beam energy is less than 60 keV for the toroidal magnetic field strength of 0.25 T. The observable area covers the upper half of the poloidal cross-section of plasmas.
- 10) To develop the high temperature first wall with tungsten (W) armour for the QUEST, the Advanced Multi-Step Brazing (AMSB) was applied to fabricate the prototype joint structure of W armour with a thickness of 0.254 mm and the stainless steel (SUS) substrate, in which the oxide dispersion strengthened copper alloy (ODS-Cu) with a thickness of 1 mm was inserted between W and SUS as an intermediate material. The staggered joint structure of W/ODS-Cu/SUS was successfully obtained by AMSB. Each joint interface showed no sign of exfoliations and macro defects. The hydrogen retention properties will be confirmed in the 2021 fiscal year.
- 11) A magnetic probe that is suitably designed for measuring ECH generated plasma at QUEST has been examined to investigate magnetic phenomena during plasma equilibration and various plasma instabilities. The growth of flux during current ramp-up was detected by the probe, in which a vertical shift of the current with flux perturbation was also observed in the measurement data.
- 12) A layered material with tungsten coating and a substrate of type 316 stainless steel was prepared by hot rolling. Small samples prepared from the rolled sheet were installed and exposed to plasma in the 2020 spring/summer experimental campaign of QUEST. No thick deposition layer was formed on the plasma-exposed surfaces of the samples. However, impurities such as oxygen and carbon were found around scratch marks formed by the rolling. Surface finishing seems to be important for controlling plasma-surface interaction of a rolled material.
- 13) Increasing the operation days of the Thomson scattering system was an important issue to be solved. Two members of joined the Thomson scattering team, and they contributed to the operation, the calibration and the analysis. As a result, the plasma measurement days increased from 15 days in AY2019 to more than 40 days in AY2020. Remote participation from the University of Tokyo was tested using a VPN, in which monitors and windows necessary for the operation and analysis were shared successfully.
A laser beam position monitor system was tested and the best optical configuration was found.
- 14) On CT injection at QUEST, a new drift tube, inside of which is a CT guiding tube made of OFC-Cu, has been prepared to improve CT transport and fueling efficiency. The performance of the Cu tube was numerically verified, resulting in substantial improvement. A verification experiment has been also planned to be carried out with a small size plasma gun at Univ. Hyogo.
- 15) In order to apply the framework developed for a carbon divertor in the LHD to QUEST, we implemented the tungsten EAM potential developed by L.-F. Wang *et. al.* (L. F. Wang, *et. al.*, J. Phys. Condens. Matter 29, 435401 (2017)) into the hydrogen recycling model. The developed model was employed to estimate the release time of hydrogen atoms and molecules from the tungsten wall. The simulation results show that, similar to carbon walls, the release of molecular hydrogen takes longer than the release as atoms.

Kazuaki Hanada (Kyushu University) 1), 2)
Arseniy Kuzmin (Kyoto University) 3)
Manabu Takechi (QST) 4)
Hiroshi Idei (Kyushu University) 5)
Yoshihiko Hirooka (Chubu University) 6)
Yoshihiko Nagashima (Kyushu University) 7)
Roger Raman (University of Washington) 8)

Takeshi Ido (Kyushu University) 9)
Masayuki Tokitani (NIFS) 10)
Kengoh Kuroda (Kyushu University) 11)
Yuji Hatano (University of Toyama) 12)
Akira Ejiri (University of Tokyo) 13)
Naoyuki Fukumoto (University of Hyogo) 14)
Seiki Saito (NIFS) 15)

(K. Hanada)

University of Toyama

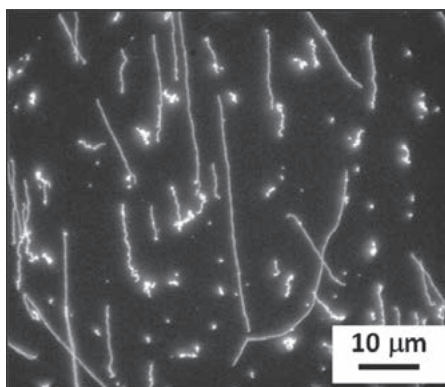


Fig. 1 Fluorescence image of genome-sized DNA molecules of T4 GT7 bacteriophage. The rate of double strand breaks was evaluated by measuring the change in the lengths of DNA molecules after immersion in tritiated water.

Highlight

Research Activities in Hydrogen Isotope Research Center, Organization for Promotion of Research, University of Toyama

A simple experimental system to examine the rate of double strand breaks (DSBs) of genome-sized DNA molecules in tritiated water under well-controlled conditions was established for the validation of computer simulation on interactions of biomolecules and ionizing radiation. No noticeable irradiation effects were observed at a tritium (T) concentration of 1300 Bq/cm^3 , indicating that the effects of β -ray irradiation were far smaller than those of oxidation and/or thermal motion at the low dose rate ($43 \mu\text{Gy/h}$). Radiation-induced DSBs were clearly recognizable at high T concentrations of $4.0\text{--}5.2 \text{ MBq/cm}^3$. The dependence of the DSB rate on water temperature and DNA concentration was examined by using the high concentration tritiated water.

[Double-strand breaks in a genome-sized DNA caused by beta-ray under cellular environment (T. Kenmotsu, Doshisha U.)]

Tritium Transport in Fusion Reactor Materials: Development of T removal technique from plasma-facing materials (PFMs) after the service in a fusion reactor is important for safe and cost-effective disposal. Lattice defects induced by neutron irradiation in tungsten (W) act as traps against hydrogen isotopes. Hence, it is important to understand the influence of radiation-induced defects on T removal efficiency. For this purpose, T release from a W sample irradiated with heavy ions was examined in this study. A plate of W was irradiated with 6.4 MeV Fe ions to 0.5 displacement per atom (dpa) at the damage peak at 500 °C, using the accelerator DuET at Kyoto University to simulate neutron irradiation effects. The depth of the damaged zone was about 1.1 μm. The irradiated and non-irradiated samples were exposed to DT mixture gas (4% T) at 500 °C. Then, the sample was heated under Ar gas flow sequentially to 200–500 °C.

The released T was collected in water bubblers and its amount was evaluated using a liquid scintillation counter. Non-destructive depth profiling of T was performed using β-ray induced X-ray spectrometry and Monte Carlo simulation, considering generation and attenuation of X-rays in the sample and Ar gas. The fraction of hydrogen isotopes to W in the damaged zone reached $([D]+[T])/[W] = 7 \times 10^{-4}$, while that in the non-irradiated sample was $\sim 10^{-7}$. As shown in Fig. 2, the detrapping rate of T from irradiated W was comparable with that of the non-irradiated sample, indicating that the detrapping of T from radiation-induced defects was negligibly small at 250 and 300 °C. The significant T release from the damaged zone started at 400 °C. A sharp concentration gradient of T was developed in the damaged zone during T release, indicating the rate of T release was controlled by a diffusion process under the trapping effects. The majority of T was released not as HT but as HTO via isotope exchange with moisture in Ar gas. In addition, T permeation experiments through a metallic wall from and to high temperature, high pressure water was started to examine T transport to coolant water in a future fusion reactor.

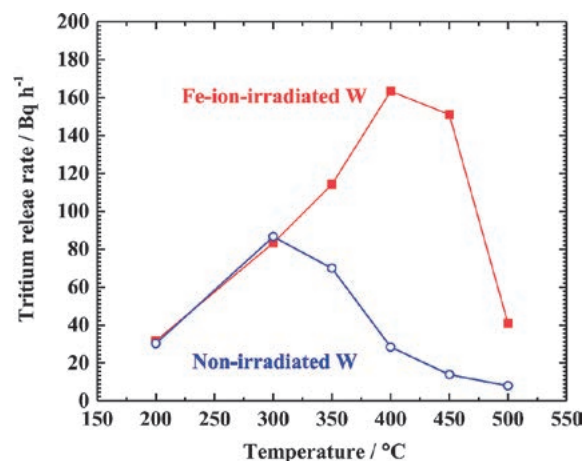


Fig. 2 Tritium release rate from W sample damaged with 6.4 MeV Fe ions to 0.5 dpa and non-irradiated W sample during heating under Ar gas flow.

Other experimental studies performed in the Hydrogen Isotope Research Center in the fiscal year 2020 are the followings:

- *Hydrogen isotope transport through plasma modified fusion reactor materials* (H. T. Lee, Osaka U.);
- *High temperature and high flux irradiation effect on hydrogen isotope retention in damaged W* (Y. Oya, Shizuoka U.);
- *Hydrogen isotope exchange on metallic plasma facing walls* (N. Ashikawa, NIFS);
- *Tritium retention on facing materials modified by plasma wall interactions* (K. Tokunaga, Kyushu U.);
- *Synergistic effects of bulk helium and damages on hydrogen isotope retention behaviors in plasma facing materials* (F. Sun, Shizuoka U.);
- *Application of GD-OES analysis to efficient grasping major controlling factors of complicate PWI in high-temperature plasma confinement devices* (N. Yoshida, Kyushu U.);
- *Evaluation of hydrogen isotope retention and release of SiC and SiC/SiC composite* (H. Kishimoto, Muroran Inst. Technol.);
- *Gamma-ray irradiation effect on hydrogen isotopes at fusion material surfaces* (T. Chikada, Shizuoka U.);
- *Suppression of tritium permeation in metals by laser-doping of impurities* (Y. Nobuta, Hokkaido U.); and
- *Development of high concentration tritium heavy water and monitoring of the concentration* (Y. Arikwa, Osaka U.).

(Y. Hatano, University of Toyama)

8. Activities of Rokkasho Research Center

At Rokkasho village in Aomori Prefecture, the International Fusion Energy Research Centre (IFERC) project and the International Fusion Materials Irradiation Facility/Engineering Validation and Engineering Design Activities (IFMIF/EVEDA) project have been conducted under the Broader Approach (BA) agreement between the EU and Japan from June 2007, in order to complement ITER and to contribute to an early realization of the DEMO reactor. The roles of the NIFS Rokkasho Research Center (RCE) established in May 2007 are to assist NIFS and universities to cooperate with those activities, and to prepare the environment for promoting various collaborative research including technology between activities at Rokkasho and at universities. As cooperation activities, the head of the NIFS RCE is undertaking tasks as the IFERC Project Leader (PL) from September 2010 to June 2020 and is undertaking tasks as the IFERC Deputy PL (D-PL) from July 2020 (the role of PL is to coordinate the activities by EU and JA implementing agencies and the role of D-PL is to support PL). Moreover, the head of the NIFS RCE is working as the leader of the general coordination group of the Joint Special Team for a Demonstration Fusion Reactor (DEMO) design, which is the organization set in May 2015 for establishing technological bases required for the development of DEMO as an all-Japan collaboration.

BA activities have two Phases; BA Phase I from June 2007 to March 2020 and BA Phase II from April 2020 to March 2025 or later. As reported in the NIFS annual report 2019, all the planned activities of IFERC project in the BA Phase I have been completely accomplished on time and on budget. The results were disseminated as the peer-reviewed papers (557 papers for DEMO Design, 304 papers for DEMO R&D, 693 papers for CSC [Computational Simulation Centre] and 8 papers for REC [ITER Remote Experimentation Centre]). Also, all the contributions by both EU and JA have been completely accomplished on time and on budget. After BA Phase I, the BA Phase II started in April 2020 seamlessly, and the purpose of IFERC project was re-defined by BA Steering Committee (BA SC) so as to provide support for ITER, and other BA projects such as IFMIF/EVEDA and Satellite Tokamak Programme (STP) and to consolidate know-how for future fusion reactors through the production of databases, inputs to engineering hand books, and review of lessons learned in the existing fusion projects.

The 2020 JFY (from April 2020 to March 2021) has been a year of re-organization to orient IFERC activities following the priorities given by BA SC for BA Phase II mentioned above. Hereafter, the outline is described very briefly sub-project by sub-project.

Regarding CSC activity in 2020, the IFERC Project Team (PT) and the IFERC HPC Follow-up working group conducted preparation and signature of a Procurement Arrangement (PA), exploitation of the resources provided by JA on JFRS-1 as “host contribution” for 2 years, preparation for possible joint procurement of High Performance Computer (eventually, it was concluded that there was no advantage to a joint procurement), preparation for collaboration with IO, and organization of 2 workshops on simulation projects using resources provided.

As for DEMO Design activity in 2020, despite COVID difficulties, the activities took place on sharing of information/results of major reviews (the first DEMO gate review in EU and first C&R in JA) and on planning of 8 design tasks including joint activities and development of a Work Breakdown Structure (WBS). The eight tasks are 1) Plasma scenario development, 2) Divertor and power exhaust, 3) Breeding blanket design and tritium extraction and removal, 4) Remote maintenance, 5) Safety, 6) System codes, 7) Superconducting magnets, and 8) Balance of Plant (BoP) and plant system, where the first five items have high priority, and are directly relevant for ITER and JT-60SA exploitation so joint work is foreseen in these areas. In addition, on the last three items information will be exchanged to share the whole view of DEMO.

As to DEMO R&D activity in 2020, the preliminary research and the detailed planning for 4 year activities have been performed for four task areas: 1) R&D on Tritium Technology, 2) Development of Structural Material for Fusion DEMO In-Vessel Components, 3) Neutron irradiation experiments of Breeding Functional Materials (BFMs), and 4) Development of material corrosion database. Based on such preliminary research and detailed planning for 4 year, 4 new PAs were completed with WBS, responsible people identified, schedule refined, detailed research plan.

In 2020, the REC activity has gained visibility and urgency due to the COVID 19 pandemic situation. The REC activity consists in the collaboration with ITER Organization (IO), with IFMIF/EVEDA and with STP. Regarding collaboration with IO, a kick-off meeting to discuss the collaboration between IO and IFERC-REC was held in Jan. 2020 with ITER CODAC staff in Rokkasho, based on the “Cooperation Arrangement between the BA activities and the ITER project” signed in Nov. 2019. After these activities, in 2020, one PA was signed on Oct. 2020 for the procurement of equipment and services to implement the collaboration with IO (Note that in June 2021 the Implementing Arrangement No.2 corresponding to the above Cooperation Arrangement has been signed). Concerning the collaboration with IFMIF/EVEDA, the support to implement remote participation for the Linear IFMIF/EVEDA Prototype Accelerator (LIPAc) is ongoing. In March 2020, a Central Control Room (CCR) for LIPAc was completed in the REC Building and used now as shown below.



Collaboration of IFERC with IFMIF/EVEDA for remote participation in LIPAc

Technical Coordination Meeting (TCM) was held twice for the definition of activities, and one PA was completed for preparatory activities (planning and definition of collaboration with IFMIF/EVEDA), and the 2nd PA is in preparation. Joint Task Force is actively working on providing immediate remote access to LIPAc data for commissioning purposes, and long term solutions under study. As to collaboration with JT-60SA, IFERC Integrated PT has given feedback to STP on current remote access for system commissioning, and discuss proposals for further collaboration

The head of NIFS RCE is also undertaking the role of the leader of the general coordination group of the Joint Special Team for a DEMO design. Since the collaboration among many researchers from NIFS and other institutions and technicians from companies is indispensable for the conceptual design of DEMO reactor, the head of the NIFS RCE tries to work as a coordinator.

In summary, the NIFS RCE contributes widely not only to the success of ITER but also to the realization of fusion energy through the continuous efforts mentioned above.

(N. Nakajima)

9. Research Enhancement Strategy Office

The Research Enhancement Strategy Office (RESO) was founded in October 2013, and three University Research Administrators (URAs) were assigned. Under the Research Planning Task Group, the following four Task Groups were organized.

- (1) Collaboration Research Enhancement Task Group
- (2) Young Researchers Development Task Group
- (3) Public Relations Enhancement Task Group
- (4) IR(Institutional Research)/Evaluation Task Group

(1) The collaborative research activities

1) Enhancing international collaborative research in the stellarator-heliotron (S-H) plasma, and steady-state operation (SSO) toward a fusion reactor

Wendelstein 7-X (W7-X) of the Max Planck Institute of Plasma Physics (IPP) at Greifswald in Germany was upgrading for the water-cooled divertor from November 2018. In 2020, a joint research between NIFS and IPP, such as commissioning of diagnostics installed by NIFS was conducted mainly by remote communication/participation tools as a countermeasure for the COVID-19 pandemic.

Collaborative research was also enhanced with PPPL, the University of Wisconsin and University of California, Irvine in the United States, CIEMAT in Spain, CEA in France, CONSORZIO RFX in Italy, Culham Centre in the United Kingdom, University of Belgrade in Serbia, and Peking University and Southwest Jiaotong University (SWJTU) in China. Renewing of the collaboration agreement with the ITER Organization was under progress to be signed in early 2021.

2) Promoting establishment of Agreements with Asian institutes to accelerate collaborative research

In order to enhance helical and stellarator research in Asian countries, the Chinese First Quasi-axisymmetric Stellarator (CFQS) project between NIFS and SWJTU and an international research collaboration between NIFS and Peking University has been promoted. In the CFQS project, fabrication of mock-up coils was successfully completed. The fabrications of the first modular coil (MC4) and the vacuum chamber have been started. As the collaboration between NIFS and Peking University, the design of the Time-of-Flight neutron spectrometer (TOFED) was completed for LHD. The construction of TOFED was initiated in 2019. Commissioning of the TOFED is ongoing.

(2) Supporting young researchers

In the activities for supporting young researchers, international collaboration activities of young researchers were encouraged, enhancing their basic research skills. RESO supported the international collaboration plans proposed by young researchers in NIFS. Applications were reviewed by the Young Researchers Development Task Group. One program was supported in FY2020 as follows.

1. Experimental study of the turbulent transport in TCV tokamak in Lausanne University.

RESO also assisted with the applications of young scientists to the 'Grants-in-aid Scientific Research' program. About 70 application documents were reviewed and suggestions were given to the authors for improvement.

(3) Enhancing public relations

1) Dissemination of research achievements through EurekAlert!

Three topics were released: i) “An accurate simulation of high-pressure plasma for an economical helical fusion reactor,” ii) “Weight reduction of fusion reactor components –Design optimization using a topology optimization technique-” and iii) “Development of a broadband mid-infrared source for remote sensing.” These topics were released to the media in Japan, too. Some topics attracted attention from the international media.

2) Information release about NIFS and fusion science

RESO participated in the AAAS annual online meeting and introduced NIFS and the research results in the virtual form in collaboration with other Japanese institutes, 8–11 February 2021.

3) Outreach activities based on the fusion community

RESO joined the discussion of the fusion science outreach headquarters with QST, universities and the Ministry of Education, Culture, Sports, Science and Technology.

4) Others

RESO introduced interesting science topics to the public on the occasion of the science talk of at the Open Campus Online of NIFS shown in the Figure 1.

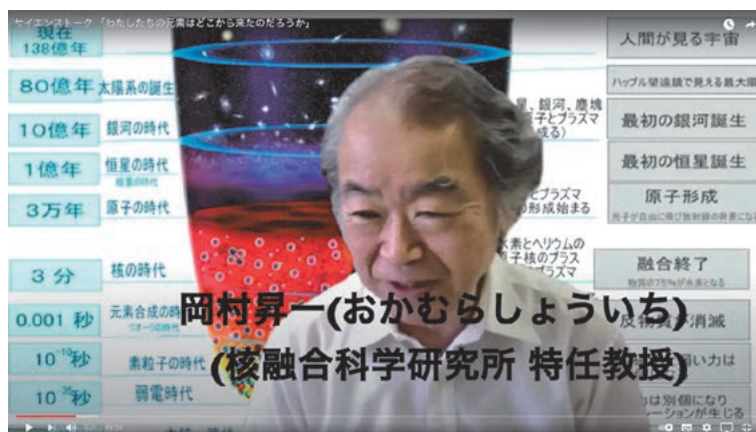


Fig. 1 The science talk at the Open Campus Online of NIFS.

(4) IR/Evaluation activities

The task group for the IR (Institutional Research) and evaluation continued its role to make systematic analyses of the present research activities of the institute. The statistical data of the publications and the scientific reports were collected using the NIFS article information system (NAIS) with complementary data obtained through SCOPUS and WoS public research resource supplying companies. The outcome results of the collaboration activities were collected through the annual collaboration reports of NIFS.

(T. Muroga, S. Okamura, T. Nishitani and K. Yaji)

10. The Division of Health and Safety Promotion

The Division of Health and Safety Promotion is devoted to preventing work-related accidents, to ensuring safe and sound operation of machinery and equipment, and to maintaining a safe and healthful environment for researchers, technical staff, coresearchers, and students. This division consists of ten offices, and various subjects related to the health and safety are discussed by office chiefs once in a month.

1. Environmental Safety Control Office

This office has the responsibility to maintain a safe workspace and environment.

- A) Management to solve the problems pointed out by the safety and health committee.
- B) Maintenance of the card-key system for the gateways of controlled areas.
- C) Maintenance and management of the vehicle gate at the entrance of the experimental zone.
- D) Maintenance of the fluorescent signs of the evacuation routes and the caution marks.
- E) Management of sewage drainage from the NIFS.

2. Health Control Office

The main role of this office is to keep the workers in the institute healthy, including co-researchers and students.

- A) Medical checkups both for general and special purposes and immunization for influenza.
- B) Mental health care services and health consultation.
- C) Accompany the inspections of the health administrator and the occupational physician.
- D) Maintenance of AEDs.
- E) Alerts and response to the COVID-19.

Various lectures were held for physical and mental health. An online stress-check was held in October 2020.

3. Fire and Disaster Prevention Office

The main role of this office is to prevent or minimize damage caused by various disasters.

- A) Making self-defense plans for fires and disasters, and implementation of various training.
- B) Promotion of first-aid workshops and the AED class.
- C) Maintenance of fire-defense facilities and attending on-site inspections by a local fire department.
- D) Review and update disaster prevention rules and disaster prevention manuals.

All workers must attend the disaster prevention training held every year (Fig.1).



Fig. 1 Fire extinguisher training

4. Radiation Control Office

The main role of this office is to maintain radiation safety for researchers and the environment. Legal procedures for radiation safety and regular education for the radiation area workers are also important roles of this office.

- A) Maintain radiation safety for the workers.
- B) Registration and dose control of radiation area workers.
- C) Observation of radiation in the radiation-controlled area and the peripheral area.
- D) Maintenance of the radiation monitor.
- E) Applications for radiation equipment to the national agencies and the local governments.
- F) Revise official regulations and establish new rules.

An educational lecture for the radiation area workers was held on March 4, 2021. We prepared an opportunity of the DVD viewing for an absentee. Non-Japanese workers were educated and trained in English.

5. Electrical Equipment and Work Control Office

The main role of this office is to maintain electrical safety for researchers, technical staff members and students.

- A) Check and control the electrical facilities according to the technical standards.
- B) Safety lecture for researchers and workers.
- C) Annual check of the electric equipment during a blackout.

The annual inspection of the academic zone was carried out on May 23, 2020, and that of the experimental zone was carried out on June 13 and June 14, 2020.

6. Machinery and Equipment Control Office

The main role of this office is to maintain the safe operation of cranes. The tasks of this office are as follows.

- A) Inspection and maintenance of cranes.
- B) Management of the crane license holders and safety lectures for the crane users.
- C) Schedule management of crane operations.

7. High Pressure Gas Control Office

The main role of this office is for safety operation and maintenance of high pressure facilities with cooling system such as LHD.

- A) Safety operation and maintenance of high-pressure gas handling facilities in NIFS.
- B) Daily operation, maintenance, system improvement, and safety education according to the law.
- C) Safety lectures for researchers and workers.

8. Hazardous Materials Control Office

The main role of this office is the management of the safe treatment of hazardous materials and maintaining safety for researchers against hazardous events.

- A) Research the requests for hazardous materials and the storage status.
- B) Management to ensure safe storage of the waste.
- C) Monitoring of discharging water to prevent water pollution.
- D) Implementation of chemical substance risk assessment.

9. New Experimental Safety Assessment Office

The main role of this office is to check the safety of experimental devices except for LHD. For this purpose, researchers who want to setup new experimental apparatus must apply for the safety review. Two reviewers are assigned from members of this office and other specialists and check the safety of these devices.

- A) Examine new experiments for safety problems and advise on safety measures.
- B) Improve safety in each experiment and reinforce the safety culture at NIFS by annual reviews by NIFS employees.

10. Safety Handbook Publishing Office

The tasks of this office are to publish the Safety Handbook in Japanese and in English, and it is updated every year. The regular safety lectures were held on May 14, 2020. All workers including the co-researchers and students must attend this safety lecture every year.

(S. Sakakibara)

11. Division of Deuterium Experiments Management

The deuterium experiment has been carried out on LHD since March 7, 2017. Objectives of the deuterium experiments are (1) to realize high-performance plasmas by confinement improvement and by the improved heating devices and other facilities, (2) to explore the isotope effect study, (3) to demonstrate the confinement capability of energetic particles (EPs) in helical system and to explore their confinement studies in toroidal plasmas, and (4) to proceed with the extended studies on Plasma-Material Interactions (PMI) with longer time scales.

The division of deuterium experiments management was founded to establish the safety management system and to consolidate experimental apparatus related to the deuterium experiments. After the start of the deuterium experiment on the LHD, the function of this division was shifted to the management of the safe and the reliable operation of the deuterium experiment. Under this division, a taskforce named 'Deuterium experiment management assistance taskforce' was established. The main jobs of the taskforce were (1) the establishment and improvement of manuals to operate LHD and peripheral devices safely during deuterium experiments, (2) check and improvement of the regulations related to proceeding with the deuterium experiments safely, (3) the upgrade of the LHD itself, its peripheral devices and the interlock systems for safe operation during the deuterium experiments, (4) upgrade and optimization of heating devices and diagnostic systems for the deuterium experiments, (5) remodeling the LHD building and related facilities, and so on. These jobs are proceeding with the cooperation with the LHD board meeting and the division of health and safety promotion. In addition, the necessary tasks related to the safety evaluation committee founded by NIFS and those related to the safety inspection committee for the National Institute for Fusion Science (NIFS) founded by local government bodies are proceeding in this division. The publication of an annual report for the radiation management of the LHD deuterium experiment is another important task of this division.

During the fiscal year of 2019, the safety evaluation committee meeting was held three times. The main topic of the committee is the evaluation of the annual report for the radiation management at the deuterium experiment and the evaluation of the safety operation of the deuterium experiment in the experiment campaign of 2019. In addition, the prospect for the next three years of the deuterium experiment was discussed.

The cooperation of the safety inspection committee for NIFS, which is organized by the local government bodies, such as Gifu-prefecture, Toki-city, Tajimi-city, and Mizunami-city, is an important task for the division of the deuterium experiments management. The environmental neutron dose monitoring at NIFS and the tritium concentration monitoring in the environmental water around NIFS has been performed by the committee since 2015. In 2019 FY, these monitoring activities were performed twice as scheduled under the cooperation with the division of the deuterium experiment management.

a)



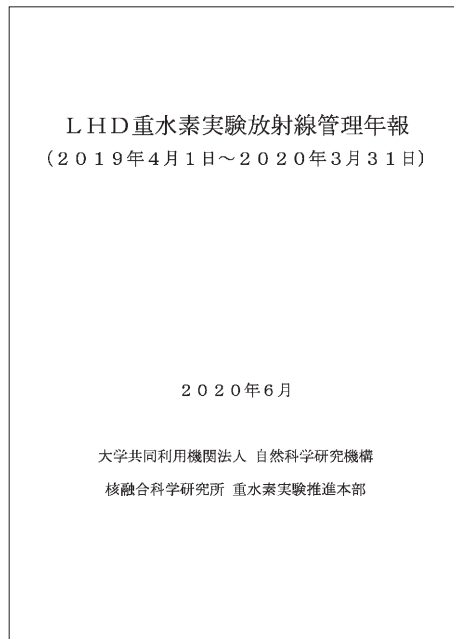
b)



c)



d)



(a) The photographs at the environmental water sampling with the secretariat of the safety inspection committee. (b) The real-time radiation monitoring post where the cooperative environmental neutron monitoring is performed with the secretariat. (c) Additional neutron dosimeters placed by the secretariat of the safety inspection committee (left) and by the division of deuterium experiment management (right) near the radiation monitoring post at the cooperative environmental neutron monitoring with the secretariat. (d) The front cover of the annual report for the radiation management at the first LHD deuterium experiment (written in Japanese).

(M. Osakabe and M. Isobe)

12. Division of Information and Communication Systems

The Department of Information and Communication System (ICS) was founded in 2014 in order to develop and maintain the information and network systems of NIFS efficiently. All of the information system experts in NIFS belong to the ICS. There are one office and four TASK groups which correspond to the job classifications in NIFS. The Information Security Office, established in 2020, oversees the overall information security of the institute. The Network Operation task group manages and maintains the communication systems in NIFS, such as the E-mail system including security issues. The Experimental Data System task group performs operation and development of data acquisition systems for the LHD experiment. The Backbone Information Systems task group, which was created by merging the Institutional Information Task Group and Integrated ID management and Authentication System task group in 2020, carries out the maintenance and development of the management systems for collaboration research and its output. The Atomic and Molecule Database task group maintains the atom and molecule database which is open to researchers around the world.

The ICS works as follows: the request for the maintenance, improvement, and development of the information and communication system from each section is submitted to the ICS. The deputy division directors of ICS check all the requests, establish the priority among them, and assign them to the appropriate Task Group. Because all the experts belong to the Technical Service Section of ICS, each Task Group Leader asks the Section Leader to allot the required number of experts for a prescribed period of time so as to finish the job.

In NIFS, three research projects extend across the research divisions. It can be said that the ICS is another “project” which lies across all the divisions in the institute for keeping the information and communication systems stable, secure, and up-to-date.

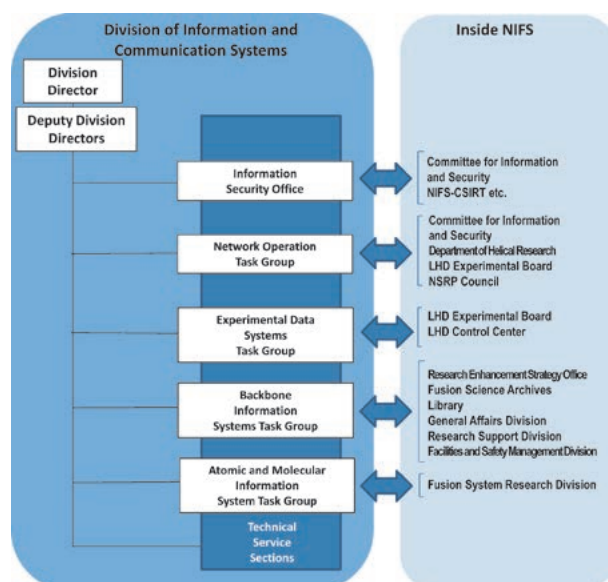


Fig. 1 Structure of Division for Information and Communication Systems.

Migration of e-mail service to Gmail and Google Groups

The mail service of the National Institute for Fusion Research (NIFS) had been operated by on-premises servers consisting of MailSuite and DeepAnchor of Qualitia (then DEEPSOFT) running on a virtual server system, and a secondary server built on Linux server. DeepAnchor provides a variety of services, but we used it to convert large attachments into a URL for the download.

As the maintenance period of MailSuite expires at the end of FY2020, we decided to adopt Google Gmail as the next mail system based on various conditions such as spam filters, stability of e-mail transmission, convenience, and incident cases.

The operation start time of Gmail was set to the beginning of August 2020 in consideration of the influence on the plasma experiment of NIFS. A migration period of about one month was set so that the migration of the mail system would not be concentrated at a certain point but could be done at the user’s convenience. During the transition period, new mail was delivered to both the old and new systems, so that there would be no interruption in business operations regardless of which system was used.

In order to carry out the migration work in a short period of time, it was decided that the administrators would treat almost all of the migration work of Gmail and Google Group, the mailing list, in order to reduce the time required for explanations and inquiries to the users. In order to carry out these migration tasks, a special team was formed within the Information and Communication Systems Department.

The two-step authentication is mandatory for Gmail in the same way of MailSuite, and as the second factor, we encouraged users to select multiple options from voice guidance over the phone, SMS to their smartphones, and authentication applications (Google Authenticator). In addition, a YubiKey was procured and distributed to all users for whom did not have or did not want to use a smartphone or for their backup. All users were able to complete the two-step verification within the scheduled period.

Currently, Gmail and Google Groups are operating without problems along with other G Suite apps.

Backbone Information Systems Task Group

Two task groups in the Division of Information and Communication Systems, that is the Institutional Information Systems task group (IIS-TG) and the Integrated ID Management and Authentication System task group (IDMAS-TG), are evolutionally merged into the Backbone Information Systems Task Group (BIS-TG) in April 2020. Japanese name of the task group is '*Kikan-Joho*', which is the same pronunciation as of IIS-TG.

In May of 2020, NIFS changed the license plan of Microsoft products from OVS-ES to EES. To adapt the EES, BIS-TG established a regime for user administration under Azure Active Directory. On the ramp-up period, existing user account was exported from the email system operated by the NetTG and imported into Azure AD via a web interface and customized with use of PowerShell scripts. This enables cloud-based Microsoft 365 services such as Microsoft Teams, OneDrive for Business, Yammer and so on, which is suitable for the COVID-19 situation.

BIS-TG develops *JUOE* system and deploys in March 2021. This web-based system intends to support workflows related to the Joint Use of Measurement Instruments program and is expected to reduce complicated coordination works.

Major services provided by BIS-TG are the followings:

NAIS (NIFS Article Information System): accumulates information of research achievements made by NIFS staffs and the collaborators. This system is used also for an internal approval for publication/presentation. It becomes one of essential information systems supporting research activities in NIFS. The total number of registered records at the end of the fiscal year was about 17,000.

Icarus and Workshop: a web-based online service for assisting various host operation to hold international conferences and for hosting relatively small workshops/meetings, respectively. 'Workshop' system was used by 20 workshops/meetings in FY2020.

GakuNin: the academic access management federation consisting of universities and academic institutes in Japan. NIFS joined in FY 2017. The status of the service in NIFS is experimental.

Eduroam: a world-wide Wi-Fi roaming infrastructure. NIFS joined in FY 2018. BIS-TG provides a user authentication function for Eduroam.

Colid: an ID management system for collaborators of NIFS research collaboration program, which is based on SAML under Shibboleth IdP and LDAP similar to GakuNin. This service is utilized for information disclosure to collaborators via web sites.

(S. Ishiguro)

13. International Collaboraiton

Many research activities in NIFS are strongly linked with international collaborations with institutes and universities around the world. These collaborations are carried out in various frameworks, such as 1) coordination with foreign institutes, 2) bilateral coordination with intergovernmental agreements, and 3) multilateral coordination under the International Energy Agency (IEA).

The coordination with foreign institutes is important as a basis of collaborative research. From 1991, NIFS concluded 32 coordination through FY2019.

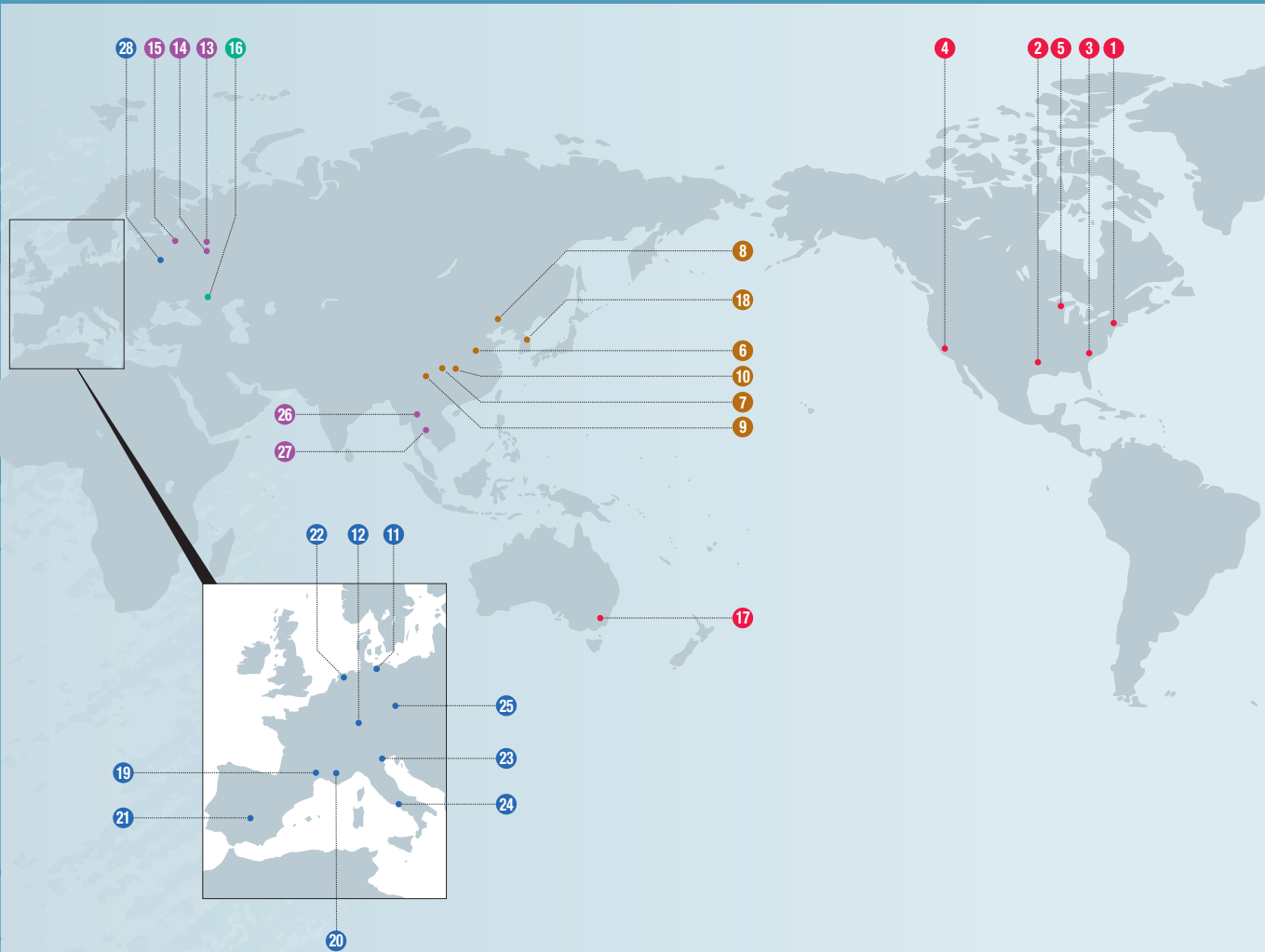
NIFS is the representative institute for the three bilateral coordination with intergovernmental agreements (J-US, J-Korea, and J-China), and for the four multilateral coordination under the IEA (Plasma Wall Interactions (PWI), Stellarator-Heliotron concept, Spherical Tori, and Steady State Operation). For the three bilateral coordination, and the multilateral coordination PWI Technology Collaboration Program (TCP), NIFS coordinates the collaborative research not only for NIFS researchers, but also for researchers in universities. The activities of the bilateral and the multilateral coordination activities are reported in the following subsections, respectively.

Since the beginning of 2020, for the COVID-19 pandemic, social activities have been strongly limited to prevent the outbreak of COVID-19 all over the world. Many of international activities with personal exchanges could not be conducted, and many of international conferences were postponed or held online. For example, IAEA FEC planned to be held in October 2020 was postponed to May 2021. Online communications drastically increased, and people became very familiar with such communications though the time difference is a serious problem to hold an international online conference.

Under such situation, the 29th International Toki Conference on Plasma and Fusion Research was held in Toki, Japan on 27–30 October 2020, and NIFS hosted the meeting. More than 220 researchers from 11 countries participated. For reducing the risk of the expansion of COVID-19, the conference was held under online connection for video conferencing.

(S. Masuzaki)

Academic Exchange Agreements



- U.S.A.** 1 Princeton Plasma Physics Laboratory (PPPL)
 - 2 Institute for Studies, The University of Texas at Austin (IFS)
 - 3 Oak Ridge National Laboratory (ORNL)
 - 4 Center for Energy Science and Technology Advanced Research, University of California, Los Angeles (UCLA)
 - 5 College of Engineering, University of Wisconsin, Madison
 - China** 6 Institute of Plasma Physics, Chinese Academy of Sciences (ASIPP)
 - 7 Southwestern Institute of Physics (SWIP)
 - 8 Peking University
 - 9 Southwest Jiaotong University (SWJTU)
 - 10 Huazhong University of Science and Technology
 - Germany** 11 Max Planck Institute for Plasma Physics (IPP)
 - 12 Karlsruhe Institute of Technology (KIT)
 - Russia** 13 Russian Research Center, Kurchatov Institute (KI)
 - 14 A. M. Prokhorov General Physics Institute, Russian Academy of Sciences (GPI)
 - 15 Peter the Great St. Petersburg Polytechnic University
 - Ukraine** 16 National Science Center of the Ukraine Khar'kov Institute of Physics and Technology Institute of Plasma Physics (KIPT)
 - Australia** 17 Australian National University (ANU)
 - South Korea** 18 National Fusion Research Institute (NFRI)
 - France** 19 Aix-Marseille University (AMU)
 - 20 Commissariat à l'énergie atomique et aux énergies alternatives (CEA)
 - Spain** 21 National Research Center for Energy, Environment and Technology (CIEMAT)
 - Netherlands** 22 Dutch Institute for Fundamental Energy Research (FOM)
 - Italy** 23 CONSORZIO RFX
 - 24 Institute of Ionized Gas (IGI)
 - Czech** 25 HiLASE Center, Institute of Physics CAS (FZU)
 - Thailand** 26 Chiang Mai University
 - 27 Thailand Institute of Nuclear Technology (TINT)
 - Poland** 28 Institute of Plasma Physics and Laser Microfusion (IPPLM)
- The ITER International Fusion Energy Organization (ITER)

US – Japan (Universities) Fusion Cooperation Program

The US-Japan Joint Activity has been continued from 1977. The 41th CCFE (Coordinating Committee for Fusion Energy) meeting was held on March 11, 2021 via televideo conference system. The representatives from the MEXT, the DOE, Universities and Research Institutes from both Japan and the US participated. At the meeting, the current research status of both countries was reported together with bilateral technical highlights of the collaborations. The FY 2020 cooperative activities were reviewed, and the FY 2021 proposals were approved. It should be noted that because of COVID-19 pandemic, most of the personnel exchange and workshops were cancelled. However, some collaborative activities were maintained by remote participation and web meetings.

Fusion Technology Planning Committee (FTPC)

In this category of the US-Japan collaboration, there are six research fields, namely, the superconducting magnets, low-activation structural materials, plasma heating related technology, blanket engineering, in-vessel/high heat flux materials and components, and power plant studies and related technologies. In usual years, personal exchanges are conducted and workshops are held in these research fields. However, in the fiscal year FY2020, due to the spreading of the COVID-19 pandemic, all the programs were either differed or canceled, including four J-to-US personal exchanges (differed), one J-to-US personal exchange (canceled), three US-to-J personal exchanges (differed), one J-to-US workshop (differed), and one US-to-J workshop (differed). For all these activities, information exchanges were done among responsible members and participants via e-mails and/or video conferences to make agreement about resumption of each program in the coming fiscal year FY2021.

Fusion Physics Planning Committee (FPPC)

In the area of fusion physics, 2 committee meetings and 11 personnel exchanges were performed remotely, amid the COVID-19 pandemic. However, due to travel restrictions, 3 Workshops and 13 personnel exchanges



Fig. 1 (a) “Virtual” LHD Control Room (b) “Vacant” DIII-D Control Room during operation.

from the JA to U.S. were deferred to next FuY. In spite of the unusual situation in this year, scientists from both sides have endeavored to continue their collaborative research activities. Some experiments were carried out with remote participation enabled by new tele-communication tools and data transport systems.

Joint Institute for Fusion Theory (JIFT)

Most plans of workshops and personal exchanges that had been scheduled for the 2020–2021 JIFT programs were changed due to the influence of COVID-19. Three workshops “US-Japan collaborations on co-designs of fusion simulations for extreme scale computing,” “Theory and simulation on the high field and high energy density physics,” and “Progress on advanced optimization concept and modeling in stellarator-heliotrons” were decided to be postponed to 2021–2022 based on online discussions among corresponding organizers. In the category of personnel exchanges, ten programs were also decided to be postponed to 2021–2022 by online discussions between corresponding researchers. A personnel exchange program for a Visiting Professor on “Electromagnetic turbulence in fusion plasmas” was carried out as a remote program in which online discussions were made for presenting collaborative research results in the APS DPP Annual Meeting and the journal Nuclear Fusion. Another personnel exchange program on “Kinetic-MHD hybrid simulations of energetic-particle driven instabilities” was also carried out as a remote program in which discussions on a simulation code benchmark study for kink and fishbone instabilities in a tokamak plasma were made by email. At the JIFT Steering Committee meeting that was held using Zoom on November 19, 2020, the status of JIFT activities for 2020–2021 was reviewed and the recommendation plans for 2021–2022 were discussed. The JIFT discussion meeting was held at Toki on September 17, 2020, in the Plasma Simulator Symposium.

US-Japan Joint Project: FRONTIER

The FRONTIER collaboration started in April 2019 to provide the scientific foundations for reaction dynamics in interfaces of plasma facing components for DEMO reactors. This project consists of 3 tasks: Irradiation Effects on Reaction Dynamics at Plasma-Facing Material/Structural Material Interfaces (Task 1), Tritium Transport through Interface and Reaction Dynamics in Accidental Conditions (Task 2) and Corrosion Dynamics on Liquid-Solid Interface under Neutron Irradiation for Liquid Divertor Concepts (Task 3). All tasks perform neutron irradiation in High Flux Isotope Reactor (HFIR) at Oak Ridge National Laboratory (ORNL) and examine neutron-induced modifications in microstructure, mechanical strength, tritium transport, corrosion behavior, etc. Many hundreds of joined and composite materials samples were prepared in Japan and shipped to ORNL to be accommodated in irradiation capsules. The conceptual design was completed for the first-of-the-kind irradiation capsule for *in-situ* compatibility tests between structural material and liquid Sn as shown in Fig. 4.

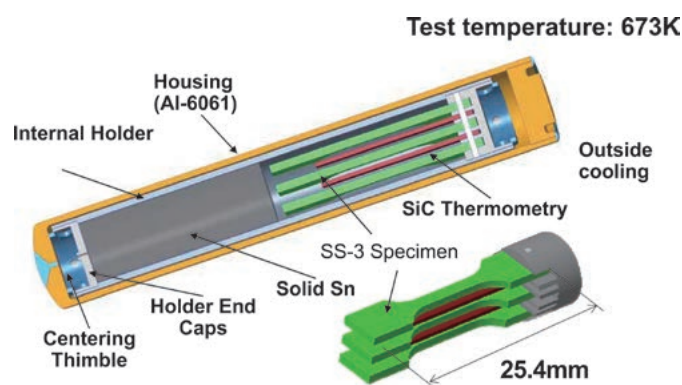


Fig. 4 Schematic diagram of liquid Sn rabbit capsule for compatibility study under neutron irradiation in High Flux Isotope Reactor (M. Kondo *et al.*, Plasma Fusion Res. **16** (2021) 2405040).

(T. Muroga, N. Yanagi, T. Morisaki, H. Sugama and Y. Hatano)

Japan–China Collaboration for Fusion Research (Post–CUP Collaboration)

I. Post–CUP collaboration

The post-Core University Program (Post-CUP) collaboration is motivated by collaboration on fusion research with institutes and universities in China including Institute of Plasma Physics Chinese Academy of Science (ASIPP), Southwestern Institute of Physics (SWIP), Peking University, Southwestern Jiaotong University (SWJTU), Huazhong University of Science and Technology (HUST) and other universities both in Japan and China. The Post-CUP collaboration is carried out for both studies on plasma physics and fusion engineering. Based on the following implementation system, the Post-CUP collaboration is executed.

Table 1 Implementation system of Japan-China collaboration for fusion research

Category	① Plasma experiment				② Theory and simulation	③ Fusion engineering research
Subcategory	①-1	①-2	①-3	①-4	—	—
Operator	A. Shimizu	S. Kubo	M. Isobe	T. Oishi	Y. Suzuki	T. Tanaka

①-1: Configuration optimization, transport, and magnetohydrodynamics, ①-2: Plasma heating and steady-state physics, ①-3: Energetic particles and plasma diagnostics, ①-4: Edge plasma and divertor physics, and atomic process

II. Primary research activities of collaboration in FY 2020

The 3rd steering committee meeting for the NIFS-SWJTU joint project for CFQS quasi-axisymmetric stellarator, was held on Nov. 12, 2020 online as shown in Fig. 1. Progress of engineering design, results of various tests for the mockup of modular coil (MC) which is the most complicated in shape, current status of the construction of actual MCs, and vacuum vessel (VV) were reviewed [1]. Renovation plan of experiment building in the Jiuli campus in SWJTU was also discussed. As for the MC mockup, heat-run test was performed, by which the temperature increase of the mockup coil and the cooling capability by water were checked, and the expected performance was confirmed. For the first actual MC, winding mould construction was completed. For VV, the mould for press work was manufactured. Construction of MCs and VV is steadily in progress.

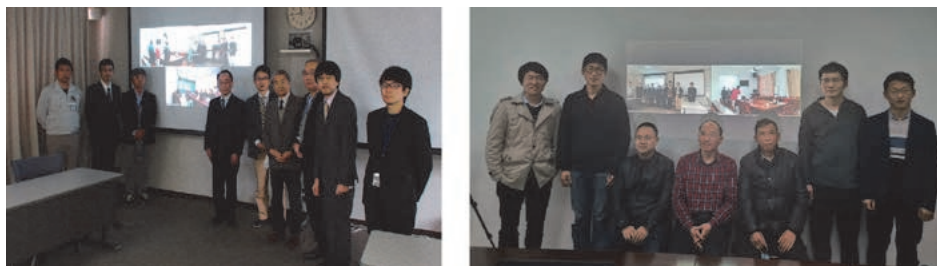


Fig. 1 The 3rd steering committee meeting of NIFS-SWJTU joint project for CFQS held on Nov. 12, 2020 online. The left and right pictures show participants from NIFS and SWJTU, respectively.

In the research of energetic particles, NIFS and ASIPP have been discussing about execution of collaborative research to measure a velocity distribution function of neutral beam (NB)-injected energetic ions in EAST and LHD through deuterium-deuterium (DD) fusion born neutron spectroscopy. Based on this discussion, we installed

a new 7Li -enriched $\text{Cs}_2\text{LiYCl}_6:\text{Ce}$ (CLYC-7) fast-neutron scintillation detector having a tangential sightline onto LHD. The significant shift of DD neutron energy according to the direction of tangential NB injection was clearly observed as expected in the FY2020 campaign of LHD [2]. Comparison of neutron energy spectra measured in LHD with the neutron energy spectra predicted by numerical simulation was initiated. As for the DD fusion born 1 MeV triton confinement research, NIFS and SWIP discussed performing collaborative research for triton confinement in HL-2M deuterium plasmas in the future and comparison with the experimental results in LHD. The predictive analysis of triton burnup ratio, which is the index of triton confinement ability, in HL-2M deuterium plasmas was performed using NUBEAM code as well as FBURN and LORBIT codes developed by NIFS. A relatively high triton burnup ratio of $\sim 1.3\%$ in relatively low-density and high-plasma-current conditions was predicted for HL-2M as a result of joint work [3].

In the research of the edge and divertor plasmas, the 3rd Japan Society for the Promotion of Science (JSPS)-Chinese Academy of Science (CAS) Workshop on “*Control of Wall Recycling on Metallic Plasma-Facing Materials in Fusion Reactors*” was held on 23-24 September 2020, as the remote meeting. A group photo of this workshop is shown in Fig. 2. Based on research activities involving overseas travels in FY2019, researching results were presented [4]. Especially young researchers had a lot of discussions in English, in this workshop, and it was a good experience from the viewpoint of training young researchers. A collaborative study on the extreme-ultraviolet (EUV) spectroscopy had also continued progress. A new space-resolved EUV spectrometer was installed in HL-2A and data acquisition started for the spatial profiles of impurity emission lines [5], which provides us with an opportunity to compare the results in HL-2A with those obtained by EAST and LHD.

In the research of fusion engineering, tritium recovery characteristics from a $\text{Li}_2\text{TiO}_3\text{-Li}_4\text{SiO}_4$ mixed ceramic material developed in SWIP have been examined in Shizuoka University. The results and future plan were discussed in a remote seminar.



Fig. 2 The 3rd meeting of the JSPS-CAS Bilateral Joint Research Projects held on 23-24 September 2020. A total of 25 participants joined the remote meeting.

- [1] CFQS TEAM, NIFS-PROC-119, 2021.
- [2] S. Sangaroon *et al.*, European Conference on Plasma Diagnostics (ECPD) 2021, 7–11 June 2021, online, and submitted to Journal of Instrumentation.
- [3] K. Ogawa *et al.*, Plasma Physics and Controlled Fusion **63** (2021) 045013.
- [4] J. Huang *et al.*, Plasma Science and Technology **23** (2021) 084001.
- [5] C.F. Dong *et al.*, Fusion Engineering and Design **159** (2020) 111785.

(M. Isobe)

Plasma Wall Interaction (PWI) Collaboration

This collaboration is based on the IEA Technical Collaboration Programme (TCP) of the “Development and Research on Plasma Wall Interaction Facilities for Fusion Reactors” (in short, PWI TCP). The objective of this TCP is to advance physics and technologies of the plasma-wall interaction research by strengthening cooperation among plasma-wall interaction facilities (in particular, by using dedicated linear plasma devices), to enhance the research and development effort related to the first wall materials and components for fusion reactor.

Every year, NIFS collects proposals of international collaborative studies based on the PWI TCP from domestic universities. The proposals are reviewed in the PWI technical committee in which members are domestic senior researchers in universities, QST and NIFS, and some of proposals are approved. Proponents of the approved collaborative researches are sent to the foreign institutes by NIFS, and conduct the studies.

Unfortunately, for the COVID-19 pandemic, collaborative activities based on the PWI TCP could not be conducted in FY2020 though three proposals were approved.

(S. Masuzaki)



14. Division of External Affairs

The Division of External Affairs, as a core organization responsible for public relations and outreach activities, promotes “dialogue” with society including the local area through a variety of activities. The organization has undergone a review in 2019 and now consists of five offices: Society Cooperation Office, Content Production Office, Event Planning Office, Public Relations and Tour Guide Office, and Outreach Promotion Office. A summary of the offices is depicted in Fig. 1. Many of the NIFS staff are active as members of the department. The main activities are: holding public explanatory meetings (Fig. 2), holding academic lectures for the public (Fig. 3), providing tours of the NIFS facilities (Fig. 4), and science classroom activities (Fig. 5). Face-to-face activities were limited due to COVID-19, but new activities utilizing online were initiated.



Fig. 1 Organization chart of Division of External Affairs

Activities held in 2020 include the following.

- Public explanatory meetings held at 5 places; 137 people participated
- Tours of the NIFS facilities (any time) held 87 times; more than 635 people participated
- Open academic lectures for the public held online; There were 561 accesses
- Science classroom activities held 7 times
- Release of information through Web pages, mailing lists, and SNS (Twitter and Facebook)
- Publication of NIFS official pamphlet (in Japanese and in English)
- Publication of public relations magazine: NIFS News (6 issues) (Fig. 6)
- Publication of public relations magazine: Letters from Plasma-kun (6 issues)



Fig. 2 Public explanatory meeting in Toki-city



Fig. 3 Online academic lectures



Fig. 4 Tour of the NIFS facilities



Fig. 5 Science classroom



Fig. 6 Public relations magazine: NIFS News

15. Department of Engineering and Technical Services

The Department of Engineering and Technical Services covers a wide range of work in the design, fabrication, construction, and operation of experimental devices in the fields of software and hardware.

The department consists of the following five divisions. The Fabrication Technology Division oversees the construction of small devices and the quality control of parts for all divisions. The Device Technology Division works on the Large Helical Device (LHD) and its peripheral devices except for heating devices and diagnostic devices. The Plasma Heating Technology Division supports the ECH system, the ICRF system, and the NBI system. The Diagnostic Technology Division supports plasma diagnostic devices and radiation measurement devices, and oversees radiation control. Finally, the Control Technology Division concentrates on the central control system, the cryogenic system, the current control system, and the NIFS network.

The total number of staff is now 59 (2020). We have carried out the development, the operation, and the maintenance of the LHD and those peripheral devices together with approximately 57 operators.

(S. Kobayashi)

1. Fabrication Technology Division

The main work of this division is the fabrication of experimental equipment. We also take care of technical consultation and experimental parts supplies related to the LHD experiment. In addition, we manage the administrative procedures of the department.

The number of machined requests was 127, and the production parts total number was 533 in this fiscal year (FY). The total numbers of electronic engineering requests and articles were 16 and 45, respectively. The details of some of this division's activities follow below.

(M. Yokota)

(1) Fabrication of Corrugated Conductor

A cylindrical cavity wall with periodical corrugation to excite a cylindrical Bloch wave at the frequency of 100 GHz was fabricated as shown in Fig. 1.

The cylindrical conductor has 80 corrugations on the outside. The parameters of the rectangular corrugation are a width of 0.3 mm, a depth of 0.6 mm, and a periodic length of 0.5 mm.

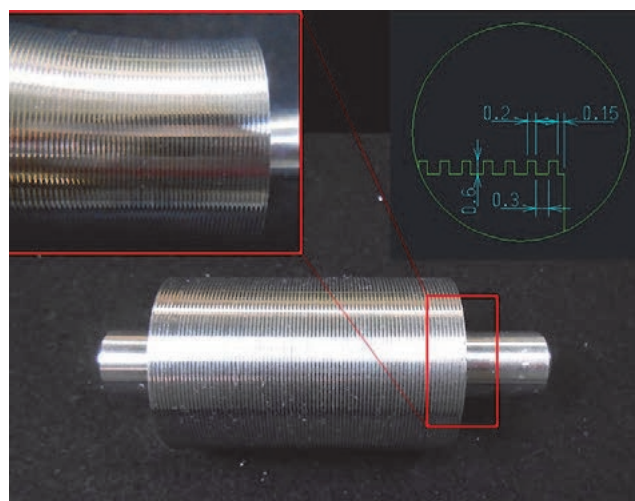


Fig. 1 Corrugated Conductor.

(K. Okada)

(2) Fabrication of 56 GHz notch filter

A 56 GHz Notch filter was fabricated for the Electron Cyclotron Emission Imaging System(Fig. 2). It consists of 6 cavities and a waveguide in the internal space.

The parameters of the cavity analyzed for electromagnetic fields are a diameter of 4.12 mm, and a depth of 4.63 mm. And the parameters of the rectangular waveguide are a length of 5.69 mm, and a width of 2.845 mm.

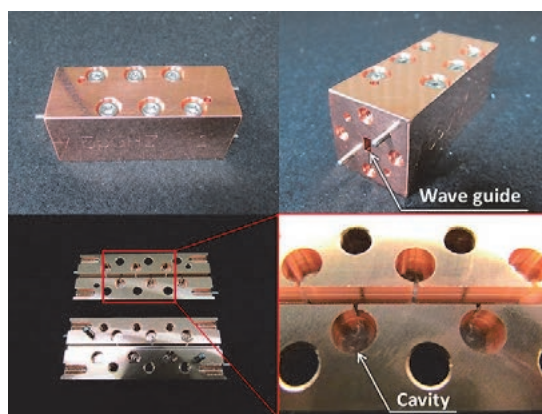


Fig. 2 56 GHz notch filter.

(T. Shimizu)

(3) Fabrication of 35ch PN photo diode array amplifier

A 35ch PN photo diode array amplifier is used to amplify the emission spectral signal when the solid hydrogen pellets melt in the plasma (Fig. 3).

This circuit has the specifications that the frequency bandwidth is DC to 2 MHz, and the current-voltage conversion resistance is 1 M Ω .

A problem of mutual interference, because the amplifiers were densely packed around the PN element, was solved by a noise reduction effect using a guard electrode for the signal line.

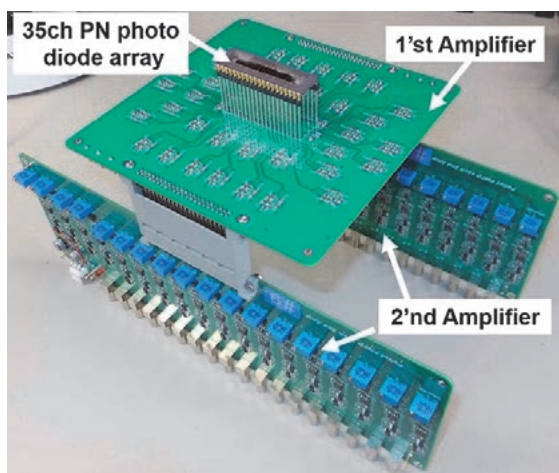


Fig. 3 35ch PN photo diode array amplifier.

(Y. Ito)

2. Device Technology Division

This Division supports the operation, improvement, and maintenance of LHD.

(1) LHD operation

We started pumping the cryostat vessel for cryogenic components on August 27, 2020 and pumping the plasma vacuum vessel on August 28, 2020. Subsequently, we checked for air leakage from the flanges on the plasma vacuum vessel. Fifty-nine flanges were inspected. Consequently, we observed leakage in one device and repaired the device.

The pressure of the cryostat vessel reached the adiabatic condition ($< 2 \times 10^{-2}$ Pa) on August 28, 2020, and the pressure of the plasma vacuum vessel was below 1×10^{-5} Pa on September 7, 2020.

The LHD experiments of the 22nd LHD experimental campaign were started on October 15, 2020, and carried out until February 18, 2021. The total number of days of the plasma experiments was 60.

During this experimental campaign, the vacuum pumping system eliminated air from both vessels without difficulty. In addition, no significant problems were reported for the utilities (for example, compressed air system, water-cooling system, GN2-supply system) of the LHD and the exhaust detritiation system. The LHD operation was completed on March 12, 2021.

(H. Hayashi)

(2) Development of bonding technique with W and Cu alloys using an advanced spark plasma sintering method

A bonding technique was developed using a tungsten (W) and copper (Cu) alloy, with chromium zirconium copper (CuCrZr) as a divertor material in the LHD. The two materials were bonded using the powder solid bonding (PSB) method, as shown in Fig. 4, an advanced spark plasma sintering method. Based on this method, a hydrogen environment was prepared, where the bonding process was performed to suppress the oxidation of W effectively, which would otherwise reduce the bonding strength of the materials. Furthermore, a mixed powder of W and Cu was inserted between W and CuCrZr to minimize the thermal stress generated at the bonded interface owing to the difference in the thermal expansion coefficients between W and CuCrZr. Shear strength tests were performed on the test specimens to evaluate the quality and strength of the bonding between the two materials, and the bond strength at the bonded interface was measured. The quality of the bonded interface was further verified through electron microscopy, qualitative and quantitative analysis, elemental mapping images, hardness measurements, and ultrasonic testing. The results showed that the intermediate layer of the W–Cu mixed powder was sufficiently dense, and no undesirable defects appeared on the intermediate layer or at the bonded interface. The proposed method will help manufacture more reliable and effective heterometallic bonding materials without defects in fusion experimental devices.

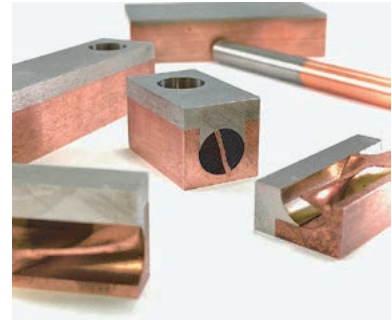


Fig. 4 Bonding samples fabricated using PSB method.

(T. Murase)

(3) Development of water bubbler system for tritium measurements in gas flow

When a deuterium (D) plasma experiment is conducted, tritium is generated through the D-D fusion reaction, and then a part of the tritium is implanted in the plasma-facing materials (PFMs). A water bubbler system was

designed and constructed as equipment for the tritium analysis system to evaluate the amount of tritium in the PFMs. A flow diagram of the water bubbler system is shown in Fig. 5.

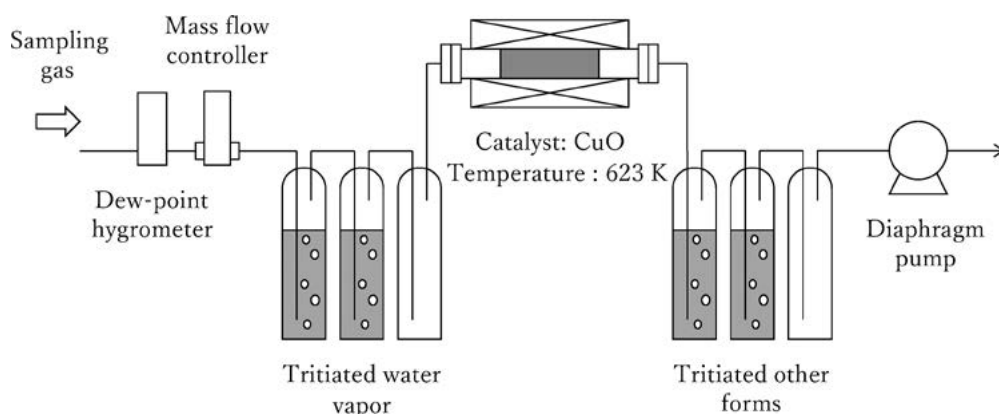


Fig. 5 A flow diagram of the water bubbler system.

The water bubbler system can collect tritium in water, and the chemical forms of tritium, such as water vapor and other chemical forms, are discriminated by a catalytic reactor packed with copper oxide (CuO wire approximately 0.65×6 mm, PN: 1.02767, Millipore Corporation). The catalytic heater can be heated to 723 K. This system is controlled using a programmable logic controller that incorporates the settings of the sampling time or temperature control and, the interlock of the catalytic heater.

After the sampling operation, the water sample containing tritium was mixed with a liquid scintillator (Ultimate Gold LLT, PerkinElmer) in a polyethylene vial. Then mixed sample was measured using a liquid scintillation counter (Tri-Carb 4910TR, PerkinElmer).

The performance of the developed system was compared with that of a conventional system. The results showed a good agreement, as summarized in Table 1.

Table 1 Measurement results

Devices	Run1 (Bq/cm ³)	Run2 (Bq/cm ³)
Conventional system	$10.7 \times 10^{-5} \pm 9.4 \times 10^{-6}$	$7.9 \times 10^{-5} \pm 7.5 \times 10^{-6}$
Developed system	$8.1 \times 10^{-5} \pm 7.0 \times 10^{-6}$	$7.9 \times 10^{-5} \pm 7.4 \times 10^{-6}$

(H. Kato)

(4) Development of a new ion source for heavy ion beam probes

The plasma potential is a critical parameter in plasma research, and it has been measured using heavy ion beam probes (HIBP).

Currently, the problem of HIBP is that it is difficult to measure the plasma potential in high-density regions. It is necessary to develop a new ion source as shown in Fig. 6 to increase the ion beam current. The target beam current is 100 μ A, which is five times higher than the current ion beam current.

In the current ion source, argon is ionized using a heater and sputtered onto gold to produce negative gold ions. In the new ion source, the heater is bowl-shaped, and it ionizes cesium and collects it at one point, similar to a lens. This process efficiently spatters the cesium onto gold to produce negative gold ions.

In developing the new ion source, five power supplies, including a heater power supply for cesium vaporization, a beam current measurement device, and a device for cooling the equipment, were selected, purchased, and installed. Additionally safety measures were implemented.

The performance test of the new ion source showed that the beam current was only 28 μA at the center of the beam. The new ion source is integrated into the HIBP system of the LHD after adjustment to improve beam focusing.

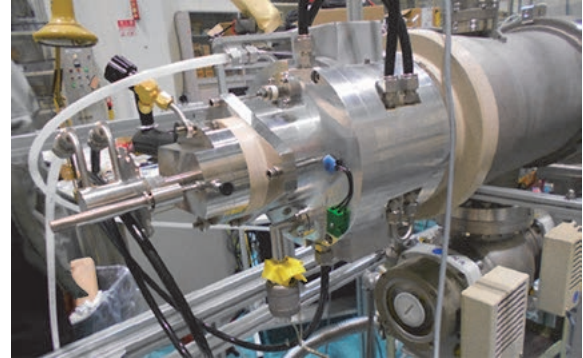


Fig. 6 New ion source for the HIBP.

(H. Takubo)

(5) Development of scroll pump load current monitoring system

We built a load current monitoring system for scroll pumps. This action was performed to check for a pump failure rapidly. We monitored the load current of the scroll pump during operation and determined the state of the pump.

We installed one Rogowski coil clamp on each pump and recorded the condition of the pumps. We stopped running the pump because we observed an increase in current, signifying the failure of the pump as shown in Fig. 7. Consequently, the pump damage was minimized. We believe that the proposed system is effective for preventing pump damage.

In the future, we will expand the scope of this system and strengthen the management of pumps.



Fig. 7 Increased load current.

(H. Chimura)

3. Plasma Heating Technology Division

The main tasks of this division are the operation and the maintenance of three different types of plasma heating devices and their common facilities. We have also performed technical support for improving, developing and

newly installing these devices. In this fiscal year, we mainly carried out device improvement and modification for a deuterium plasma experiment. The details of these activities are as follows.

(T. Kondo)

(1) ECH

(a) Gyrotron Operation for LHD experiments and Developments of devices

During the 22nd experimental campaign, we injected power up to 4 MW to assist plasma experiments. That contributed to the accomplishment of high performance plasmas with high ion and electron temperatures. Low power and long pulse injection can sustain the ECH plasma. Some trouble happened, but all ECH technical staff of the LHD experimental group contributed to the various plasma experiments.

The gyrotron have three kinds of high-voltage power supply (Anode, Body, and Collector). We designed the high-voltage switch device, which can connect or disconnect three power supplies in simultaneously by a pneumatic actuator (Fig. 8).

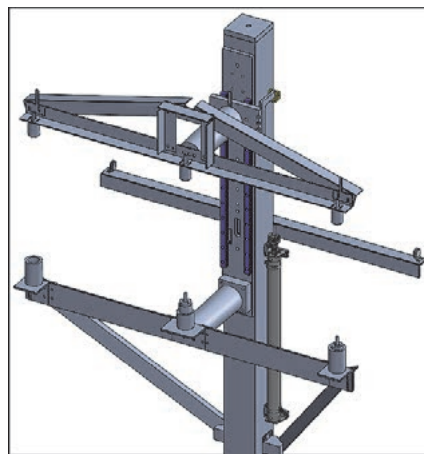


Fig. 8 A picture of the high-voltage switch device.

(S. Ito and T. Takeuchi)

(2) ICH

(a) The operation of ICH in the 22nd experimental campaign of LHD experiments

In the 22nd experimental campaign, HAS (Handshake type) antennas with two antenna straps were installed at the 3.5U&L ports of the LHD. Thus, in addition to the FAIT (Field-Aligned Impedance-Transforming) antenna with two antenna straps at the 4.5U&L ports, we carried out the LHD experiments with in total two antennas with four antenna straps.

We decided the combination of an RF transmitter and an antenna strap. Then, the transmitters #3 and #4 were connected to the 3.5U&L antenna straps and transmitters #6A and #6B were connected to the 4.5U&L antenna straps. The total injection power from the four antenna straps into the plasma reached about 3.4 MW in the short pulse of 1 second at the RF wave frequency of 38.47 MHz.

(b) Development of high-speed optical measurement system “Ha-fast”

We developed an optical measurement system to detect the passive emissions of $H\alpha$ (656.3 nm), HeI

(587.6 nm), and HeII (468.6 nm) with time resolution higher than 1 MS/s. These data are registered with LABCOM as the diagnostic name “Ha-fast”. Fig. 9 shows a diagram of this system, and Fig. 10 shows a measurement example. This system has observed the optical emissions of the ICH plasma successfully.

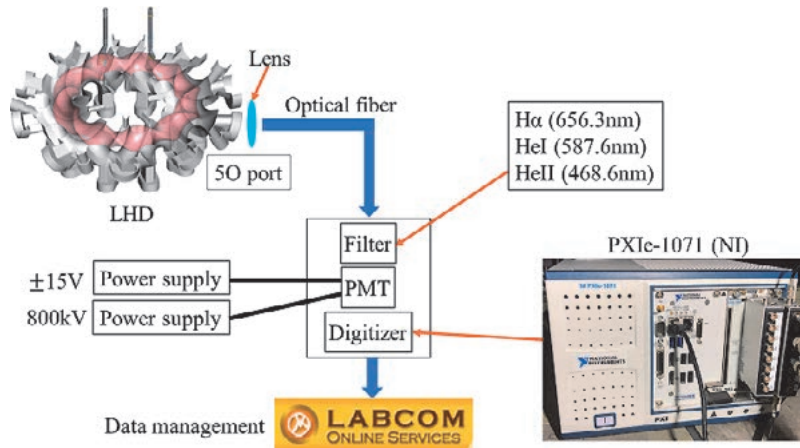


Fig. 9 A diagram of an optical measurement system.

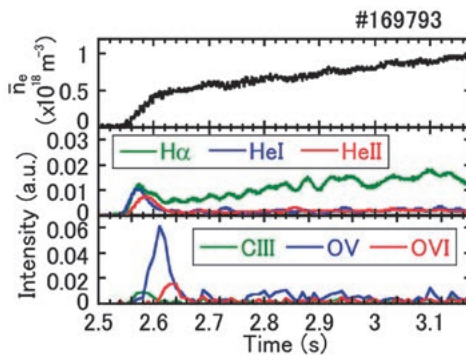


Fig. 10 A measurement example.

(G. Nomura and M. Kanda)

(3) NBI

(a) The operation and maintenance of NBI in the 22nd campaign of LHD experiments

In this campaign, approximately 8,000 shots of beams were injected into the LHD plasmas with three negative-NBIs (BL1, BL2, and BL3). The injection history of the total injection power for the negative-NBIs is shown in Fig. 11. The maximum injection power in this campaign was about 12MW. As for the positive-NBIs (BL4 and BL5), the maximum total injection power of the positive-NBIs was about 20MW. The NBIs had no troubles that lead to serious problems in the plasma experiments.

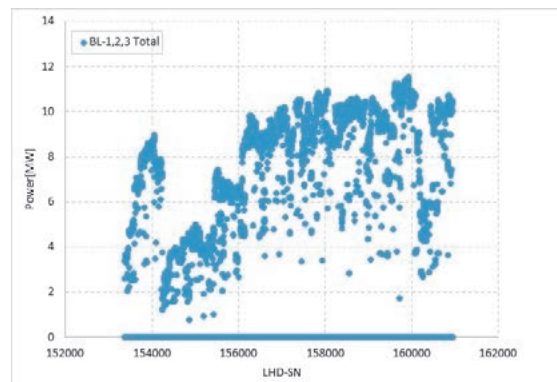


Fig. 11 A history of the total injection power for the negative-NBIs.

(b) Evaluation of NBI injection power

NBI injection power is evaluated from the temperature rise of Calorie-Meter Arrays (CMA), which consist of molybdenum chips and are installed in armor tiles at the wall opposite to the NBI injection-port. The temperatures of calorie-meter chips are measured by sheath type thermocouples via isolation amplifiers using a WE (YOKOGAWA Co.) data acquisition system. Under the weak magnetic field configuration of LHD, energetic particles from plasmas often hit some of molybdenum chips of the CMA. In this case, the temperatures of these chips are not used in the evaluation.

The NBI injection efficiency is estimated by normalizing the evaluated NBI injection power by the output power of the acceleration power supplies. Here, the monitor signals of the power-supply outputs are acquired by the CAMAC data acquisition system. The typical estimated injection efficiencies for three tangential NBIs, are shown for the 22nd campaign of LHD experiments, as follows.

NBI1: 0.333(H), 0.334(D)

NBI2: 0.256(H), 0.226(D)

NBI3: 0.325(H), 0.275(D)

(M. Sato and S. Komada)

(4) Motor-Generator (MG)

The MG is used to supply the pulsed power to the NBI and the ECH for LHD. The MG has supplied power for 20,740 shots in this fiscal year and 674,473 shots since its construction. The operation time was 1,208 hours. 136 batteries have been replaced for control and braking.

(Y. Mizuno)

4. Diagnostics Technology Division

This division mainly supports the development, the operation and the maintenance of plasma diagnostic devices and radiation measurement devices for LHD. In addition, we also have taken charge of radiation control.

(T. Kobuchi)

(1) Plasma diagnostic device

Some plasma diagnostics devices have functioned for more than 20 years and thus require maintenance.

For the Nd:YAG Thomson scattering system, we replaced a noise cut transformer and outlets for the data acquisition system power supplies with new ones (Fig. 12). As a result of them, fast bus error incidence decreased by about 40% in the data acquisition system from the previous experimental campaign.

For the FIR interferometer (far-infrared laser measuring device), we have updated from the recording device using an analog chart paper and a pen to the magnetic recording device as shown in Fig. 13. It became possible to collect the data in more detail, to read the data from memory and to create graphs, when necessary.

For the integrated radiation monitoring system, we are developing the programs to operate some equipment. The program which reads personal data from an ID card has been developed for identifying the person who is operating.

The LHD data acquisition system began acquiring images from 15 surveillance camera measurements in the 22nd experimental campaign and acquired a total data volume of approximately 312.7 TB in compressed size. This is more than three times the amount of data collected in the 21st experimental campaign, so both RAID storage and optical disk storage were suddenly expanded to store a large amount of data during the experiment.



Fig. 12 Outlets for data acquisition system power supplies in the Thomson scattering system.

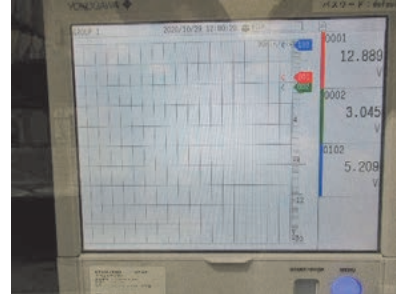


Fig. 13 Display of the new recording device.

(C. Iwai, T. Nishimura and M. Ohsuna)

(2) Radiation measurement and radiation control

In order to control the safety of radioactivity, we carried out the operation and maintenance of three high-purity germanium (HPGe) detectors, seven liquid scintillation counters, a 2π gas-flow counter, an auto well gamma system, three stack tritium monitoring systems, two gas monitoring systems, two dust monitoring systems, and the drain water monitoring system. The liquid scintillation counters are used for exhaled tritium measurement, exhaust tritium measurement, wastewater measurement, and environmental water measurement.

In the application system for radiation worker registration, the SQRC for access control to be pasted on the Luxcel badge had been printed by receiving the EXCEL list, converting it to CSV, and using a special application, but a program was developed to allow direct printing from the WWW browser to improve the efficiency of the work (Fig. 14).

We are developing the program to operate some equipment connected to the integrated radiation monitoring system. The program which reads personal data from an ID card has been developed for identifying the person who operates the equipment.



Fig. 14 Pressing the button indicated by the red circle will start printing the SQRC (in Japanese).

(M. Nakada, S. Hashimoto, M. Nonomura and Y. Yamamoto)

5. Control Technology Division

The Control Technology Division is in charge of the important engineering tasks in the LHD project, such as system development, project management and system operation, which are mainly targeted to the central control

system, cryogenic system, coil power supply and super-conducting coils.

We are also responsible for the IT infrastructures, e.g. LHD experiment network, NIFS campus information network and internet servers, in every phase of the projects including requirements analysis, system design, implementation, operation and user support.

The essential topics of the activities for last fiscal year are described below.

(H. Ogawa)

(1) LHD cryogenic system and power supply system for superconducting coils

The cooling operation in the 22nd experimental campaign has been executed without significant accident.

In the power supply system, we replaced the monitoring and logging devices for coil energization before the 21st experimental campaign. This fiscal year we have developed the waveform display application for the long-time data monitoring and logging using LabVIEW (Fig. 15) because the application originally attached to the device had a limited display time of up to 1 second.

Major functions are as follows: 1) 48 simultaneous monitoring channels, 2) automatic logging start/stop, 3) variable length of data display time up to 2 hours and 4) device status monitoring.

The new application monitored and recorded all signals with no severe problems in the 22nd experimental campaign.

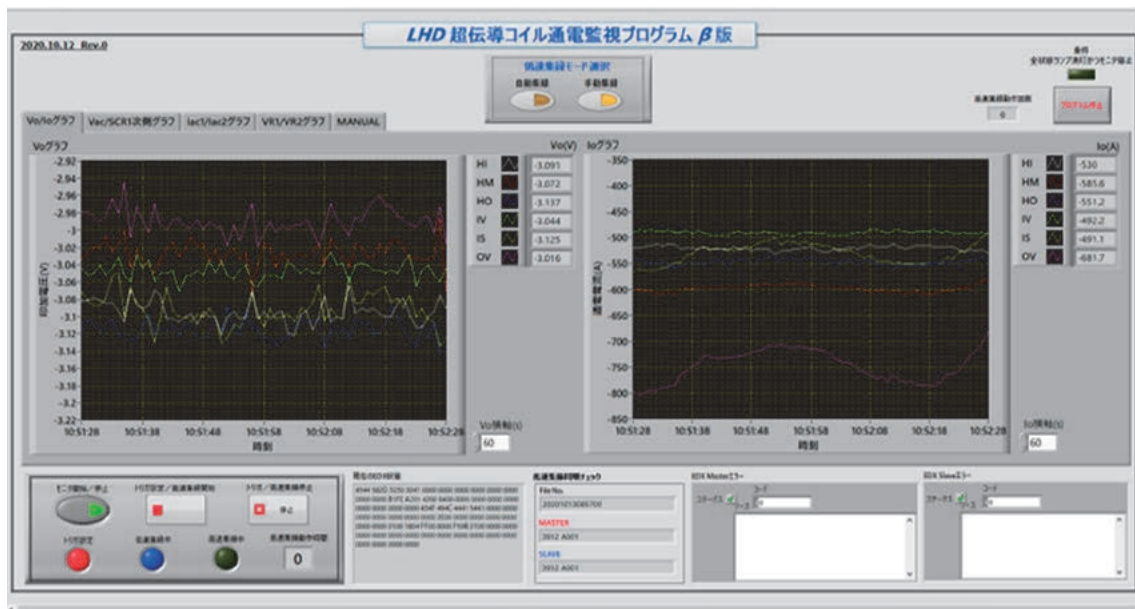


Fig. 15 Newly developed waveform display application.

(H. Tanoue)

(2) Development of current Timing Modulator

In the LHD plasma experiment, the current Timing Modulator, which provides timing signals to the measurement equipment, has been used for over 20 years since the 1st experimental campaign. Therefore, we developed the replacement modulator in case of an unpredictable failure caused by deterioration.

Once the modulator receives a pulse signal from the Central Control System, it sends modulated signals to

the demodulators. Then, the demodulators control measurement equipment according to the signal type they have received.

The new modulator adopts a FPGA board with a Zynq processor called Microzed, manufactured by Xilinx Inc., and the same functions as the current modulator are implemented using development tools, Vivado and PetaLinux (Fig. 16).

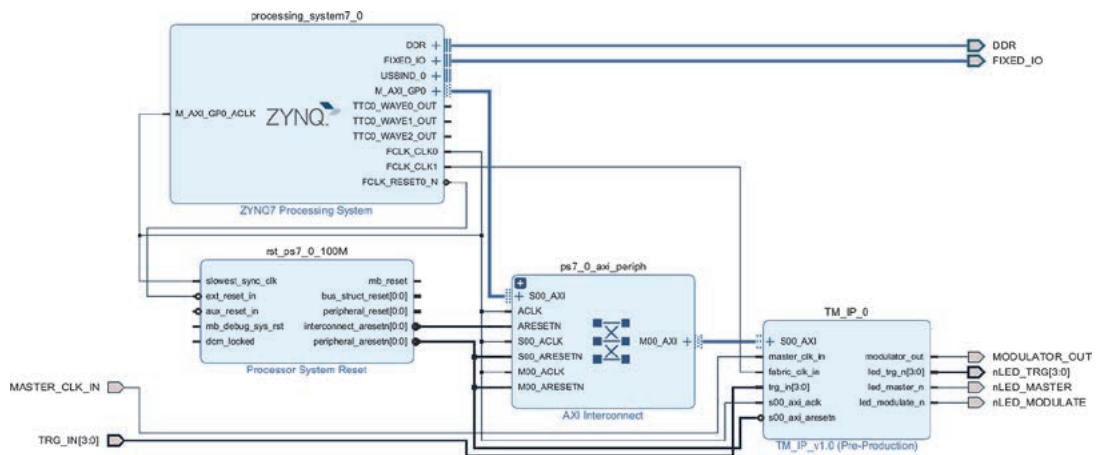


Fig. 16 Block design of the timing modulator.

(H. Maeno)

(3) Network management

The NIFS campus information networks consist of several clusters. We manage the Research Information Cluster (NIFS-LAN) and the LHD Experiment Cluster (LHD-LAN).

The achievements in FY 2020 are as follows:

(a) Introduction of G suite for Education

Along with the introduction of G suite for Education, a cloud service provided by Google, the mail system was migrated from an on-premise mail server system to Gmail.

(b) Upgrade of the virtual server system

The virtual server system has been upgraded (Fig. 17). Although the number of servers was reduced from four to three, the number of virtual machines that could be installed to the server increased due to the upgrade of the CPU, memory size and the other resources.

(c) LHD-LAN

It is required in our security policy that the network management staff needs to be present when connecting a new device to the LHD-LAN.



Fig. 17 Virtual server system.

In FY 2020, the 66 new devices were connected to the LHD-LAN, 88 were updated and 26 IP addresses made available due to device removal.

(T. Inoue and O. Nakamura)

6. Development of a double-barreled Tracer-Encapsulated Solid Pellet (TESPEL) injection system (TESPEL#4)

We have developed and installed a TESPEL#4 system, which will be one of the important experimental tools for the LHD. We have already made two TESPEL injection systems (one for the LHD, and the other for the German magnetic fusion experiment device, Wendelstein 7-X). Therefore, we have enough knowledge and technique for developing a new TESPEL injector. Thus, we accepted a request from a researcher to make the TESPEL#4 for the LHD. The significant features of the TESPEL#4 are that 1) it is a double-barreled system, and then it is possible to inject two TESPELs almost simultaneously, 2) the exchange cycle of the TESPEL holding disk can be reduced.

A compact design is necessary due to the limited available space for the TESPEL#4. For ensuring the performance of the TESPEL#4 system, we spent a lot of time on TESPEL injection tests and He leak tests. Fig. 18 shows a TESPEL#4 installed on the LHD. We developed the TESPEL#4 operation control system using a PLC. We also developed the remote control system for the TESPEL#4 operation with Microsoft Visual Studio. Fig. 19 shows an operation screen of the remote control system for the TESPEL#4. Fig. 20 shows the PLC and controllers

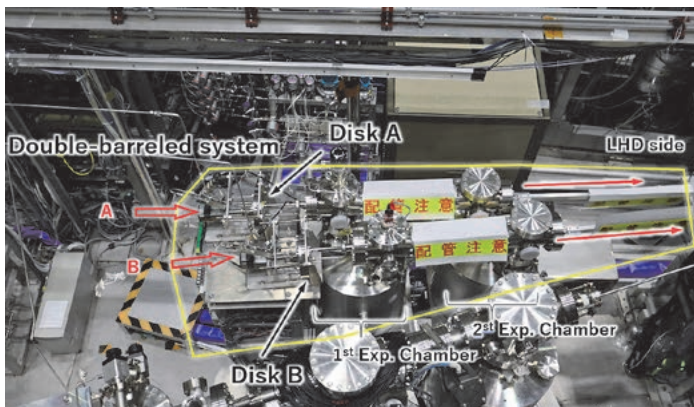


Fig. 18 TESPEL#4 installed on the LHD.

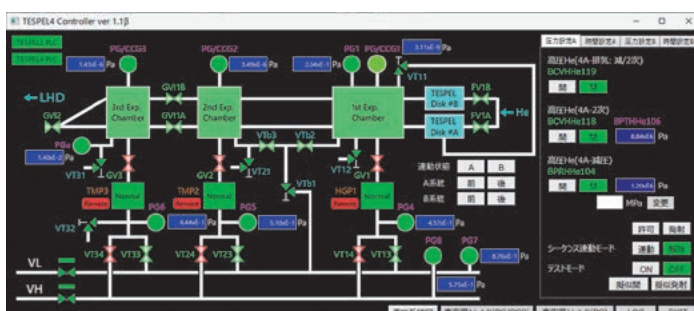


Fig. 19 Operation screen of remote control system for the TESPEL#4.



Fig. 20 PLC and controllers of the TESPEL#4.

of the TESPEL#4. The development of the TESPEL#4 system by the NIFS Engineering Department could keep development costs down., and it also can provide fast troubleshooting. In the 22nd LHD experiment campaign, we confirmed a successful injection of two TESPELs into a single discharge with the TESPEL#4 system.

(Hiromi Hayashi, H. Maeno and H. Furuta)

7. NIFS Article Information System (NAIS)

A list of rehearsal materials for the conference was made available on the NAIS so that we can check the materials to be presented online. As a result, we no longer need to post the materials, so we do not need to print them and can check them on our own PC (Fig. 21).

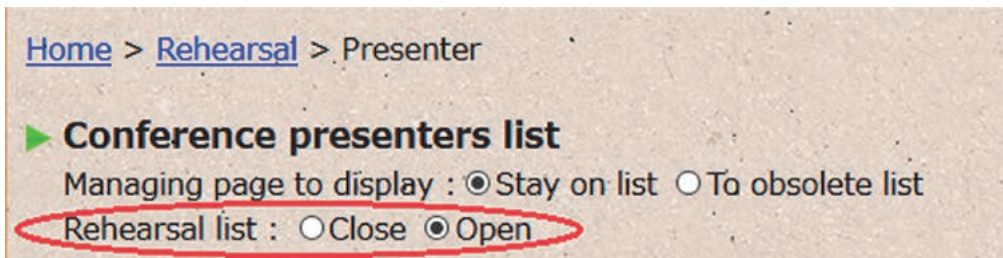


Fig. 21 The person in charge of the meeting can choose to make materials open or closed.

(M. Nonomura)

8. Activities of technical exchange and technical cooperation

(1) Fourth technical exchange meeting: “Computational technology using finite element method”

On February 25, 2021, we held a technical exchange meeting on numerical computational technology based on the finite element method (FEM). This meeting was the fourth, and there were seven presenters and 40 participants, including those who used a remote web conference application (ZOOM), as shown in Fig. 22.

In this meeting, four outside presenters presented reports on reduced-order modeling technology using a commercial FEM code (ANSYS), the heat-transfer analysis of beam dumps and an accelerator production target using ANSYS Mechanical, the electromagnetic (EM)-force analysis of a port plug for JT60SA using ANSYS Emag, and the EM and structural analyses of toroidal-field magnetic coils on a reversed field pinch device, RELAX. In addition, three presenters within NIFS presented EM shield performance evaluation by comparing



Fig. 22 Technical exchange meeting using ZOOM meeting system.

the experimental and FEM results using ANSYS Maxwell, the modal and structural analyses of control cabinets required for experimental fusion devices, and the EM analysis and fabrication of a microwave notch filter using ANSYS HFSS. We engaged in discussions related to all the presentations.

(T. Murase)

(2) Fabrication of a model of the plasma experimental device “RT-1”

A model of the plasma experimental device “RT-1” was fabricated using a 3D printer at the request of the University of Tokyo as a technical cooperation.

This is a 1/30 size model, we delivered two units in a case with a two-color printed base (Fig. 23).



Fig. 23 1/30 size model of “RT-1”.

(S. Nakagawa and Y. Yamamoto)

16. Department of Administration

The Department of Administration handles planning and external affairs, general affairs, accounting, research support, and facility management work.

The major operations of this department are to support the promotion of the Institute's regular research and the development of the collaborative research.

The department consists of the following four divisions, namely, the General Affairs Division, the Financial Affairs Division, the Research Support Division, and the Facilities and Safety Management Division. Details of these divisions are described below.

General Affairs Division

The General Affairs Division handles administrative work and serves as the contact point with the outside. This Division consists of four sections. The General Affairs Section is in charge of secretarial work for the Director General and the Deputy Director General, support for the Advisory Committee meetings, and enacting rules and regulations. The Planning and Evaluation Section is in support for assessment of the institution's performance including scientific achievement and management efficiency. The Personnel and Payroll Section is in charge of general personnel affairs, salary, and public welfare. And the Communications and Public Affairs Section focuses on outreach and publicity activities.

Number of Staff Members

(※ This list was compiled as of March 31, 2021.)

Director General	1
Researchers	121
Technical and Engineering Staff	46
Administrative Staff	41
Employee on Annual Salary System	12
Research Administrator Staff	3
Visiting Scientists	8
Total	232

Financial Affairs Division

The Financial Affairs Division consists of six sections: The Audit Section, the Financial Planning Section, the Accounts and Properties Administration Section, the Contracts Section, the Procurement Section, and the Purchase Validation Section.

The major responsibilities of the division are to manage and execute the budget, to manage corporate property, revenue/expenditure, and traveling expenses of staff, and to purchase supplies and receive articles.

(JFY 2020)

Settlement

(in million of Yen)

Salaried Wages	2,097
Operating Costs	7,054
Equipment	0
Site and Buildings	150
Grant-in-Aid for Scientific Research	149
Total	9,450

Research Support Division

The Research Support Division consists of four sections and one center. These are the Graduate Student Affairs Section, the Academic Information Section which includes the Library at NIFS, the Research Support Section and the International Collaboration Section, which is in charge of inter-university coordination and arranging international cooperation. The Visitor Center assists collaborating researchers and visitors.

Collaboration Research Programs

(JFY 2020)

	Applications Applied	Applications Accepted	Researchers Accepted
LHD Project Collaboration Research	25	24	296
Joint Research	249	247	1,854
Joint Research Using Computers	134	132	373
Workshops	31	31	643
Bilateral Collaboration Research	101	101	1,304
Total	540	535	4,470

Number of Graduate School Students

(SOKENDAI: The Graduate University for Advanced Studies)

(As of March 31, 2021)

Doctoral Course					
Grade 1	Grade 2	Grade 3	Grade 4	Grade 5	Total
6	2	4	4	5	21

(The Joint Program of Graduate Education)

Graduate course education is given in NIFS apart from SOKENDAI in joint programs with the Department of Energy Science and Engineering of the Graduate School at Nagoya University, Division of Particle and Astrophysical Science of the Graduate School of Science at Nagoya University, Division of Quantum Science of the Graduate School of Engineering at Hokkaido University, Department of Energy Science of the Graduate School of Science and Engineering at University of Toyama, Interdisciplinary Graduate School of Engineering Science in Kyushu University and the Graduate School of Engineering at Tohoku University. In total, 29 graduate students are involved in the programs as of March 31, 2021.

The Special Research Collaboration Program for Education

(As of March 31, 2021)

Affiliation \ Degree	Bachelor's Course	Master's Course	Doctoral Course	Total
National Graduate School	3	22	4	29
Public Graduate School	0	0	0	0
Private Graduate School	0	0	0	0
Total	3	22	4	29

Books and Journals

(JFY 2020)

Books in Japanese	19,817
Books in Other Languages	50,691
Total (volumes)	70,508
Journals in Japanese	272
Journals in Other Languages	816
Total (titles)	1,088

Facilities and Safety Management Division

The Facilities and Safety Management Division consists of three sections: The Safety and Health Management Section, the Facilities Planning Section, and the Facilities Maintenance Section. They are in charge of planning, designing, making contracts, supervising the construction and maintenance of all facilities at NIFS, such as buildings, campus roads, electricity, telephone, power station, air conditioning, water service, gas service, elevators, and cranes. The Facilities and Safety Management Division submits a budget request and administers the budget for those facilities.

The Safety and Health Management Section also arranges medical examination and disaster drills. These three sections promote facilities' environment better for all staff.

Site and Buildings

(JFY 2020)

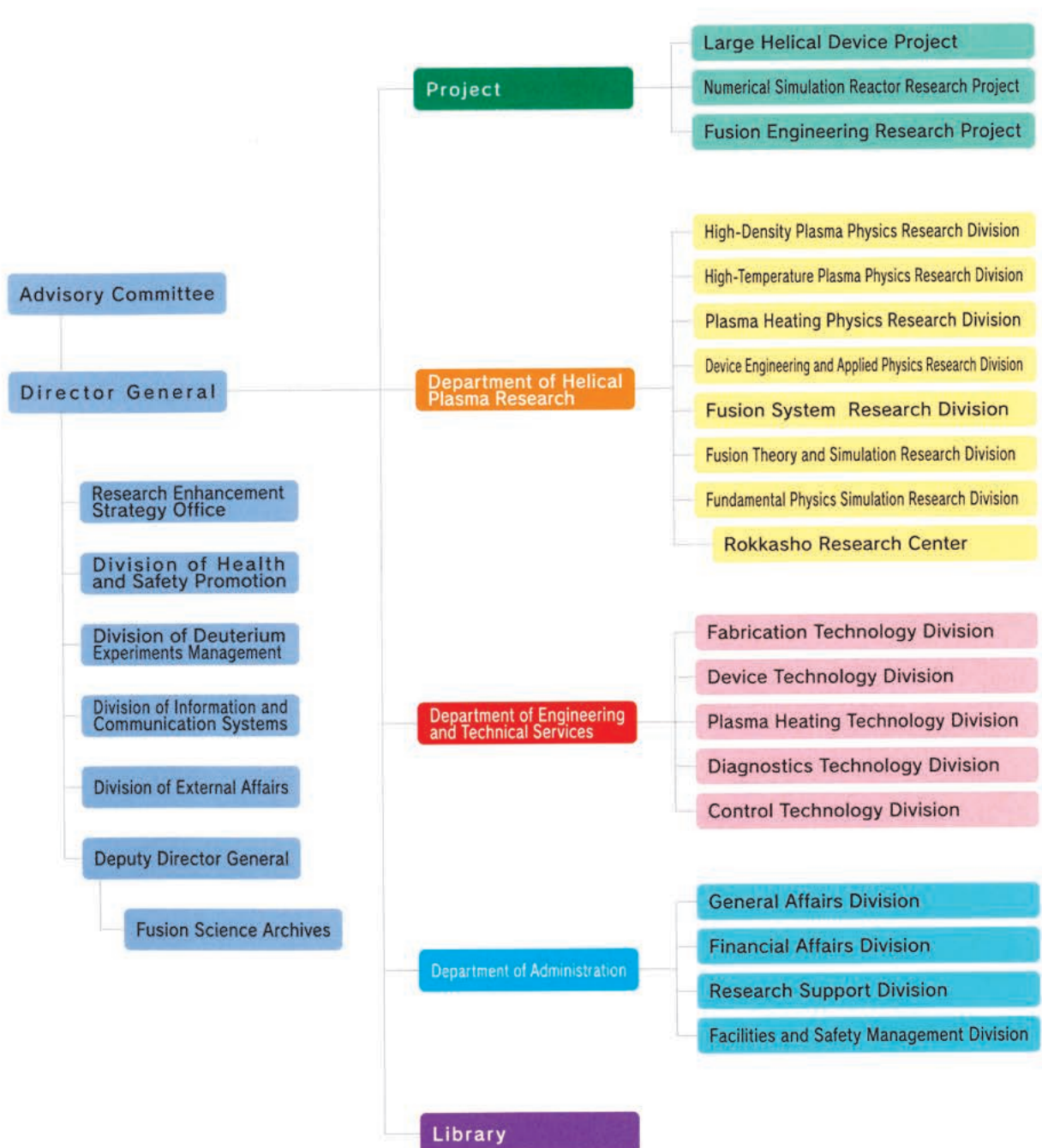
Toki	
Site	464,445 m ²
Buildings	
Total Building Area	39,557 m ²
Total Floor Space	71,830 m ²

APPENDIX

APPENDIX 1. Organization of the Institute

NATIONAL INSTITUTE for FUSION SCIENCE

Organization



APPENDIX 2. Members of Committees

Advisory Committee

ANDO, Akira	Professor, Graduate School of Engineering, Tohoku University
USHIGUSA, Kenkichi	Managing Director, Fusion Energy Research and Development Directorate, National Institutes for Quantum and Radiological Science and Technology
OHNO, Noriyasu	Director, Graduate School of Engineering, Nagoya University
OGAWA, Yuichi	Professor, Graduate School of Frontier Science, The University of Tokyo
KODAMA, Ryouzuke	Director, Institute of Laser Engineering, Osaka University
NAGASAKI, Kazunobu	Professor, Institute of Advanced Energy, Kyoto University
NAKASHIMA, Yousuke	Director, Plasma Research Center, University of Tsukuba
HANADA, Kazuaki	Director, Research Institute for Applied Mechanics, Kyushu University
WATANABE, Tomohiko	Professor, Department of Physics, Nagoya University
WADA, Motoi	Professor, Faculty of Science and Engineering, Doshisha University
MUROGA, Takeo	Deputy Director General, NIFS and Executive Director of Fusion Engineering Research Project, NIFS
MORISAKI, Tomohiro	Executive Director of Large Helical Device Project (on Science), NIFS
OSAKABE, Masaki	Executive Director of Large Helical Device Project (on Device), NIFS
SUGAMA, Hideo	Executive Director of Numerical Simulation Research Project, NIFS
YANAGI, Nagato	Executive Director of Fusion Engineering Research Project, NIFS
KUBO, Shin	Director of Plasma Heating Research Division, NIFS
MITO, Toshiyuki	Director of Device Engineering and Applied Physics Research Division, NIFS
MURAKAMI, Izumi	Director of Fusion Systems Research Division, NIFS
TODO, Yasushi	Director of Fusion Theory and Simulation Research Division, NIFS
ISHIGURO, Seiji	Director of Fundamental Physics Simulation Research Division, NIFS
NISHIMURA, Kiyohiko	Division Director for Health and Safety Promotion, NIFS

※ This list was compiled as of March 31, 2021

APPENDIX 3. Advisors, Fellows, and Professors Emeritus

Advisors

Michael Tendler Professor
 Royal Institute of Technology
 Alfvén Laboratory

Fellows

YAMADA, Hiroshi

Professors Emeritus

ICHIKAWA, Yoshihiko (1993)	MATSUOKA, Keisuke (2010)
MIZUNO, Yukio (1994)	TOI, Kazuo (2012)
FUJITA, Junji (1996)	NARIHARA, Kazumichi (2012)
KURODA, Tsutomu (1997)	KUMAZAWA, Ryuhei (2012)
AMANO, Tsuneo (1998)	UDA, Tatsuhiko (2012)
MOMOTA, Hiromu (1998)	SATO, Motoyasu (2012)
IYOSHI, Atsuo (1999)	YAMAZAKI, Kozo (2013)
HATORI, Tadatsugu (1999)	KAWAHATA, Kazuo (2013)
TANAHASHI, Shugo (2000)	OKAMURA, Shoichi (2014)
KAWAMURA, Takaichi (2000)	KOMORI, Akio (2015)
SATO, Tetsuya (2001)	SUDO, Shigeru (2015)
FUJIWARA, Masami (2002)	SKORIC, Milos (2015)
TODOROKI, Jiro (2003)	MUTO, Takashi (2016)
KAMIMURA, Tetsuo (2003)	NAGAYAMA, Yoshio (2017)
OHKUBO, Kunizo (2005)	NAKAMURA, Yukio (2017)
HAMADA, Yasuji (2007)	SAGARA, Akio (2017)
KATO, Takako (2007)	ITOH, Kimitaka (2017)
NODA, Nobuaki (2008)	HORIUCHI, Ritoku (2017)
WATARI, Tetsuo (2008)	HIROOKA, Yoshihiko (2018)
MOTOJIMA, Osamu (2009)	MORITA, Shigeru (2019)
SATO, Kohnosuke (2010)	NISHIMURA, Arata (2019)
OHYABU, Nobuyoshi (2010)	

※ This list was compiled as of March 31, 2021

APPENDIX 4. List of Staff

Director General

YOSHIDA, Zensho

Deputy Director General

MUROGA, Takeo

Department of Helical Plasma Research

Prof. MUROGA, Takeo (Director)

High-Density Plasma Physics Research Division

Prof. SAKAMOTO Ryuichi (Director)
Prof. WATANABE, Kiyomasa
Prof. SAKAMOTO, Ryuichi
Prof. OHDACHI, Satoshi
Assoc. Prof. YOSHIMURA, Shinji
Assoc. Prof. SHOJI, Mamoru
Assoc. Prof. TOKUZAWA, Tokihiko
Assoc. Prof. KOBAYASHI, Masahiro
Assoc. Prof. MOTOJIMA, Gen

Asst. Prof. NARUSHIMA, Yoshiro
Asst. Prof. TAKEMURA, Yuki
Asst. Prof. TSUCHIYA, Hayato
Asst. Prof. OISHI, Tetsutaro
Asst. Prof. NISHIMURA, Shin
Asst. Prof. HAYASHI, Yuki
Asst. Prof. KAWAMOTO, Yasuko
Asst. Prof. GOTO, Yuki
Specially Asst. Prof. OHTSUBO, Yohko

High-Temperature Plasma Physics Research Division

Prof. IDA, Katsumi (Director)
Prof. SAKAKIBARA, Satoru
Prof. TANAKA, Kenji
Prof. ISOBE, Mitsutaka
Prof. PETERSON, Byron Jay
Assoc. Prof. GOTO, Motoshi
Assoc. Prof. TAMURA, Naoki
Assoc. Prof. YAMADA, Ichihiko
Assoc. Prof. YASUHARA, Ryo
Assoc. Prof. OZAKI, Tetsuo
Assoc. Prof. NAKANISHI, Hideya

Assoc. Prof. OGAWA, Kunihiko
Asst. Prof. KOBAYASHI, Tatsuya
Asst. Prof. MUTO, Sadatsugu
Asst. Prof. FUNABA, Hisamichi
Asst. Prof. YOSHINUMA, Mikirou
Asst. Prof. SUZUKI, Chihiro
Asst. Prof. SHIMIZU, Akihiro
Asst. Prof. EMOTO, Masahiko
Asst. Prof. MUKAI, Kiyofumi
Asst. Prof. UEHARA, Hiyori

Plasma Heating Physics Research Division

Prof. KUBO, Shin (Director)
Prof. SIMOZUMA, Takashi
Prof. OSAKABE, Masaki
Prof. TSUMORI, Katsuyoshi
Assoc. YOSHIMURA, Yasuo
Assoc. Prof. NISHIURA, Masaki
Assoc. Prof. KASAHARA, Hiroshi
Assoc. Prof. IGAMI, Hiroe
Assoc. Prof. TAKAHASHI, Hiromi
Assoc. Prof. SAITO, Kenji
Assoc. Prof. SEKI, Tetsuo

Prof. NAGAOKA, Kenichi
Asst. Prof. TSUJIMURA, Toru
Asst. Prof. NAKANO, Haruhisa
Asst. Prof. KAMIO, Shuji
Asst. Prof. IKEDA, Katsunori
Asst. Prof. KISAKI, Masashi
Asst. Prof. SEKI, Ryosuke
Asst. Prof. FUJIWARA, Yutaka
Asst. Prof. NUGA, Hideo
Asst. Prof. YANAI, Ryohma

Device Engineering and Applied Physics Research Division

Prof. MITO, Toshiyuki (Director)
Prof. TAKAHATA, Kazuya
Prof. IMAGAWA, Shinsaku
Prof. YANAGI, Nagato
Prof. NISHIMURA, Kiyohiko
Prof. HIRANO, Naoki
Assoc. Prof. IWAMOTO, Akifumi
Assoc. Prof. HAMAGUCHI, Shinji

Assoc. Prof. CHIKARAIISHI, Hirotaka
Assoc. Prof. TAKAYAMA, Sadatsugu
Assoc. Prof. TANAKA, Masahiro
Assoc. Prof. SAZE, Takuya
Asst. Prof. TAKADA, Suguru
Asst. Prof. OBANA, Tetsuhiro
Asst. Prof. KOBAYASHI, Makoto
Asst. Prof. ONODERA, Yuta

Fusion Systems Research Division

Prof. MURAKAMI, Izumi (Director)
Prof. MUROGA, Takeo
Prof. MIYAZAWA, Junichi
Prof. NISHIMURA, Arata
Prof. MASUZAKI, Suguru
Assoc. Prof. TANAKA, Teruya
Assoc. Prof. TAMURA, Hitoshi
Assoc. Prof. NAGASAKA, Takuya
Assoc. Prof. HISHINUMA, Yoshimitsu

Assoc. Prof. KATO, Daiji
Assoc. Prof. TOKITANI, Masayuki
Asst. Prof. GOTO, Takuya
Asst. Prof. ASHIKAWA, Naoko
Asst. Prof. NOTO, Hiroyuki
Asst. Prof. SAKAUE, Hiroyuki
Asst. Prof. HAMAJI, Yukinori
Asst. Prof. YAJIMA, Miyuki
Asst. Prof. SHEN, Jingjie

Fusion Theory and Simulation Research Division

Prof. TODO, Yasushi (Director)
Prof. SUGAMA, Hideo
Prof. ICHIGUCHI, Katsuji
Prof. YOKOYAMA, Masayuki
Assoc. Prof. MIZUGUCHI, Naoki
Assoc. Prof. TODA, Shinichiro
Assoc. Prof. SATAKE, Shinsuke
Assoc. Prof. KANNO, Ryutaro
Assoc. Prof. SUZUKI, Yasuhiro

Assoc. Prof. NUNAMI, Masanori
Asst. Prof. YAMAGISHI, Osamu
Asst. Prof. ISHIZAKI, Ryuichi
Asst. Prof. NAKATA, Motoki
Asst. Prof. WANG, Hao
Asst. Prof. KAWAMURA, Gakushi
Asst. Prof. SATO, Masahiko
Asst. Prof. YAMAGUCHI, Hiroyuki
Asst. Prof. MATSUOKA, Seikichi

Fundamental Physics Simulation Research Division

Prof. ISHIGURO, Seiji (Director)
Prof. MIURA, Hideaki
Prof. NAKAMURA, Hiroaki
Prof. SAKAGAMI, Hitoshi
Assoc. Prof. USAMI, Shunsuke
Assoc. Prof. OHTANI, Hiroaki
Assoc. Prof. ITO, Atsushi M.

Assoc. Prof. TOIDA, Mieko
Assoc. Prof. YAMAMOTO, Takashi
Asst. Prof. HASEGAWA, Hiroki
Asst. Prof. MORITAKA, Toseo
Asst. Prof. ITO, Atsushi
Asst. Prof. TAKAYAMA, Arimichi

Rokkasho Research Center

Prof. NAKAJIMA, Noriyoshi
Asst. Prof. SATO, Masahiko (Additional Post)

Project

Large Helical Device Project

Prof. IDA, Katsumi
Prof. OSAKABE, Masaki

Numerical Simulation Reactor Research Project

Prof. SUGAMA, Hideo

Fusion Engineering Research Project

Prof. MUROGA, Takeo
Prof. YANAGI, Nagato

Research Enhancement Strategy Office

Prof. MUROGA, Takeo (Director)
Specially Appointed Prof. OKAMURA, Shoichi
Specially Appointed Prof. ROBINSON, Kenneth
Specially Appointed Prof. YAJI Kentaro

Division of Health and Safety Promotion

Prof. NISHIMURA, Kiyohiko (Division Director)

Division for Deuterium Experiments Management

Prof. OSAKABE, Masaki (Division Director)

Division of Information and Communication Systems

Prof. ISHIGURO, Seiji (Division Director)

Division of External Affairs

Prof. TAKAHATA, Kazuya (Division Director)

Fusion Science Archives

Prof. KUBO, Shin (Director)

Library

Prof. MURAKAMI, Izumi (Director)

※ This list was compiled as of March 31, 2021

Guest Professor

(None)

COE Research Fellows

SIMON Partric
SHIN Shogeth
JACOBO Varela Rodriguz
MALIK Idouakass
CHEN Hengjiun
ISLAM Md. Shahinul

Research Fellow (Science research)

(None)

Research Fellow (Industrial-Academic coordination)

(None)

JSPS Research Fellow

(None)

Department of Administration

NODA, Takao Department Director

General Affairs Division

NISHIO, Naoaki Director
ICHIOKA, Akihiro Senior Advisor
ARAI, Masanori Chief/General Affairs Section
SHIMIZU, Kazuma Chief/Planning and Evaluation Section
MAEDA, Yoshikazu Chief/Employee Section
UESUGI, Kotaro Chief/Personnel and Payroll Section
MATSUBARA, Tomohisa Chief/Communications and Public Affairs Section

Financial Affairs Division

SHIMIZU, Naomi Director
TSUDA, Makoto Deputy Director
FUJII, Kazuki Chief/Financial Planning Section
Iwashima, Itsuki Chief/Accounts and Properties Administration Section
FUKUOKA, Miwa Chief/Audit Section
HIBINO, Atsushi Chief/Procurement Section

Research Support Division

FUJITA, Hirotada Director
URUSHIHARA, Satona Deputy Director
SUZUKI, Takayuki Chief/Research Support Section
SOGA, Shihoko Chief/International Collaboration Section
KAWAI, Sanae Chief/Graduate Student Affairs Section
OHTA, Masako Chief/Academic Information Section
URUSHIHARA, Satona Leader/Visitor Center (Additional Post)
KONDO, Takahiko Chief/Visitor Center

Facilities and Safety Management Division

SHIRAHIGE, Tamio Director
WAKASHIMA, Masahiro Deputy Director
MIYATA, Kazuaki Chief/Facilities and Equipment Section
IKEDA, Katsumi Facility Planning Section

※ This list was compiled as of March 31, 2021

APPENDIX 5. List of Publications I (NIFS Reports)

- NIFS-1128 Osamu Mitarai and Nagato Yanagi
Suppression method of COVID-19 infection by isolation time control based on the SIR model and the analogy of nuclear fusion research
Dec. 01, 2020
- NIFS-MEMO-87 CHS-qa design team
Proposal of the CHS-qa experiment
July 22, 2020 (In Japanese)
- NIFS-PROC-120 Edited by Izumi Tsutsui (KEK) and Shin Kubo (NIFS)
Proceedings of the meetings on Archives in Fields of Natural Sciences in FY2019
Feb. 26, 2021 (In Japanese)
- NIFS-PROC-119 NIFS-SWJTU JOINT PROJECT FOR CFQS -PHYSICS AND ENGINEERING DESIGN-
VER.3.1 2020. NOV.
National Institute for Fusion Science, National Institutes of Natural Sciences
Institute of Fusion Science, School of Physical Science and Technology, Southwest Jiaotong University
Hefei Keye Electro Physical Equipment Manufacturing Co. Ltd.
Jan. 25, 2021
- NIFS-PROC-118 Edited by Tetsuo Ozaki and Sunao Katsuki
New Development of Beam Physics and the Application by New Generation Pulsed Power Technology
June 29, 2020
- NIFS-PROC-117 Edited by E. Kikutani (KEK) and S. Kubo (NIFS)
Proceedings of the meeting on Archives in Fields of Natural Sciences in FY2018
June 9, 2020 (In Japanese)

※ This list was compiled as of March 31, 2021

APPENDIX 6. List of Publications II (Journals, etc.)

1. Abe Y., Johzaki T., Sunahara A., Arikawa Y., Ozaki T., Ishii K., Hanayama R., Okihara S., Miura E., Komeda O., Sakata S., Matsuo K., Morita H., Takizawa R., Mizutani R., Iwamoto A., Sakagami H., Sentoku Y., Shiraga H., Nakai M., Fujioka S., Mori Y., Kitagawa Y.
Monte Carlo particle collision model for qualitative analysis of neutron energy spectra from anisotropic inertial confinement fusion
High Energy Density Physics 36 100803 2020
2. Akata N., Iwata C., Nakada M., Tanaka M., Kakiuchi H., Kovács T., Yanagisawa F., Kanai Y.
Characterization of atmospheric ²¹⁰Pb concentration and its relation to major ion species at Tsukuba, Japan
Journal of Radioanalytical and Nuclear Chemistry 327 755-760 2021
3. Araki K., Miura H.
Asymmetry of Quadratic Energy Transfer Between Ion Cyclotron and Whistler Modes in Fully Developed Hall Magnetohydrodynamic Turbulence
Plasma and Fusion Research 15 Special Issue 1 2401024 2020
4. Bando T., Ohdachi S.
Research and Technology Notes: Separation of fluctuation component with Singular Spectrum Analysis
Journal of Plasma and Fusion Research 96 5 262-266 2020
5. Berkel M., Van kampen R., Vandersteen G., Kobayashi T., Ravensbergen T., Igami H., Lammers J., Oosterwegel G., Galperti C., Felici F., Baar M.
Correcting for non-periodic behaviour in perturbative experiments: application to heat pulse propagation and modulated gas-puff experiments
Plasma Physics and Controlled Fusion 62 9 94001 2020
6. Chen H., Uehara H., Kawase H., Yasuhara R.
Efficient visible laser operation of Tb:LiYF₄ and LiTbF₄
Optics Express 28 8 10951-10959 2020
7. Chen H., Uehara H., Yasuhara R.
Compact deep ultraviolet frequency-doubled Tb:LiYF₄ lasers at 272 nm
Optics Letters 45 19 5558 2020
8. Chen H., Yao W., Uehara H., Yasuhara R.
Graphene Q-switched Tb:LiYF₄ green laser
Optics Letters 45 9 2596-2599 2020
9. Ejiri A., Aoi Y., Yamazaki H., Tsujii N., Takase Y., Watanabe O., Ko Y., Rice J., Peng Y., Iwasaki K., Matsuzaki K., Osawa Y., Yoshimura Y.
Development of a Compact Hard X-Ray Camera on the TST-2 Spherical Tokamak
Plasma and Fusion Research 15 Regular Issue 1202023 2020
10. Fujita K., Satake S., Kanno R., Nunami M., Nakata M., García-regaña J., Velasco J., Calvo I.
Global calculation of neoclassical impurity transport including the variation of electrostatic potential
Journal of Plasma Physics 86 3 905860319 2020
11. Fujiwara Y., Kamio S., Yamaguchi H., Garcia A., Stagner L., Nuga H., Seki R., Ogawa K., Isobe M., Yokoyama M., Heidbrink W., Osakabe M., LHD Experiment Group.
Fast-ion D alpha diagnostic with 3D-supporting FIDASIM in the Large Helical Device
Nuclear Fusion 60 11 112014 2020
12. Geiger B., Stagner L., Heidbrink W., Dux R., Fischer R., Fujiwara Y., Garcia A., Jacobsen A., Vuuren A., Karpushov A., Liu D., Schneider P., Sfiligoi I., Poloskei P., Weiland M.
Progress in modelling fast-ion D-alpha spectra and neutral particle analyzer fluxes using FIDASIM
Plasma Physics and Controlled Fusion 62 10 105008 2020
13. Goto M., Ramaiya N.
Polarization of Lyman- α Line Due to the Anisotropy of Electron Collisions in a Plasma
Symmetry 13 2 297 2021

14. Goto M., Ramaiya N., Oishi T., Kawamoto Y., Kawate T.
Measurement of anisotropic electron velocity distribution function in LHD by polarization spectroscopy
Plasma and Fusion Research 16 Special Issue 1 2402029 2021
15. Goya K., Mori A., Tokita S., Yasuhara R., Kishi T., Nishijima Y., Tanabe S., Uehara H.
Broadband mid-infrared amplified spontaneous emission from Er/Dy co-doped fluoride fiber with a simple diode-pumped configuration
Scientific Reports 11 5432 2021
16. Haba Y., Nagaoka K., Tsumori K., Kisaki M., Takahashi K., Nakano H., Ikeda K., Yoshimura S., Osakabe M.
Response of beam focusing to plasma fluctuation in a filament-arc-type negative ion source
Japanese Journal of Applied Physics 59 SH SHHA01 2020
17. Habara H., Lad A., Nagami R., Singh P., Chatterjee G., Adak A., Dalui M., Jha J., Brijesh P., Mishima Y., Nagai K., Sakagami H., Tata S., Talluri M., Krishnamurthy M., Tanaka K., Kumar G.
Micro-optics for ultra-intense lasers
AIP Advances 11 3 35214 2021
18. Hashida M., Furukawa Y., Inoue S., Sakabe S., Masuno S., Kusaba M., Sakagami H., Tsukamoto M.
Uniform LIPSS on titanium irradiated by two-color double-pulse beam of femtosecond laser
Journal of Laser Applications 32 2 22054 2020
19. Hirano N., Nagai S., Xie Y., Okamura T.
Basic research of HTS coil cooling assist technology by magnetic refrigeration
Journal of Physics: Conference Series 1559 12090 2020
20. Hu K., Wang Q., Koyamada K., Ohtani H., Goto T., Miyazawa J.
Visualization of The Plasma Shape in a Force Free Helical Reactor, FFHR
Journal of Advanced Simulation in Science and Engineering 7 1 151-167 2020
21. Hu W., Kobayashi T., Suzuki Y., Yoshinuma M., Tokuzawa T., Ida K.
Correlation analysis between density and magnetic field low frequency fluctuations in improved confinement mode on LHD
Plasma and Fusion Research 16 Special Issue 1 2402031 2021
22. Ida K.
Bifurcation phenomena in magnetically confined toroidal plasmas
Advances in Physics: X 5 1 1801354 2020
23. Ida K., Yoshinuma M., Tanaka K., Nakata M., Kobayashi T., Fujiwara Y., Sakamoto R., Motojima G., Masuzaki S., The LHD Experimental Group.
Characteristics of plasma parameters and turbulence in the isotope-mixing and the non-mixing states in hydrogen–deuterium mixture plasmas in the large helical device
Nuclear Fusion 61 1 16012 2021
24. Imagawa S., Obana T., Hamaguchi S., Yanagi N., Mito T.
Normal-zone propagation in helical coils of Large Helical Device
Journal of the Cryogenic Society of Japan 55 5 357-365 2020
25. Ishiyama S., Chikaraishi H., Sagara A.
Operating scenario of 3GWth class FFHR power plant with bypass controlled supercritical CO₂ gas turbine power generation system
Fusion Engineering and Design 164 112194 2021
26. Islam M., Nakashima Y., Iijima T., Nojiri K., Ezumi N., Yoshikawa M., Kariya T., Minami R., Hirata M., Hoshino K., Hatayama A., Hasegawa H., Ishiguro S., Matsuura H., Sakamoto M.
Study of the Transient Behavior of Detached Plasma during Xe Gas Injection into the D-Module of GAMMA 10/PDX
Plasma and Fusion Research 15 Regular Issue 1402074 2020
27. Islam M., Nakashima Y., Ishiguro S., Hoshino K., Hatayama A., Hasegawa H., Sakamoto M.
Numerical Simulation Study of the Magnetic Flux Tube Expansion on the Divertor Plasma Parameters by the LINDA Code
Plasma and Fusion Research 16 Special Issue 1 2403049 2021

28. Ito A.
Saloon: An Encouragement of Writing with Markdown
Journal of Plasma and Fusion Research 96 7 379-387 2020
29. Ito A., Nakajima N.
Two-fluid and finite Larmor radius effects on high-beta tokamak equilibria with flow in reduced magnetohydrodynamics
Physica Scripta 96 3 35602 2021
30. Ito A., Takayama A., Watanabe O., Singh V., Tyagi S., Singh S.
Tuning of Density Functional Theory Simulation on Vector Processor System – Plasma Simulator Raijin –
Plasma and Fusion Research 15 Regular Issue 1203085 2020
31. Ito D., Yazawa H., Tomitaka M., Kumagai T., Kono S., Yamauchi M., Misawa T., Kobuchi T., Hayashi H., Miyake H., Ogawa K., Nishitani T., Isobe M.
Development of a Wide Dynamic Range Neutron Flux Measurement Instrument Having Fast Time Response for Fusion Experiments
Plasma and Fusion Research 16 Regular Issue 1405018 2021
32. Iwamoto A., Kodama R.
Conceptual design of a subcritical research reactor for inertial fusion energy with the J-EPoCH facility
High Energy Density Physics 36 100842 2020
33. Kageyama A., Sakamoto N., Miura H., Ohno N.
Interactive Exploration of the In-Situ Visualization of a Magnetohydrodynamic Simulation
Plasma and Fusion Research 15 Regular Issue 1401065 2020
34. Kamio S., Fujiwara Y., Nagaoka K., Ogawa K., Seki R., Yamaguchi H., Nuga H., Isobe M., Osakabe M., Cheng C.
Observation of clump structure in transported particle orbit using an upgraded neutral particle analyzer during TAE burst in LHD
Nuclear Fusion 60 11 112002 2020
35. Kamio S., Fujiwara Y., Ogawa K., Kobayashi M., Sangaroon S., Isobe M., Seki R., Nuga H., Osakabe M., Matsuyama S., Miwa M., Toyama S.
Neutron-induced signal on the single crystal chemical vapor deposition diamond-based neutral particle analyzer
Review of Scientific Instruments 91 11 113304 2020
36. Kamio S., Fujiwara Y., Ogawa K., Seki R., Nagaoka K., Nuga H., Sangaroon S., Isobe M., Osakabe M., Cheng C.
Initial Results of Hydrogen and Deuterium Beam Ion Simultaneous Transport due to Toroidal Alfvén Eigenmode in the Large Helical Device
Plasma and Fusion Research 16 Special Issue 1 2402044 2021
37. Kamitani A., Takayama T., Saitoh A., Nakamura H.
Acceleration Techniques for Linear-System Solver in Shielding Current Analysis of Cracked HTS Film
Plasma and Fusion Research 16 Special Issue 1 2405005 2021
38. Kawase H., Uehara H., Yao W., Chen H., Yasuhara R.
Optical chopper based mechanically Q-switched ~3 μm Er:YAP single-crystal laser
Japanese Journal of Applied Physics 60 1 12002 2021
39. Kawate T., Tsuzuki T., Shimizu T., Imada S., Katsukawa Y., Hara H., Suematsu Y., Ichimoto K., Hattori T., Narasaki S., Warren H., Teriaca L., Korendyke C., Brown C., Auchere F.
A sensitivity analysis of the updated optical design for EUVST on the Solar-C mission
Proceedings of SPIE 11444 114443J 2020
40. Kobayashi M., Angelone M., Yoshihashi S., Ogawa K., Isobe M., Nishitani T., Sangaroon S., Kamio S., Fujiwara Y., Tsubouchi T., Uritani A., Sakama M., Osakabe M., The LHD Experimental Group.
Thermal neutron measurement by single crystal CVD diamond detector applied with the pulse shape discrimination during deuterium plasma experiment in LHD
Fusion Engineering and Design 161 112063 2020

41. Kobayashi M., Ogawa K., Isobe M., Nishitani T., Nishimura T., Mukai K., Yoshihashi S., Osakabe M.
Design of neutron spectrum-shaping assembly around the pneumatic tube-end in the LHD torus hall for the medical research application
Plasma and Fusion Research 15 Special Issue 1 2405043 2020
42. Kobayashi M., Tokar M.
Time-dependent plasma transport simulation for the study of edge impurity radiation dynamics with magnetic island in large helical device
Contributions to Plasma Physics 60 5-6 e201900138 2020
43. Kobayashi T.
The physics of the mean and oscillating radial electric field in the L–H transition: the driving nature and turbulent transport suppression mechanism
Nuclear Fusion 60 9 95001 2020
44. Kobayashi T., Ida K., Tanaka K., Yoshinuma M., Tsujimura T., Inagaki S., Tokuzawa T., Tsuchiya H., Tamura N., Igami H., Yoshimura Y., Itoh S., Itoh K.
Isotope effect in transient electron thermal transport property and its impact on the electron internal transport barrier
Nuclear Fusion 60 7 76015 2020
45. Kobayashi T., Kin F., Kawachi Y., Sasaki M., Kosuga Y., Yamasaki K., Inagaki S.
Impact of helium neutral gas puff on plasma turbulence in linear magnetized argon plasmas
Physics of Plasmas 27 6 62309 2020
46. Kobayashi T., Yanai R., Tsujimura T., Tokuzawa T., Ida K.
Transient Electron Thermal Transport Analysis Accounting Oblique Electron Cyclotron Resonance Heating Injection to Magnetic Field Line
Plasma and Fusion Research 15 Regular Issue 1402072 2020
47. Kobayashi T., Yoshinuma M., Ida K.
Two-dimensional beam emission spectroscopy for hydrogen isotope negative neutral beam in Large Helical Device
Plasma Physics and Controlled Fusion 62 12 125011 2020
48. Kocsis G., Tamura N., Bussiahn R., McCarthy K., Baldzuhn J., Biedermann C., Cseh G., Damm H., Kornejew P., König R., Panadero N., Szepesi T.
Investigation of TESPEL cloud dynamics in Wendelstein 7-X stellarator
Nuclear Fusion 61 1 16006 2021
49. Koschinsky J., Akaslompolo S., Biedermann C., Bozhenkov S., Isobe M., Kontula J., Ogawa K., Schneider W., Warmer F., Wurden G., Wolf R., W7-x team T.
Estimation of 14 MeV neutron rate from triton burn-up in future W7-X deuterium plasma campaigns
Contributions to Plasma Physics 60 8 e201900186 2020
50. Kuzmin A., Kobayashi M., Hanada K., Idei H., Onchi T., Mori S., Yoneda N., Shikama T., Hasuo M., Ido T., Nagashima Y., Ikezoe R., Hasegawa M., Kuroda K., Kono K., Matsuo S., Nagata T., Shimabukuro S., Higashijima A., Niiya I., Zushi H.
Investigation of radial distribution of atomic hydrogen flux to the plasma facing components in steady state discharges in QUEST tokamak
Nuclear Materials and Energy 26 100872 2021
51. Langenberg A., Wegner T., Pablant N., Marchuk O., Geiger B., Tamura N., Bussiahn R., Kubkowska M., Mollén A., Traverso P., Smith H., Fuchert G., Bozhenkov S., Damm H., Pasch E., Brunner K., Knauer J., Beurskens M., Burhenn R., Wolf R.
Charge-state independent anomalous transport for a wide range of different impurity species observed at Wendelstein 7-X
Physics of Plasmas 27 5 52510 2020
52. Leconte M., Kobayashi T.
Zonal profile corrugations and staircase formation: Role of the transport crossphase
Physics of Plasmas 28 1 14503 2021
53. Li H., Fujiwara S., Nakamura H., Mizuguchi T., Nakata A., Miyazaki T., Saito S.
Structural change of damaged polyethylene by beta-decay of substituted tritium using reactive force field
Japanese Journal of Applied Physics 60 SA SAAB06 2021

54. Liu B., Dai S., Kawamura G., Zhang L., Yang Z., Feng Y., Wang D.
EMC3-EIRENE modelling of the toroidally asymmetric heat flux distribution with neon impurity injection on EAST
Nuclear Materials and Energy 26 100844 2021
55. Ma B., Hishinuma Y., Noto H., Shimada Y., Muroga T.
Development of Y2O3 dispersion strengthened Cu alloy using Cu6Y and Cu2O addition through the MA-HIP process
Fusion Engineering and Design 161 112045 112045 2020
56. Ma B., Hishinuma Y., Shimada Y., Noto H., Kasada R., Oono N., Ukai S., Muroga T.
The size dependence of microstructure and hardness on the MA powders for the MA-HIP processed Cu-Y2O3 dispersion-strengthened alloys
Nuclear Materials and Energy 24 100773 2020
57. Masuzaki S., Yajima M., Ogawa K., Motojima G., Tanaka M., Tokitani M., Isobe M., Otsuka T.
Investigation of the distribution of remaining tritium in divertor in LHD
Nuclear Materials and Energy 26 100884 2021
58. Matsunaga S., Narushima Y., Onodera Y., Terazaki Y., Miyazawa J., Yanagi N.
HTS-WISE Conductor and Magnet Impregnated with Low-Melting Point Metal
IEEE Transactions on Applied Superconductivity 30 4 4601405 2020
59. Matsuura H., Sugiyama S., Kimura K., Kajimoto S., Nishitani T., Ogawa K., Kawamoto Y., Isobe M., Osakabe M.
Observation of a nuclear-elastic-scattering effect caused by energetic protons on deuteron slowing-down behaviour on the Large Helical Device
Nuclear Fusion 60 6 66007 2020
60. Mitarai O., Sugiyama S., Yanagi N., Narushima Y., Sakamoto R., Goto T., Matsuura H., Sagara A.
Comparative Studies on the Control Algorithm for the High-Density Ignition Regime in FFHR-d1
Plasma and Fusion Research 15 Special Issue 1 2405059 2020
61. Morishita Y., Murakami S., Yokoyama M., Ueno G.
Data assimilation system based on integrated transport simulation of Large Helical Device plasma
Nuclear Fusion 60 5 56001 2020
62. Morishita Y., Murakami S., Yokoyama M., Ueno G.
Special Topic Articles: Progress of Physical Modeling by Data-Driven Approach in Magnetically Confined Fusion Plasmas 3.Transport Modeling Applying Data Assimilation Techniques -PracticalCases in LHD-
Journal of Plasma and Fusion Research 97 2 72-78 2021
63. Moseev D., Laqua H., Stange T., Abramovic I., Nielsen S., Akaslompolo S., Avramidis K., Braune H., Gantenbein G., Illy S., Jelonnek J., Jin J., Kasperek W., Krier L., Korsholm S., Lechte C., Marek A., Marsen S., Nishiura M., Pagonakis I., Salewski M., Rasmussen J., Tancetti A., Thumm M., Wolf R.
Collective Thomson Scattering Diagnostic for Wendelstein 7-X at 175 GHz
Journal of Instrumentation 15 C05035 2020
64. Motojima G., Masuzaki S., Morisaki T., Kobayashi M., Sakamoto R., Tsuchibushi Y., Murase T., Takeiri Y., The LHD Experimental Group.
Application of Divertor Pumping to Long-Pulse Discharge for Particle Control in LHD
Plasma and Fusion Research 16 Regular Issue 1202014 2021
65. Mukai K., Masuzaki S., Hayashi Y., Oishi T., Suzuki C., Kobayashi M., Tanaka H., Peterson B., The LHD Experimental Group.
Divertor Detachment with Multi-Species Impurity Seeding in LHD
Plasma and Fusion Research 15 Regular Issue 1402051 2020
66. Murakami I., Kato D., Oishi T., Goto M., Kawamoto Y., Suzuki C., Sakaue H., Morita S.
Progress of tungsten spectral modeling for ITER edge plasma diagnostics based on tungsten spectroscopy in LHD
Nuclear Materials and Energy 26 100923 2021
67. Murakami I., Kato M., Emoto M., Kato D., Sakaue H., Kawate T.
NIFS Atomic and Molecular Numerical Database for Collision Processes
Atoms 8 4 71 2020

68. Murase T., Nakagawa S., Kinoshita S., Shimizu A., Okamura S., Isobe M., Xiong G., Xu Y., Liu H., Liu H., Yin D.
Eddy current analyses for vacuum vessel of CFQS quasi-axisymmetric stellarator
Fusion Engineering and Design 161 111869 2020
69. Muroga T., Möslang A., Diegele E.
Users' perspective on D-Li neutron sources (A-FNS and IFMIF-DONES) for DEMO and beyond
Journal of Nuclear Materials 535 152186 2020
70. Nagayama Y., Ejiri A., Takase Y., Tsujii N., Nakanishi H., Ohsuna M., Tsuchiya H., Yamaguchi S.
Measurement of Electron Density Fluctuations by Using the O-mode Microwave Imaging Reflectometry (O-MIR) in TST-2 Spherical Tokamak
Plasma and Fusion Research 15 Special Issue 1 2402060 2020
71. Nakagawa S., Murase T., Shimizu A., Kinoshita S., Isobe M., Okamura S., Xu Y., Liu H., Xiong G., Liu H., Yin D., Wan Y.
Engineering Analysis for Vacuum Vessel of CFQS Quasi-Axisymmetric Stellarator
Plasma and Fusion Research 15 Special Issue 1 2405066 2020
72. Nakanishi H., Yamanaka K., Tokunaga S., Ozeki T., Homma Y., Ohtsu H., Ishii Y., Nakajima N., Yamamoto T., Emoto M., Ohsuna M., Imazu S., Inoue T., Nakamura O., Abe S., Urushidani S.
Demonstration of High-speed Data Replication Relay across Multiple Repository Sites Using a Global Loop Path
Plasma and Fusion Research 16 Special Issue 1 2405017 2021
73. Nakano H., Kisaki M., Ikeda K., Tsumori K., Nagaoka K., Haba Y., Masaki S., Fujiwara Y., Kamio S., Osakabe M.
Deuterium experiment with large-scale negative ion source for large helical device
Japanese Journal of Applied Physics 59 SH SHHC09 2020
74. Nakasone S., Ishimine A., Shiroma S., Masuda N., Nakamura K., Shiroma Y., Ooka S., Tanaka M., Kato A., Hosoda M., Akata N., Yasuoka Y., Furukawa M.
Temporal and Spatial Variation of Radon Concentrations in Environmental Water from Okinawa Island, Southwestern Part of Japan
International Journal of Environmental Research and Public Health 18 3 998 2021
75. Nakasone S., Yokoyama S., Takahashi T., Ota M., Kakiuchi H., Sugihara S., Hirao S., Momoshima N., Tamari T., Shima N., Atarashi-Andoh M., Fukutani S., Ishimine A., Furukawa M., Tanaka M., Akata N.
Preliminary Investigation of Pretreatment Methods for Liquid Scintillation Measurements of Environmental Water Samples Using Ion Exchange Resins
Plasma and Fusion Research 15 Special Issue 1 2405027 2020
76. Nakasone S., Yokoyama S., Takahashi T., Ota M., Kakiuchi H., Sugihara S., Hirao S., Momoshima N., Tamari T., Shima N., Atarashi-Andoh M., Fukutani S., Nakamura K., Ishimine A., Furukawa M., Tanaka M., Akata N.
Simple Pretreatment Method for Tritium Measurement in Environmental Water Samples using a Liquid Scintillation Counter
Plasma and Fusion Research 16 Special Issue 1 2405035 2021
77. Narushima Y., Miyazawa J., Matsunaga S., Yanagi N.
Edgewise-strain-free helical winding using high-temperature superconducting tape conductor
Plasma and Fusion Research 15 Regular Issue 1405076 2020
78. Nimavat N., Goto M., Segueineaud G., Oishi T., Morita S.
Measurement of polarization in Lyman- α line caused by anisotropic electron collisions in LHD plasma
Journal of Quantitative Spectroscopy and Radiative Transfer 260 107430 2021
79. Nishijima D., Tokitani M., Patino M., Nagata D., A G., Doerner R.
Impact of seeded plasma impurities on D retention in RAFM steels
Nuclear Materials and Energy 23 100740 2020
80. Nishimura A.
Neutron irradiation effect on critical current of Nb3Sn wire under 8 T to 15.5 T
IOP Conference Series: Materials Science and Engineering 756 12013 2020

81. Nishimura A.
Study on Assembly of TF Coil and Vacuum Vessel for Fusion DEMO
Plasma and Fusion Research 16 Special Issue 1 2405036 2021
82. Nishiura M., Shimizu T., Kobayashi S., Tokuzawa T., Ichinose K., Kubo S.
Q-band high-performance notch filters at 56 and 77 GHz notches for versatile fusion plasma diagnostics
Review of Scientific Instruments 92 3 34711 2021
83. Noto H., Hishinuma Y., Muroga T., Benoki H.
Formation Mechanism of Nano-Strengthening Particles in Dispersion Strengthened W-Ti Alloys
Plasma and Fusion Research 15 Regular Issue 1205021 2020
84. Noto H., Hishinuma Y., Muroga T., Benoki H.
Microstructure and mechanical properties of dispersion strengthened tungsten by HIP treatment followed by thermal annealing
Results in Materials 7 100116 2020
85. Nuga H., Seki R., Ogawa K., Kamio S., Fujiwara Y., Osakabe M., Isobe M., Nishitani T., Yokoyama M.
Studies of the fast ion confinement in the Large Helical Device by using neutron measurement and integrated codes
Journal of Plasma Physics 86 3 815860306 2020
86. Nunami M., Nakata M., Toda S., Sugama H.
Gyrokinetic simulations for turbulent transport of multi-ion-species plasmas in helical systems
Physics of Plasmas 27 5 52501 2020
87. Obana T., Ogitsu T.
Design of Lightweight Superconducting Magnets for a Rotating Gantry with Active Shielding
IEEE Transactions on Applied Superconductivity 30 4 8957464 2020
88. Obana T., Takahata K., Murakami H.
Investigation into quench detection for a multi-stacked pancake coil wound with Nb₃Sn CIC conductors
Plasma and Fusion Research 15 Special Issue 1 2405028 2020
89. Ogawa K., Isobe M., Osakabe M.
Progress on Integrated Neutron Diagnostics for Deuterium Plasma Experiments and Energetic Particle Confinement Studies in the Large Helical Device During the Campaigns from FY2017 to FY2019
Plasma and Fusion Research 16 Regular Issue 1102023 2021
90. Ogawa K., Isobe M., Seki R., Nuga H., Sangaroon S., Jo J., Osakabe M.
Neutron Emission Rate Characteristics of an Electron Cyclotron Heated Large Helical Device Deuterium Plasma
Plasma and Fusion Research 16 Special Issue 1 2402008 2021
91. Ogawa K., Isobe M., Sugiyama S., Matsuura H., Spong D., Nuga H., Seki R., Kamio S., Fujiwara Y., Yamaguchi H., Osakabe M., LHD Experiment Group.
Energetic particle transport and loss induced by helically-trapped energetic-ion-driven resistive interchange modes in the Large Helical Device
Nuclear Fusion 60 11 112011 2020
92. Ogawa K., Yokoyama M., Isobe M.
Regression Approach for Acquiring a Quantitative Guidance toward Updating the Deuterium-Deuterium Fusion Neutron Emission Rate in the Large Helical Device
Plasma and Fusion Research 15 Regular Issue 1202087 2020
93. Ogawa K., Zhong G., Zhou R., Li K., Isobe M., Hu L.
1 MeV triton orbit analysis in EAST plasma
Plasma and Fusion Research 15 Special Issue 1 2402022 2020
94. Ohtani Y., Tanaka K., Igami H., Ida K., Suzuki Y., Takemura Y., Tsuchiya H., Sanders M., Yoshinuma M., Tokuzawa T., Yamada I., Yasuhara R., Funaba H., Shoji M., Bando T.
Effects of core stochastization on particle and momentum transport
Nuclear Fusion 61 3 34002 2021

95. Oishi T., Morita S., Kato D., Murakami I., Sakaue H., Kawamoto Y., Goto M., The LHD Experimental Group.
Identification of Forbidden Emission Lines from Highly Ionized Tungsten Ions in VUV Wavelength Range in LHD for ITER Edge Plasma Diagnostics
Nuclear Materials and Energy 26 100932 2021
96. Oishi T., Morita S., Kato D., Murakami I., Sakaue H., Kawamoto Y., Goto M., The LHD Experimental Group.
Observation of line emissions from Ni-like W46 + ions in wavelength range of 7–8 Å in the Large Helical Device
Physica Scripta 96 2 25602 2021
97. Oishi T., Morita S., Kobayashi M., Mukai K., Kawamura G., Masuzaki S., Hayashi Y., Suzuki C., Kawamoto Y., Goto M., The LHD Experimental Group.
EUV and VUV Spectra of NeIII-NeX Line Emissions Observed in the Impurity Gas-puffing Experiments of the Large Helical Device
Plasma and Fusion Research 16 Special Issue 1 2402006 2021
98. Okamura S., Liu H., Shimizu A., Kinoshita S., Isobe M., Xiong G., Xu Y.
Island divertor configuration design for a quasi-axisymmetric stellarator CFQS
Journal of Plasma Physics 86 4 815860402 2020
99. Ozaki T., Kamio S., Saito K.
Measurements of D/H Ratio Using Compact Neutral Particle Analyzer in LHD Deuterium Experiments
Plasma and Fusion Research 15 Special Issue 1 2402034 2020
100. Saito K., Seki R., Kamio S., Kasahara H., Seki T.
Schemes for ICRF heating of high-density core plasma in LHD
Plasma and Fusion Research 15 Special Issue 1 2402015 2020
101. Saito K., Wi H., Wang S., Kim H., Jang K., Lee H., Kim J., Kwak J.
Development of a compact ICRF antenna for high-power and long-pulse plasma heating in the KSTAR
Fusion Engineering and Design 154 111496 2020
102. Saito S., Nakamura H., Sawada K., Kobayashi M., Kawamura G., Hasuo M.
Development of a Molecular Dynamics Method with Heat Transfer into Bulk for Ion Injection into Materials
Plasma and Fusion Research 15 Special Issue 1 2403073 2020
103. Saito S., Nakamura H., Sawada K., Kobayashi M., Kawamura G., Sawada T., Hasuo M.
Molecular dynamics simulation for hydrogen recycling on tungsten divertor for neutral transport analysis
Japanese Journal of Applied Physics 60 SA SAAB08 2021
104. Sangaroon S., Ogawa K., Isobe M., Fujiwara Y., Yamaguchi H., Kamio S., Seki R., Nuga H., Kobayashi M., Osakabe M.
Characterization of the New Vertical Neutron Camera Designed for the Low Neutron Emission Rate Plasma in Large Helical Device
Plasma and Fusion Research 16 Regular Issue 1402039 2021
105. Sangaroon S., Ogawa K., Isobe M., Kobayashi M., Fujiwara Y., Kamio S., Seki R., Nuga H., Yamaguchi H., Osakabe M., LHD Experiment Group.
Performance of the newly installed vertical neutron cameras for low neutron yield discharges in the Large Helical Device
Review of Scientific Instruments 91 8 83505 2020
106. Sasaki M., Kobayashi T., Dendy R., Kawachi Y., Arakawa H., Inagaki S.
Evaluation of abrupt energy transfer among turbulent plasma structures using singular value decomposition
Plasma Physics and Controlled Fusion 63 2 25004 2021
107. Sasaki M., Kobayashi T., Inagaki S., Kasuya N., Kosuga Y.
Neutral particle drag on parallel flow shear driven instability
Physics of Plasmas 27 8 82105 2020
108. Satake S., Kanno R., Honda M., Usami S.
Lecture Note: Introduction to Random Numbers for Simulations
Journal of Plasma and Fusion Research 96 6 290-299, 367-378, 405-419 2020
109. Satake S., Nakata M., Pianpanit T., Sugama H., Nunami M., Matsuoka S., Ishiguro S., Kanno R.
Benchmark of a new multi-ion-species collision operator for δf Monte Carlo neoclassical simulation
Computer Physics Communications 255 107249 2020

110. Sato M., Todo Y.
Ion kinetic effects on linear pressure driven magnetohydrodynamic instabilities in helical plasmas
Journal of Plasma Physics 86 3 815860305 2020
111. Seki R., Kamio S., Kasahara H., Saito K., Seki T., Ogawa K., Isobe M., Nuga H., Takahashi H., Kubo S., Osakabe M.
Initial result of neutron emission rate analysis for ion cyclotron range of frequency heated deuterium plasmas in LHD
Plasma and Fusion Research 15 Regular Issue 1202088 2020
112. Seki R., Todo Y., Suzuki Y., Ogawa K., Isobe M., Spong D., Osakabe M.
Hybrid simulation of NBI fast-ion losses due to the Alfvén eigenmode bursts in the Large Helical Device and the comparison with the fast-ion loss detector measurements
Journal of Plasma Physics 86 5 905860520 2020
113. Shen J., Nagasaka T., Muroga T., Yang H., Kano S., Abe H.
Microstructural evolution of two-way cold rolled 12Cr ODS steel under 1073–1373 K annealing
Nuclear Materials and Energy 25 100792 2020
114. Shoji M.
Radiation Resistant Camera System for Monitoring Deuterium Plasma Discharges in the Large Helical Device
Plasma and Fusion Research 15 Special Issue 1 2402039 2020
115. Shoji M., Kawamura G., Romazanov J., Kirschner A., Eksaeva A., Borodin D., Masuzaki S., Brezinsek S.
Boron transport simulation using the ERO2.0 code for real-time wall conditioning in the Large Helical Device
Nuclear Materials and Energy 25 100853 2020
116. Shoji M., Kawamura G., Romazanov J., Kirschner A., Eksaeva A., Borodin D., Masuzaki S., Brezinsek S.
Simulation of Impurity Transport and Deposition in the Closed Helical Divertor in the Large Helical Device
Plasma and Fusion Research 16 Special Issue 1 2403004 2021
117. Shoji M., Kawamura G., Smirnov R., Tanaka Y., Masuzaki S., Uesugi Y., Ashikawa N., Gilson E., Lunsford R.
Full-torus impurity transport simulation for optimizing plasma discharge operation using a multi-species impurity powder dropper in the large helical device
Contributions to Plasma Physics 60 5-6 e201900101 2020
118. Sugama H., Ichiguchi K., Suzuki Y., Sato M., Miura H., Ishizaki R., Furukawa M., Toda S., Nakata M., Nunami M., Matsuoka S., Satake S., Kanno R., Todo Y., Toida M., Yamaguchi H., Wang H., Seki R., Kawamura G., Nakamura H., Ito A., Takayama A., Fujiwara S., Yokoyama M., Nuga H., Suzuki C., Murakami S., Morishita Y., Ishiguro S., Ito A., Usami S., Ohtani H., Sakagami H., Hasegawa H., Moritaka T., Horiuchi R., Miyazawa J., Ohno N., Kageyama A., Tamura Y., Kitazawa S., Katagiri T., Ohshima S., Nagai T., Nagura S., Kawahara S., Hu K., Koyamada K., Goto T., Kamuki N., Takamaru H., Petrosky T., Tanaka S.
Project Review: Numerical Simulation Reactor Research Project at the National Institute for Fusion Science
Journal of Plasma and Fusion Research 96 10 576-635 2020
119. Sugama H., Matsuoka S., Nunami M., Satake S.
The Eulerian variational formulation of the gyrokinetic system in general spatial coordinates
Physics of Plasmas 28 2 22312 2021
120. Sugiyama S., Nishitani T., Matsuura H., Isobe M., Ogawa K., Tanaka T., Yoshihashi S., Uritani A., Osakabe M.
Observation of neutron emission anisotropy by neutron activation measurement in beam-injected LHD deuterium plasmas
Nuclear Fusion 60 7 76017 2020
121. Sumida S., Shinohara K., Nishitani T., Ogawa K., Bando T., Sukegawa A., Ishikawa M., Takada E., Bierwage A., Oyama N.
Conceptual design of a collimator for the neutron emission profile monitor in JT-60SA using Monte Carlo simulations
Review of Scientific Instruments 91 11 113504 2020
122. Suzuki C., Dipti D., Yang Y., Gall A., Silwal R., Sanders S., Naing A., Tan J., Takacs E., Ralchenko Y.
Identifications of extreme ultraviolet spectra of Br-like to Ni-like neodymium ions using an electron beam ion trap
Journal of Physics B: Atomic, Molecular and Optical Physics 54 1 15001 2021
123. Suzuki Y.
Effect of pressure profile on stochasticity of magnetic field in a conventional stellarator
Plasma Physics and Controlled Fusion 62 10 104001 2020

124. Suzuki Y., Purohit S., Ohdachi S., Yamamoto S., Nagasaki K.
New tomographic reconstruction technique based on Laplacian eigenfunction
Plasma Science and Technology 22 10 102002 2020
125. Suzuki Y., Watanabe K., Sakakibara S.
Theoretical studies of equilibrium beta limit in LHD plasmas
Physics of Plasmas 27 10 102502 2020
126. Tachibana Y., Kalak T., Nogami M., Tanaka M.
Combined use of tannic acid-type organic composite adsorbents and ozone for simultaneous removal of various kinds of radionuclides in river water
Water Research 182 116032 2020
127. Takayama T., Yamaguchi T., Saitoh A., Kamitani A., Nakamura H.
Multi-Objective Optimization of Superconducting Linear Acceleration System for Pellet Injection by Using Finite Element Method
Plasma and Fusion Research 16 Special Issue 1 2401025 2021
128. Takemura Y., Watanabe K., Sakakibara S., Ohdachi S., Narushima Y., Ida K., Yoshinuma M., LHD Experiment Group.
External RMP effect on locked-mode-like instability in helical plasmas
Nuclear Fusion 61 2 26011 2021
129. Tamura H., Goto T., Miyazawa J., Tanaka T., Yanagi N.
Topology optimization for superconducting magnet system in helical fusion reactor
Journal of Physics: Conference Series 1559 12108 2020
130. Tanaka H., Fujii K., Shikama T., Morita S., Goto M., Hasuo M., LHD Experiment Group.
Plasma Spectroscopy on an Aluminum-Pellet Ablation Cloud in an LHD Plasma with an Echelle Spectrometer
Atoms 8 4 81 2020
131. Tanaka H., Hayashi Y., Kajita S., Meiden H., Yoshikawa M., Vernimmen J., Scholten J., Classen I., Morgan T., Ohno N.
Cross-field transport in detached helium plasmas in Magnum-PSI
Plasma Physics and Controlled Fusion 62 11 115021 2020
132. Tanaka H., Kawamura G., Hoshino K., Kobayashi M., Matsunaga G., Suzuki Y., Lunt T., Feng Y., Ohno N.
First EMC3-EIRENE modelling of JT-60SA edge plasmas with/without resonant magnetic perturbation field
Contributions to Plasma Physics 60 5-6 e201900114 2020
133. Tanaka H., Saeki I., Ohno N., Kajita S., Ido T., Natsume H., Hatayama A., Hoshino K., Sawada K., Goto M.
Detached helium plasma simulation by a one-dimensional fluid code with detailed collisional-radiative model
Physics of Plasmas 27 10 102505 2020
134. Tanaka M., Kato H., Suzuki N.
Analysis of hydrocarbons in the exhaust gas of a fusion test device using infrared absorption spectroscopy
Plasma and Fusion Research 15 Special Issue 1 2405008 2020
135. Tanaka M., Kato H., Suzuki N., Masuzaki S., Yajima M., Nakada M., Iwata C.
Tritium Balance in Large Helical Device during and after the First Deuterium Plasma Experiment Campaign
Plasma and Fusion Research 15 Regular Issue 1405062 2020
136. Tanaka M., Suzuki N., Kato H.
Exhaust behavior of tritium from the Large Helical Device in the first deuterium plasma experiment
Journal of Nuclear Science and Technology 57 12 1297-1306 2020
137. Tanaka M., Suzuki N., Kato H., Chimura H.
Performance of exhaust detritiation system for a fusion test device in the initial phase of the operation
Fusion Engineering and Design 164 112172 2021
138. Tanaka M., Suzuki N., Kato H., Iwata C., Akata N., Hayashi H., Miyake H.
Monitoring and Recovery of Tritium in a Fusion Test Facility
Fusion Science and Technology 76 4 475-480 2020

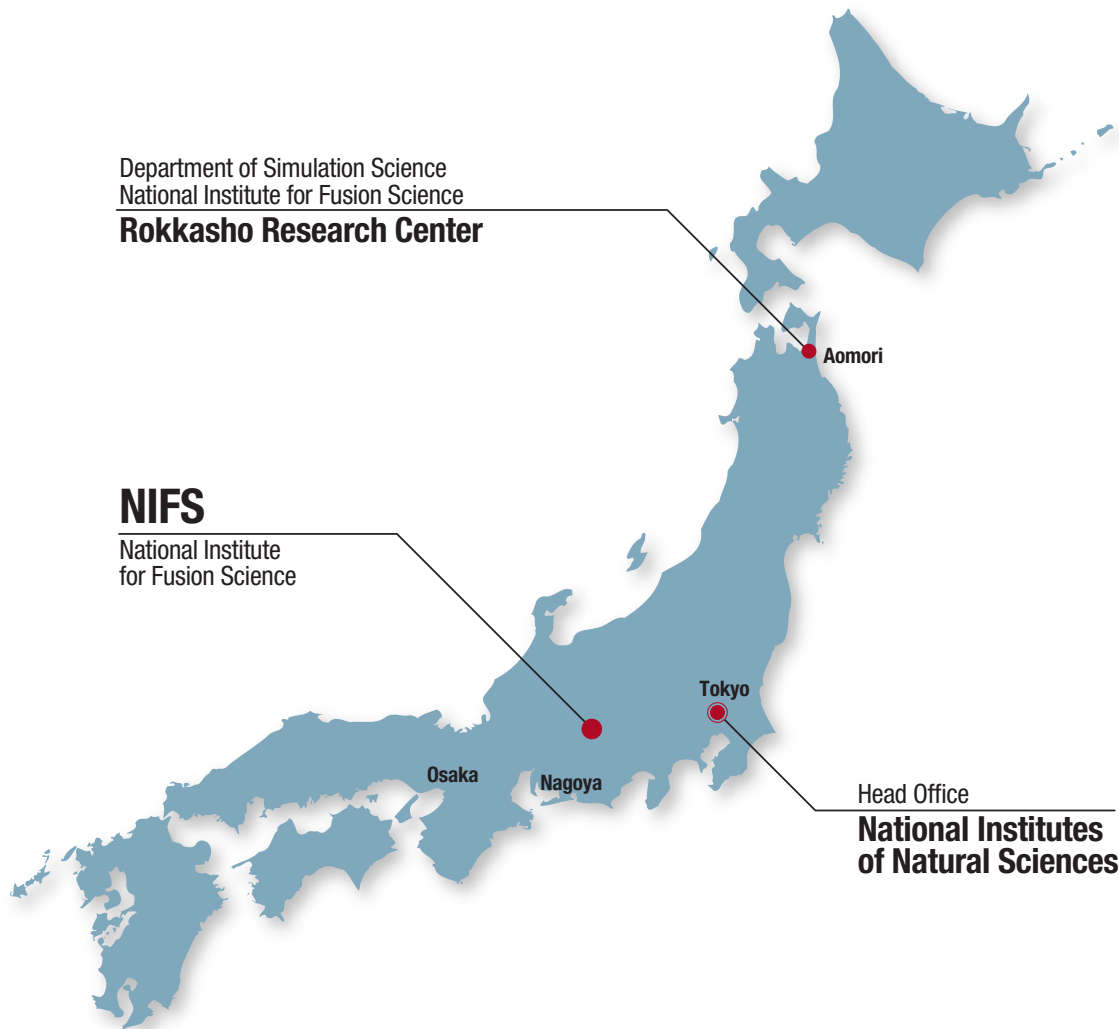
139. Tanaka M., Suzuki N., Kato H., Yokosawa M.
Initial operation results of exhaust detritiation system using a polymer membrane
Fusion Engineering and Design 160 111980 2020
140. Tanaka T., Nagasaka T., Muroga T., Yamazaki M., Toyama T.
Activation analysis for the reference low-activation vanadium alloy NIFS-HEAT-2
Nuclear Materials and Energy 25 100782 2020
141. Toda S., Nunami M., Sugama H.
Reduced models of turbulent transport in helical plasmas including effects of zonal flows and trapped electrons
Journal of Plasma Physics 86 3 815860304 2020
142. Toi K., Onchi T., Kuroda K., Kojima S., Zushi H., Hasegawa M., Fukuyama M., Kawasaki S., Higashijima A., Ikezoe T., Idei H., Ido T., Hanada K.
Effects of Toroidally Distributed Divertor Biasing on Scrape-Off-Layer Plasma in the QUEST Spherical Tokamak
Plasma and Fusion Research 16 Special Issue 1 2402024 2021
143. Toida M.
Simulation Study of Trapped Electron Effects on Positron Acceleration by a Shock Wave in an Electron-Ion-Positron Plasma
Journal of the Physical Society of Japan 90 1 14501 2021
144. Tokar M., Kobayashi M., The LHD Experimental Group.
Modeling of the resonant magnetic perturbation effect on detachment in the Large Helical Device
Plasma Physics and Controlled Fusion 62 8 85011 2020
145. Tokar M., Osakabe M., Kobayashi M., Mukai K., Nagaoka K., Takahashi H., Tanaka K., Morisaki T., The LHD Experimental Group.
A mechanism of ion temperature peaking by impurity pellet injection in a heliotron plasma
Plasma Physics and Controlled Fusion 62 7 75008 2020
146. Tokitani M., Hamaji Y., Hiraoka Y., Masuzaki S., Tamura H., Noto H., Tanaka T., Muroga T., Sagara A., Group F.
Application of the Advanced Multi-Step Brazing for fabrication of the high heat flux component
Journal of Nuclear Materials 538 152264 2020
147. Tsujimura T., Kubo S.
Propagation properties of electron cyclotron waves with helical wavefronts in magnetized plasma
Physics of Plasmas 28 1 12502 2021
148. Tsujimura T., Mizuno Y., Yanai R., Tokuzawa T., Ito Y., Nishiura M., Kubo S., Shimosuma T., Yoshimura Y., Igami H., Takahashi H., Tanaka K., Yoshinuma M., Ohshima S., The LHD Experimental Group.
Real-time control of the deposition location of ECRH in the LHD
Fusion Engineering and Design 153 111480 2020
149. Tsujimura T., Yanagihara K., Goto Y., Kubo S.
Trajectory Shift in Propagation of Electron Cyclotron Waves due to Berry Curvature in Magnetized Plasma
Plasma and Fusion Research 16 Special Issue 1 2401009 2021
150. Tsujimura T., Yanai R., Mizuno Y., Tanaka K., Yoshimura Y., Tokuzawa T., Nishiura M., Sakamoto R., Motojima G., Kubo S., Shimosuma T., Igami H., Takahashi H., Yoshinuma M., Ohshima S., The LHD Experimental Group.
Improved performance of electron cyclotron resonance heating by perpendicular injection in the Large Helical Device
Nuclear Fusion 61 2 26012 2021
151. Uehara H., Tsunai T., Han B., Goya K., Yasuhara R., Potemkin F., Kawanaka J., Tokita S.
40 kHz, 20 ns acousto-optically Q-switched 4 μm Fe:ZnSe laser pumped by a fluoride fiber laser
Optics Letters 45 10 2788-2791 2020
152. Uehara H., Yao W., Ikesue A., Noto H., Chen H., Hishinuma Y., Muroga T., Yasuhara R.
Dy-doped CaF₂ transparent ceramics as a functional medium in the broadband mid-infrared spectral region
OSA Continuum 3 7 1811-1818 2020

153. Varela J., Nagasaki K., Nagaoka K., Yamamoto S., Watanabe K., Spong D., Garcia L., Cappa A., Azegami A.
Modeling of the ECCD injection effect on the Heliotron J and LHD plasma stability
Nuclear Fusion 60 11 112015 2020
154. Varela J., Ohdachi S., Watanabe K., Spong D., Garcia L., Seki R.
Theoretical analysis of energetic-ion-driven resistive interchange mode stabilization strategies using a Landau closure model
Nuclear Fusion 60 4 46013 2020
155. Varela J., Shimizu A., Spong D., Garcia L., Ghai Y.
Study of the Alfvén eigenmodes stability in CFQS plasma using a Landau closure model
Nuclear Fusion 61 2 26023 2021
156. Varela J., Watanabe K., Shinohara K., Honda M., Suzuki Y., Shiraishi J., Spong D., Garcia L.
MHD stability of JT-60SA operation scenarios driven by passing energetic particles for a hot Maxwellian model
Nuclear Fusion 60 9 96009 2020
157. Wang H., Todo Y., Osakabe M., Ido T., Suzuki Y.
The systematic investigation of energetic-particle-driven geodesic acoustic mode channeling using MEGA code
Nuclear Fusion 60 11 112007 2020
158. Yagi-utsumi M., Tanaka T., Otsubo Y., Yamashita A., Yoshimura S., Nishida M., Kato K.
Cold Atmospheric Plasma Modification of Amyloid β
International Journal of Molecular Sciences 22 6 3116 2021
159. Yamada I., Funaba H., Lee J., Huang Y., Liu C.
Influence of Neutron Irradiation on the Large Helical Device Thomson Scattering System
Plasma and Fusion Research 15 Special Issue 1 2402075-1-4 2020
160. Yamada K., Kawashima T., Obana T., Murakami Y., Nagao M., Hozumi N.
Discrimination of partial discharges in gaseous and liquid nitrogen by using waveform characteristics
Plasma and Fusion Research 15 Special Issue 1 2401025 2020
161. Yamaguchi T., Ohtani H., Takayama T., Kamitani A.
Current Distribution Optimization by Using Genetic-Algorithm Based On-Off Method: Application to Pellet Injection System
Journal of Advanced Simulation in Science and Engineering 7 1 201-213 2020
162. Yamaguchi T., Takayama T., Kamitani A., Ohtani H.
Current Distribution Optimization in Electromagnet: Application to Superconducting Linear Acceleration System
Plasma and Fusion Research 15 Special Issue 1 2405050 2020
163. Yamamoto S., Nagasaki K., Nagaoka K., Varela J., Cappa A., Ascasíbar E., Castejon F., FONTDECABA M., García-regaña J., González-Jerez A., Ida K., Ishizawa A., Isobe M., Kado S., Kobayashi S., Liniers M., López-Bruna D., Marushchenko N., Medina F., Melnikov A., Minami T., Mizuuchi T., Nakamura Y., Ochando M., Ogawa K., Ohshima S., Okada H., Osakabe M., Sanders M., Velasco J., Weir G., Yoshinuma M.
Effect of ECH/ECCD on energetic-particle-driven MHD modes in helical plasmas
Nuclear Fusion 60 6 666018 2020
164. Yamamoto Y., Murakami S., Takahashi H., Ida K., Yoshinuma M., Chen J.
Effect of the Pfirsch-Schlüter flow on the inboard/outboard asymmetry of the toroidal flow in LHD
Physics of Plasmas 27 4 42514 2020
165. Yao W., Chen H., Uehara H., Yasuhara R.
Spectroscopic properties of Er:BZMT ceramics for laser emission
Optical Materials Express 10 12 3226-3234 2020
166. Yao W., Uehara H., Kawase H., Chen H., Yasuhara R.
Highly efficient Er:YAP laser with 6.9 W of output power at 2920 nm
Optics Express 28 13 19000-19007 2020
167. Yao W., Uehara H., Tokita S., Chen H., Konishi D., Murakami M., Yasuhara R.
LD-pumped 2.8 μm Er:Lu₂O₃ ceramic laser with 6.7 W output power and $\geq 30\%$ slope efficiency
Applied Physics Express 14 1 12001 2021

168. Yokoyama M., Yamaguchi H.
Progress of statistical modelling of thermal transport of fusion plasmas
Nuclear Fusion 60 10 106024 2020
169. Yoshimura S., Otsubo Y., Yamashita A., Ishikawa K.
Insights into normothermic treatment with direct irradiation of atmospheric pressure plasma for biological applications
Japanese Journal of Applied Physics 60 1 10502 2021
170. Yoshimura S., Terasaka K., Aramaki M.
Modification of laser-induced fluorescence spectrum by additional azimuthal Doppler effect in optical vortex beams
Japanese Journal of Applied Physics 59 SH SHHB04 2020

※ This list was compiled as of March 31, 2021

National Institute for Fusion Science



National Institute for Fusion Science
National Institutes of Natural Sciences
(TOKI Area)

322-6 Oroshi-cho
Toki-city, GIFU
509-5292

TEL: 0572-58-2222 FAX: 0572-58-2601

Rokkasho Research Center
Department of Helical Plasma Research
Located in the Aomori Research and
Development Center
Japan Atomic Energy Agency

2-166 Oaza-Obuchi-Aza-Omotodate,
Rokkasho-mura, Kamikita-gun,
AOMORI
039-3212

TEL/FAX: 0175-73-2151

How to Reach National Institute for Fusion Science



ACCESS

When you use the public transportation facility

- ◇ **from Centrair** (Central Japan International Airport)
Centrair – (μ-sky) – **Meitetsu Kanayama Sta.** (36km)
 about 25min
JR Kanayama Sta. – (JR Chuo Line) – **JR Tajimi Sta.** (33km)
 about 33min (express)
JR Tajimi Sta. – (Totetsu Bus) – **Kenkyuugakuentoshi** (7km)
 about 15min
- ◇ **from JR Nagoya Sta.**
JR Nagoya Sta. – (JR Chuo Line) – **JR Tajimi Sta.** (36km)
 about 22min (limited express) / about 30min (lapid) / about 40min (local)
JR Tajimi Sta. – (Totetsu Bus) – **Kenkyuugakuentoshi** (7km)
 about 15min

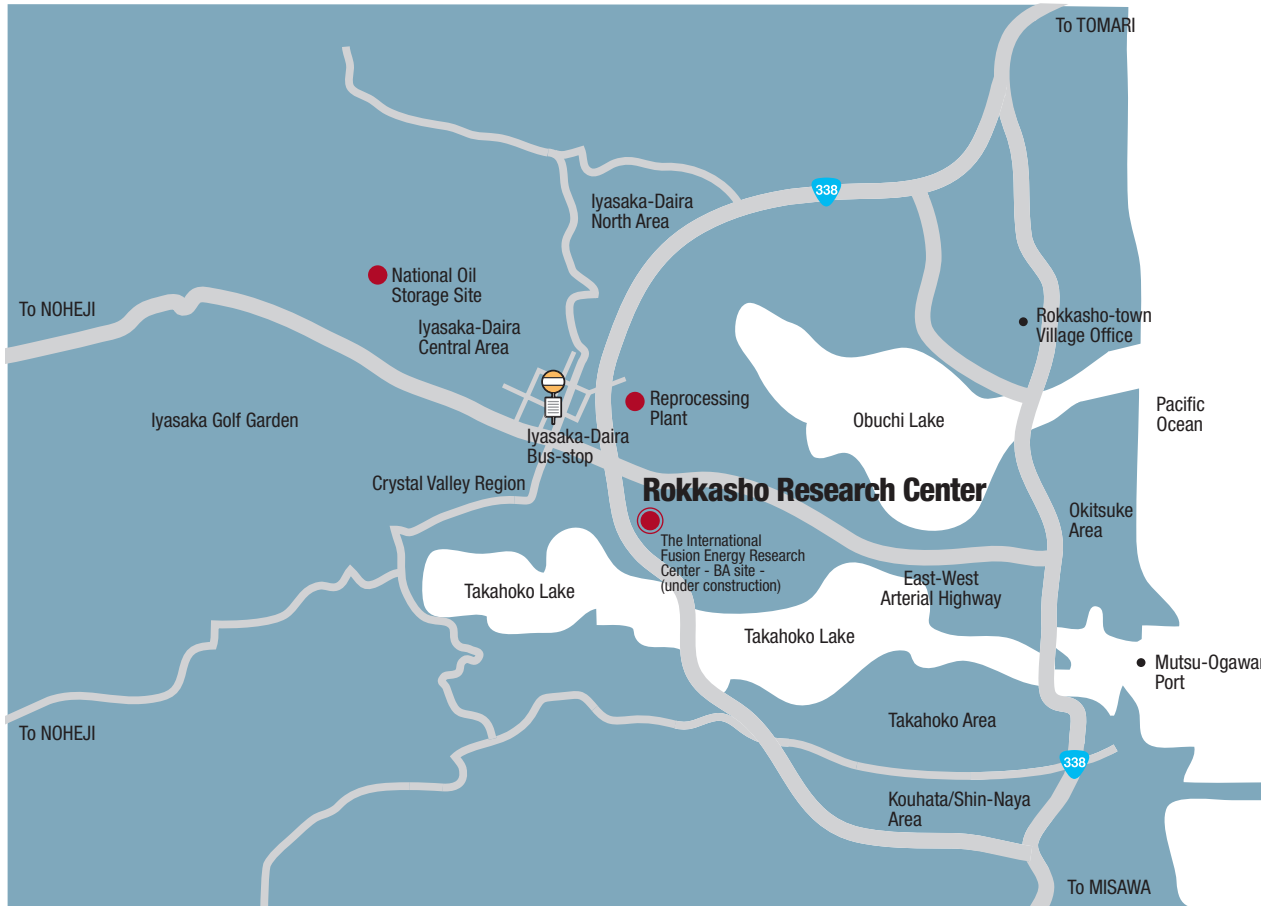
◇ from Nagoya Airport

- (Obihiro•Akita•Yamagata•Niigata•Kouchi•Matsuyama•Fukuoka•Kumamoto•Nagasaki)
- Nagoya Airport** – (Taxi) – **JR Kachigawa Sta.** (4km)
 about 10min
 - Nagoya Airport** – (Meitetsu Bus) – **JR Kachigawa Sta.** (4km)
 about 19min
 - JR Kachigawa Sta.** – (JR Chuo Line) – **JR Tajimi Sta.** (21km)
 about 20min
 - JR Tajimi Sta.** – (Totetsu Bus) – **Kenkyuugakuentoshi** (7km)
 about 15min

When you use a car

- from Chuo Expressway Toki I.C. or Tajimi I.C.** (8km)
 about 20min
- from Tokai-Kanjo Expressway Tokiminami Tajimi I.C.** (2km)
 about 5min

How to Reach Rokkasho Research Center



ACCESS

When you use the public transportation facility

◇ from Tokyo

Tokyo – (Tohoku-Shinkansen) – **Hachinohe Sta.** (630km)
about 3hr

Hachinohe Sta. – (JR Tohoku Limited Express) – **Noheji** (51km)
about 30min

Noheji – (Shimokita Koutsu Bus) – **Iyasaka-Daira** (10km)
about 40min

Iyasaka-Dairaon foot..... **Rokkasho Research Center** (0.7km)
about 8min

◇ from Misawa Airport

Misawa Airport – (Bus) – **Misawa** (2km)
about 13min

Misawa – (JR Tohoku Limited Express) – **Noheji** (30km)
about 20min

Noheji – (Shimokita Koutsu Bus) – **Iyasaka-Daira** (10km)
about 40min

Iyasaka-Dairaon foot..... **Rokkasho Research Center** (0.7km)
about 8min

◇ from Aomori Airport

Aomori Airport – (Bus) – **Aomori** (12km)
about 40min

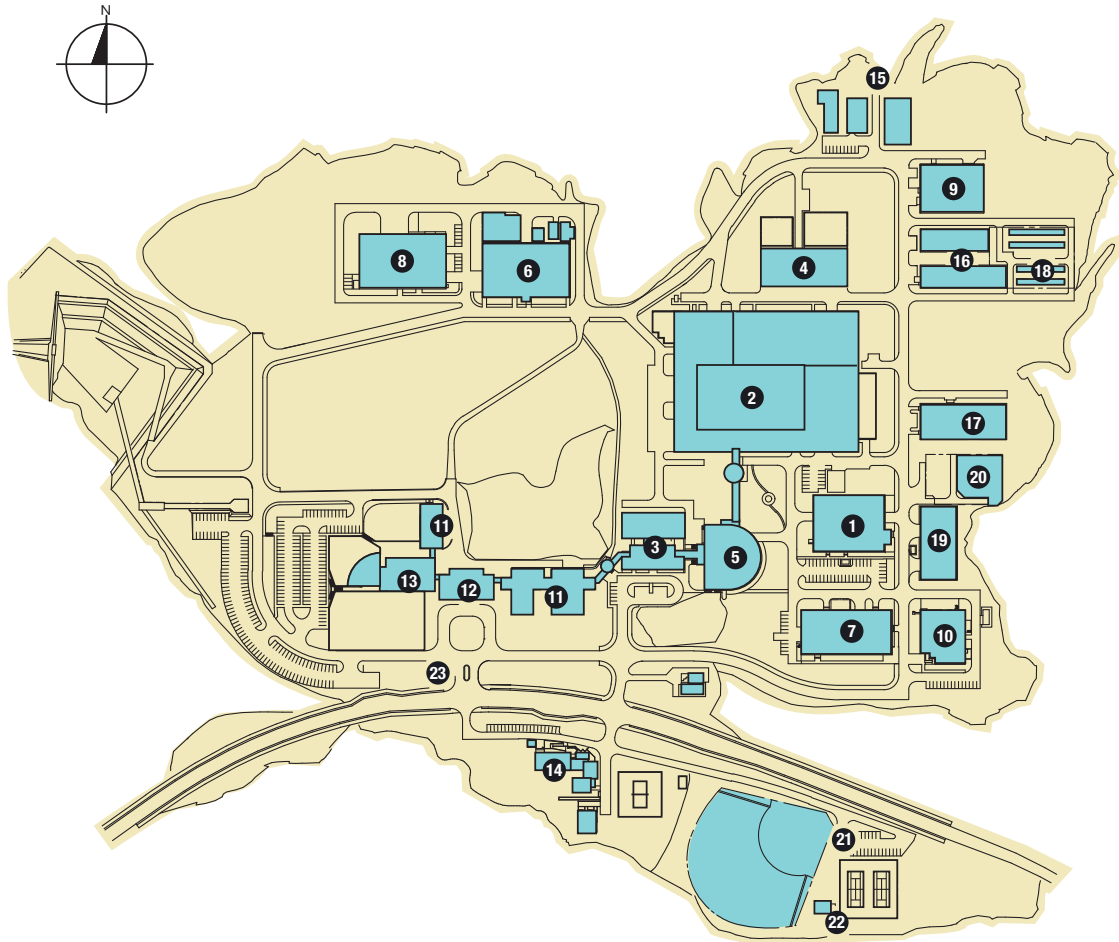
Aomori – (JR Tohoku Limited Express) – **Noheji** (45km)
about 30min

Noheji – (Shimokita Koutsu Bus) – **Iyasaka-Daira** (10km)
about 40min

Iyasaka-Dairaon foot..... **Rokkasho Research Center** (0.7km)
about 8min

National Institute for Fusion Science

Building Arrangement



NIFS plot plan

- | | |
|--|------------------------------------|
| ① Superconducting Magnet System Laboratory | ⑬ Administration Building |
| ② Large Helical Device Building | ⑭ Helicon Club (Guest Housing) |
| ③ Simulation Science Research Laboratory | ⑮ High-Voltage Transformer Station |
| ④ Heating and Power Supply Building | ⑯ Cooling Water Pump Building |
| ⑤ LHD Control Building | ⑰ Helium Compressor Building |
| ⑥ Fusion Engineering Research Laboratory | ⑱ Cooling Tower |
| ⑦ Plasma Diagnostics Laboratories | ⑲ Equipments Room |
| ⑧ R & D Laboratories | ⑳ Helium Tank Yard |
| ⑨ Motor-Generator Building | ㉑ Recreation Facilities |
| ⑩ Central Workshops | ㉒ Club House |
| ⑪ Research Staff Building | ㉓ Guard Office |
| ⑫ Library Building | |

